Development of a genetic and molecular toolkit for the oleaginous red yeast *Rhodotorula toruloides*

Submitted by George Alexander Kirke to the University of Exeter as a thesis for the degree of Master of Science by Research (Biological Sciences), April 2019.

I certify that all material in this thesis which is not my own work has been identified and that any material that has previously been submitted and approved for the award of a degree by this or any other University has been acknowledged.

(Signature) ……

George Kirke
gak203@exeter.ac.uk

Abstract

Rhodotorula toruloides is an oleaginous yeast with potential use as a biotechnological chassis for both production of industrially and pharmaceutically relevant compounds, and as a drop-in biofuel producer on low-cost substrate. Cells can accumulate lipid droplets to over 70 % weight/weight under certain growth conditions. We here summarise the currently-available genetic and molecular toolkit for the yeast and suggest further avenues for research to enable full utilisation of this yeast.

To aid in these objectives, we have constructed lipid droplet-associated GFP-tagged protein Ldp1-GFP and demonstrated how this can be used to quantify individual cell lipid quantity using confocal microscopy. Calnexin-GFP and GFP-Atg8 have also been constructed for live-cell monitoring of the intracellular machinery in lipid droplet synthesis as part of the developing *R. toruloides* molecular toolkit.

Furthermore, the induction profiles of selected heat shock protein promoters have been characterised through a GFP-reporter system. Currently, the only reported inducible promoters in *R. toruloides* are nutrient-dependent *NAR1, ICL1, MET16, CTR3, DAO1, THI4, THI5 and CTR31*, and tightly controlling these is not possible in potential use as a biofuel producer using low-cost substrate. Of the promoters highlighted herein (*ENO2, TDH3, PGK1, TPI1, SSB1, ACT1 and TDH3), ENO2* is identified as a qualitatively putative heat-shock inducible promoter, further analysis of which may allow the nutrient-dependency limitation to be overcome through exploitation of the native environmental stress response.

Contents

Abbreviations

AGPAT	Acylglycerol-3-phosphate acyltransferase
ASTM International	(formerly American Society for Testing and Materials) International
ATMT	*Agrobacterium tumefaciens*-mediated transformation
CARS	Coherent anti-Stokes Raman spectroscopy
CSM	Complete Supplement Mix
DAG	Diacylglycerol
DGAT	Diacylglycerol acyltransferase
ER	Endoplasmic reticulum
FA	Fatty acid
FAMEs	Fatty acid methyl esters
FAS	Fatty acid synthase
FFA	Free fatty acid
GHG	Greenhouse gases
HSP	Heat shock protein
HSPP	Heat shock protein promoter
LD	Lipid droplet
MIC	Minimum inhibitory concentration
MM+N	Minimal Medium + Nitrogen
MM-N	Minimal Medium - Nitrogen
OD_{600}	Optical Density (600 nm)
PA	Phosphatidic acid
PL	Phospholipid
POM	Pyruvate-oxaloacetate-malate (cycle)
PPP	Pentose phosphate pathway
SE	Sterol ester
SRS	Stimulated Raman scattering
TAG	Triacylglycerol
UNCTAD	United Nations Conference on Trade and Development
VLCFA	Very long chain fatty acid
WT	Wild-type
YPD	Yeast Peptone Dextrose
YRBC	Yeast-recombination based cloning

List of Figures

1. Introduction

Rhodotorula (formerly *Rhodosporidium*) *toruloides* (Banno) is a heterothallic basidiomycete (subphylum Pucciniomycotina) yeast (Coelho *et al.*, 2008; Wang, Q. M. *et al.*, 2015) which has recently garnered interest as a biotechnologically relevant organism. *R. toruloides* strains have been isolated from many different ecological regions around the world: from the wood-pulp of Swedish conifers (Rennerfelt, 1937), to the air in the Koishikawa Botanical Garden, Japan (Okunuki, 1931), to the gut of a captive porpoise off of the Bahamas (Kutty and Philip, 2008). However, all these strains share common traits which are potentially useful in a biotechnological capacity: their ability to naturally synthesise carotenoids (useful as nutritional supplements), and their ability to accumulate neutral lipids at high density (with potential use in the petrochemical sector). Although other uses of the oleaginous yeasts – a term to describe organisms capable of greater than 20 % weight/weight oil accumulation (Evans and Ratledge, 1984a) – and their other pharmaceutically relevant products such as D-amino acids and L-phenylalanine ammonia-lyase have been alluded to in the literature (Liu, Y. *et al.*, 2015; Park *et al.*, 2018; Tully and Gilbert, 1985), the main focus of this thesis will be on developing tools to monitor lipid droplet biogenesis and its associated molecular machinery, intrinsically associated with neutral lipid accumulation, and identifying novel non-media-dependent promoters.

Neutral lipids, the primary constituent of lipid droplets in yeast, are rapidly manifesting themselves as an alternative to fossil fuels. Although the rate of growth of greenhouse gas (GHG) emissions appears to be finally slowing, as highly industrial countries move away from coal plants and the rate of renewable energy uptake increases (Jackson *et al.*, 2016), climate change models still predict a likely anthropogenic climate change of between 1.6 °C to 3.2 °C above pre-industrial era temperatures from increasing atmospheric GHG (Rogelj *et al.*, 2012). This is predicted to lead to corresponding catastrophic global effects as habitable land and food both deplete and extreme weather variability increases (Bathiany *et al.*, 2018; Bebber *et al.*, 2013; Jackson *et al.*, 2016; Pacifici *et al.*, 2015). As of 2018, the global production of oil refinery throughput is 8.2 million barrels day^{-1}, an increase of 2.1 % over the previous year (BP, 2004). Renewable energy sources have shown a marked production rise, with a global 17 %

increase above 2017 (excluding hydroelectric energy production) but this – while significant for static energy-drawing applications and for contributing to lowered coal and natural gas-derived carbon emissions – will be unable to effectively lower the oil-derived energy demand for long-distance travel (shipping and aeroplanes). Whereas an uptake of electric-powered vehicles can reduce individual anthropogenic GHG emissions, these vehicles currently rely on low-energy-density lithium-ion batteries or underdeveloped technology in hydrogen fuel-cells with an energy density of 2.64 MJ/L and 4.5 MJ/L at 690 bar respectively (Ulvestad, 2018), compared to 33.0 MJ/L for aviation gasoline and 40.8 MJ/L for high-sulphur marine fuel oil (Figure 1). In 2012 the vast majority of the year's 961 million tonnes of CO_2 were released were from municipal marine vessels (1 806 650 vessels as of 2016). With >80 % of global trade by weight delivered through marine transportation (Walker, 2016) and an anticipated 50-250 % increase by 2050 (UNCTAD, 2016; Walker *et al.*, 2018) it is apparent that, without a process by which these GHG are carbon neutral, the shipping and long-range transportation industry will have a marked impact on anthropogenic climate change.

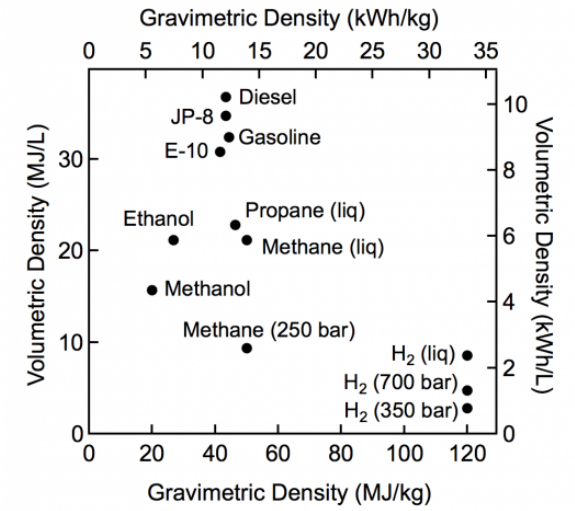

Figure 1| Energy densities of current and potential future mass-transport-energy sources. Energy densities are shown in both MJ/kg and MJ/L. JP-8 is Jet Propellant 8, an aviation fuel. Source: https://www.energy.gov/eere/fuelcells/hydrogen-storage

From the energy-density and predicted models mentioned above, it seems unlikely that the use of oil as the primary energy source of marine and aeronautical travel is likely to change in the next 50 years; prevention or reduction of further GHG will require an alternative source of the fuel. So-called 'biofuels' are carbon neutral; these sequester atmospheric CO_2 as they gain high-energy-density biomass before later releasing the GHG as they are combusted and, therefore, do not contribute to further GHG. 'First generation' biofuels have been developed successfully and these, while economical, are severely limited in their future application due to both the use of human-edible feedstocks, thereby bringing in ethical considerations as food sources become more in-demand, and bioethanol being limited to 5 % to 10 % anhydrous blending in conventional fossil fuels in unspecialised infrastructure in the EU and USA respectively (Charles *et al.*, 2010; Naik *et al.*, 2010; Tyner, 2010). In comparison, 'second generation' biofuels can use inexpensive, non-food biomass and, through generation of 'drop-in' biofuels, can be blended to 100 %, when in accordance with EN 14214:2012, and therefore reduce dependency on fossil fuels ('Biodiesel Standards & Properties').

R. toruloides is a potential second generation biofuel producer, natively capable of accumulation of lipids to over 65 % w/w (Zhang, Skerker, *et al.*, 2016) to titres of 8 g L^{-1} in shaking flasks; recent genetic overexpression of key lipid biosynthesis enzymes has raised this to 18.6 g L^{-1} and to 89.4 g L^{-1} lipid in fed-batch growth bioreactors (Zhang *et al.*, 2016). Additionally, native *R. toruloides* is resistant to many lignocellulosic biomass hydrolysate-derived compounds released during the production of monomeric carbohydrates. The compound Acetic acid (up to 70 mM), a compound which strongly inhibits *Pichia stipitis* ethanol production (Delgenes *et al.*, 1996), was found to be utilised as a lipid precursor and allowed accumulation of lipid content to 68 % w/w, though this is likely due to a shift to a carbon: nitrogen starved feedstock (Hu *et al.*, 2009; Kitahara *et al.*, 2014). The phenolic inhibitors 5-hydroxymethylfurfural (HMF), p-hydroxybenzaldehyde (PHB), syringaldehyde and vanillin did all significantly inhibit *R. toruloides* lipid biogenesis by between 5-15 %, although these were at concentrations far higher than found in actual biomass hydrolysates (Hu *et al.*, 2009). Furfural, which leads to yeast cell-growth suppression and lipid biogenesis inhibition through sequestering of reductant NADH as the compound is reduced

to detoxified furfural alcohol (Nilsson *et al.*, 2005), leads to a decrease in lipid content of *R. toruloides* by 26.5 % at concentrations 34 % and 10 % of that from spruce and corn stover hydrolysates respectively (Agbogbo and Wenger, 2007; Nilsson *et al.*, 2005). However, mutant strains of the yeast isolated for tolerance to sugarcane bagasse hydrolysate, simultaneously developed greater tolerance to furfural with a minimum inhibitory concentration (MIC) of 5 g L^{-1}; after a lag period of 36 hours (24 hours faster than the wild type (WT) *R. toruloides* mutant grew to a density comparable to non-furfural containing media containing 9.3 and 2.7 times that found in the spruce and corn stover hydrolysates at 2.5 g L^{-1} (Hu *et al.*, 2009; Kitahara *et al.*, 2014). As such, *R. toruloides* is capable of employing low-cost substrates. A 2016 pilot study by Dalmas Neto *et al.* using WT *R. toruloides* strain DEBB 5533 produced ASTM International standard biofuel when utilising sugarcane broth (40 g L^{-1} total sugars) supplemented with urea. Conversion of microbial oil to biodiesel was performed through base-catalysed transesterification using methanol and sodium hydroxide. Thliveros *et al.*, (2014) demonstrated production of fatty acid methyl esters using this transesterification method at a 97.7 % yield. The pilot study biodiesel had a total raw-material value of US\$0.26 L^{-1} biofuel produced with an additional \$0.50 L^{-1} biofuel cost associated with energy costs. With the price of crude oil at \$0.34 L^{-1} in 2017 (Robson, 1981), this yeast-derived biofuel may be close to, or even capable of undercutting, the fossil-fuel prices if lower energy costs of lipid extraction can be realised. As reviewed by Xu and Liu, 2017, recent studies using low-value waste products such as crude glycerol (Polburee *et al.*, 2016) and domestic wastewater (Ling *et al.*, 2014) reported 69.5 % w/w and 63.95 % w/w lipid content respectively, although other traditional biomass hydrolysate substrates have also been utilised. *R. toruloides* CECT 13085 has been recently grown in increasing concentrations of non-detoxified wheat straw hydrolysates to selectively evolve a mutant strain on this low-value substrate capable of 39.5 g L^{-1} lipid yield when engineered to overexpress lipid pathway genes *DGAT1* and *SCD1*.

In addition to neutral lipid accumulation, which offers specific use as a biodiesel drop-in after transesterification to fatty acid methyl esters (FAMEs), *R. toruloides* has also been used to synthesise specific high-value lipids at high titres. After expression of galactose-inducible *Fusarium verticillioides* or *Mortierella alpina* Δ12-fatty acid desaturases (FADS) genes, overproduction of the essential fatty

acid linoleic acid increased fivefold to 1.3 g L^{-1} (Wang, Y., *et al.*, 2016). Similarly, integration of Δ12-fatty acid desaturase (FAD2) and ω3 desaturase (FAD3) from *M. alpina* and *Aleurites fordii* respectively also increased essential fatty acid α-linolenic acid (C18:3) production by a 4.5-fold increase in *R. toruloides Δald1* (Lui *et al.*, 2015). Introduction of the *S. cerevisiae OLE1* gene, encoding Δ9-fatty acid desaturase, caused *R. toruloides* oleic acid (utilised in biolubricants, electrical insulation in transformers, and hydraulic fluid) content to increase fivefold, accounting for >70 % of total lipid (Park *et al.*, 2018; Tsai *et al.*, 2019). Exotic very long chain fatty acids (VLCFA) erucic acid (cis-docosa-13-enoic acid, C22:1Δ13) and nervonic acid (cis-tetracosa-15-enoic acid, C24:1 Δ15), important in production of plastics and as a treatment of human neurological pathologies such as Zellweger syndrome, adrenoleukodystrophy, schizophrenia, and multiple sclerosis, have also been produced to 10-15 g L^{-1} (20-30 % of total fatty acid content). This has been achieved through ectopic heterologous integration of codon-optimised *Brassica*-plant species *Crambe abyssinica* and *Cardamine graeca* 3-ketoacyl-CoA synthases (KCS) (Amminger *et al.*, 2012; Fillet *et al.*, 2017; Tanaka *et al.*, 2007).

Despite the recent acceleration of studies into *R. toruloides*, the molecular and genetic toolkit for *R. toruloides* remains limited; *Agrobacterium tumefaciens*-mediated transformation now allows relatively fast integration of DNA into the yeast, although codon optimisation is required for successful heterologous protein expression in this GC-rich organism, therefore necessitating custom synthesised oligonucleotides (Alexander Johns, pers. comm.). Targeted gene disruption has been demonstrated in Ku70 knockouts, required to facilitate weak homologous recombination, and CRISPR for the easily-identified *CAR2* locus, encoding a key step in the carotenoid-biosynthesis pathway and therefore generating an albino colony when mutated (Koh *et al.*, 2014; Liu, Y. *et al.*, 2018; Otoupal *et al.*, 2019).

1.1. Molecular process and organelle targeting

Having introduced the potential use of *R. toruloides* as a high-yield producer for drop-in biofuel production, the intracellular mechanisms and organelle properties of this yeast that facilitate such desirable properties will now be outlined.

1.1.1. Lipid biogenesis

Lipids are a group of organic molecules that are soluble in non-polar organic solvents and are requisite compounds for all living organisms. They are found in many diverse forms, each with differing properties, which fall within eight categories: fatty acids (FAs), glycerolipids, glycerophospholipids, sterol and sterol derivatives, sphingolipids, prenol lipids, glycolipids and polyketides (Fahy *et al.*, 2011). Complex lipids are composed of an ester-linked carboxylic acid head group and poly(un)-saturated hydrocarbon tail(s) of various lengths. Yeast lipids can either be taken up from the cell's surroundings directly, produced by *de novo* synthesis, or recycled through the hydrolysis of existing lipids to synthesise the necessary new lipids; the following section reviews each of these processes and how it is optimised in *R. toruloides* for increased lipid accumulation.

External uptake of lipids from their surrounding media by yeasts is facilitated by either diffusion of lipids, or a temperature-dependent uptake step through the transporters Ypk1 and bifunctional Fat1 very long chain transporter (and acyl-CoA synthetase), and their subsequent activation by the energy-dependent acyl-CoA-synthetase proteins Faa1/2/3/4 (Black and DiRusso, 2007; Jacquier and Schneiter, 2010). These activated FFAs (free fatty acids) can then be used as donors of acyl moieties during bi-acylation of the initial substrates glycerol or acyl-dihydroxyacetone phosphate with either the GPAT (glycerol-phosphate acyltransferase) proteins Sct1/Gpt2 or Ayr1 respectively to give lysophosphatidic acid (Lyso-PA). FFAs are then also used for acylation of Lyso-PA itself by AGPATs (acylglycerol phosphate acyl transferases) Slc1/4 or Loa1 to generate phosphatidic acid (PA). This complex lipid PA can then be used as the initial substrate in pathways for the biosynthesis of phospholipids: phosphatidylinositol (PI), phosphatidylcholine (PC), phosphatidylethanolamine (PE), phosphatidylglycerol (PG), phosphatidylinositol (PS), and cardiolipin (CL).

As detailed in Figure 2, PA can, however, also be used as the base substrate in biosynthesis of neutral lipids. Cleaving inorganic phosphate from PA catalysed by the lipins Add1, Lpp1, App1, and (predominantly) endoplasmic reticulum (ER) membrane-bound Pah1 results in a diacylglycerol (DAG) molecule and this can then be acylated with the DGAT (diacylglycerol acyl transferases) Lro1 or Dga1 to triacylglycerols (TAGs) or to sterol esters (SEs) by the Are1/2 DGAT enzymes (Chae *et al.*, 2012; Klug and Daum, 2014; Pascual and Carman, 2013; Soni *et*

al., 2009). In the ascomycete yeast *Saccharomyces cerevisiae,* deletion of *PAH1* significantly reduces the amount of DAGs available for acylation to TAGs thereby causing a proportional increase in cellular PL content; in stationary phase Δ*PAH1* mutants have a severely depleted lipid droplets (where TAG content is reduced by 80 %) and correspondingly high content of PLs (PC, +84 %; PE, +154 %; PI, +88 %; PS, +52 %; and PA; +450 %) and FFAs (+77 %) compared to WT (Fakas *et al.*, 2011). This lipid profile change leads to disruption of intracellular machinery through disruptive interactions and stresses, causing cell death through lipotoxicity (Listenberger *et al.*, 2003; Nguyen *et al.*, 2017; Wang, C. W., 2016). Curiously, *DGK1*-encoded diacylglycerol kinase, which reverses the dephosphorylation of PA to DAG back to DAG, restores the defect in lipid droplet formation back to WT but does not prevent the increased sensitivity of Δ*PAH1* mutants to lipotoxicity exhibited during growth in unsaturated FA-containing media (Fakas *et al.*, 2011).

However, biogenesis of complex lipids is not just limited to acylation from lipids taken up from media; precursor fatty acids are ubiquitously synthesised *de novo* in all yeasts for acylation of ADHP and glycerol-3-phosphate for feeding into the lipid storage or PL synthesis pathways (Klug and Daum, 2014). Oleaginous organisms (capable of lipid biogenesis greater than 20 % biomass) are particularly adept at lipid biogenesis through adaptations which overcome stoichiometric limitations in reducing power in the fatty acid synthase (FAS) enzyme complex for $C_{16:0}$-$C_{18:0}$ synthesis from glucose; as each elongation cycle of the FAS complex requires two NADPH molecules, and one glycerol-derived acetyl-CoA, synthesis of $C_{18:0}$ is undertaken in 8 condensation reactions (Ratledge, 2014). Therefore, for each mole of $C_{18:0}$ synthesised in the FAS complex 16 moles of NADPH are required. For each mole of glucose-derived acetyl-CoA in glycolysis, however, only 9 moles of NADPH are generated; oxidising cofactors generated in the mitochondria are assumed to be used almost exclusively in ATP synthesis (Ratledge, 2014). The pentose-phosphate pathway (PPP) is a second cytoplasmic pathway capable of producing an additional 6 moles of NADPH directly, but also generates an additional mole of NADPH through feeding of PPP-derived glyceraldehyde-3-phosphate into the pyruvate-oxaloacetate-malate (POM) cycle; this would satisfy the stoichiometric requirements for *de novo* FA biosynthesis. For simplicity, to assume only $C_{18:0}$

acyl groups are present in synthesised TAGs and two ATP molecules generated for each terminal oxygen in the mitochondrial electron transport chain, a theoretical yield of 31.6 g of TAG can be synthesised from 100 g of glucose (Klug and Daum, 2014; Ratledge, 2014). In the oleaginous yeast *Yarrowia lipolytica* without overexpression of cytosolic malic enzyme, overexpression of the NADP reducer is reported by Macool *et al.*, 2013 to increase lipid content by 5-10 %.

For simplicity, *de novo* TAG detailed hereafter will use only glucose as an original carbon source. Cytoplasmic glycolysis-synthesised 3-carbon dihydroxyacetone phosphate (DHAP) can either be: acylated, as detailed above, with the glycerol-phosphate acyl transferases Sct1 (GPAT2) or Gpt1 (GPAT2) to acyl-dihydroxyacetone phosphate; dehydrogenated with the NAD^+-dependent glycerol-3-phosphate dehydrogenase Gpd1 to glycerol-3-phosphate; or alternatively continue through glycolysis to generate 3-carbon pyruvate (Klug and Daum, 2014; Zheng and Zou, 2001). Passing through the mitochondrial membranes using the pyruvate decarboxylase complex, 2-carbon acetyl-CoA is generated and can be used to re-form 6-carbon citrate from 4-carbon oxaloacetate in the Krebs cycle; this citrate is crucial in facilitating oleaginous yeast lipid assimilation. Under lipid-accumulating nitrogen starvation conditions *IDH1*/*4*-encoded isocitrate dehydrogenase enzyme, responsible for the catalysis of isocitrate to oxoglutarate in the third step of the Krebs cycle, is negatively regulated leading to an increase in isocitrate and, due to the reversible nature of the aconitase enzyme, an increase in citrate in the mitochondria (Ratledge, 2014; Shi, S. and Zhao, 2017; Tang *et al.*, 2009; Yang *et al.*, 2012). This citrate can be transported to the cytoplasm through, firstly, the mitochondrial citrate transport protein across the inner membrane, before passively diffusing through a selective ion channel. Once in the cytoplasm, citrate is hydrolysed to acetyl-CoA and oxaloacetate through the action of AclI ATP-citrate lyase with the acetyl-coA feeding into the FAS complex and oxaloacetate being oxidised to malate for re-transporting back into the mitochondria and use in the Krebs cycle. This oxaloacetate, in some oleaginous yeast including *R. toruloides*, is able to instead be used to oxidise malate through the POM cycle-facilitated ‘malic enzyme’ to coupled-reaction reduce NADP to NADPH (Evans and Ratledge, 1984a; Macool *et al.*, 2013; Ratledge, 2014; Zhang, Ito, *et al.*, 2016).

De novo synthesis of FFAs in eukaryotes occurs in both the cytoplasm/ER and the mitochondria. Cytoplasmic/ER based synthesis is the principal site of TAG synthesis for lipid droplet formation and is the focus of this section. In an ATP-dependent reaction catalysed by a biotinylated acetyl-CoA carboxylase Acc1, pyruvate-derived acetyl-CoA is carboxylated to a malonyl-CoA three-carbon building block (Choudhary *et al.*, 2018; Klug and Daum, 2014; Mishina *et al.*, 1980; Wang, H. *et al.*, 2017). FA synthesis then occurs in the FA synthetase (FAS) complex; with each 'cycle' of the FAS functionally conserved proteins elongate the nascent acyl group by two carbons.

In the ascomycete *S. cerevisiae*, a giant multifunctional 2.6 MDa $\alpha_6\beta_6$ heterododecamer of the proteins 230 kDa Fas1 and 210 kDa Fas2 contains a central hexameric α wheel capped by two trimeric β domes for transfer of two carbons from malonyl-CoA to a saturated hydrocarbon chain (Leibundgut *et al.*, 2007). The *S. cerevisiae* Fas1 β-subunit contains the highly mobile 'acyl carrier protein' (ACP) acetyl transferase, enoyl reductase, dehydrase 1 & 2 and the larger part of a malonyl-palmitoyl transferase domain. The Fas1 α-subunit provides the remainder of the malonyl-palmitoyl transferase, acyl-carrier proteins, 3-ketoreductase, 3-ketosynthase, and phosphopantheteine transferase. In standard growth conditions, the FFAs produced by the cytoplasmic FAS are saturated C_{16} palmitic acid or C_{18} stearic acid molecules, synthesised in a 2:3 ratio (Fischer *et al.*, 2015; Leibundgut *et al.*, 2007; Schweizer, E. and Hofmann, 2004; Schweizer, M. *et al.*, 1986).

Interestingly, the *R. toruloides 2.7* MDa FAS type 1 protein complex contains an evolutionarily recent ACP duplication event (Fischer *et al.*, 2015). As both ACP domains show 77 % sequence identity in their mobile linker regions, with an especially high homology in the acyl-docking sequence, it is thought that these seemingly identically-functional protein subunits work to only increase relative crowding of the enlarged *R. toruloides* FAS (18 Å wider, though 20 Å shorter than the barrel found in in *S. cerevisiae*) with substrates, and this facilitates a faster reaction rate due to a localised increased substrate concentration. Gene splitting of the FAS 1 complex also appears to have occurred in the anti-parallel β-sheet between the enoyl reductase and dehydrase domains of the complex though this is not hypothesised to have any functional effect (Fischer *et al.*, 2015).

Fatty acids are activated to functional fatty acid-CoA (FA-CoA) by the synthases Faa1/4 or a Fat1; these activated molecules can then be used as acyl-donors directly in the synthesis of lyso-PA and TAGs by the GPAT or DGAT enzymes as previously mentioned, or further elongated or desaturated in the ER (Oh *et al.*, 1997; Schweizer, E. and Hofmann, 2004; Tehlivets *et al.*, 2007).

Elongation and desaturation of FAs occurs in the ER using the elongase enzymes Elo1, Elo2, and/or Elo3 – to add additional malonyl-CoA carbons – and desaturation enzyme Ole1, to generate the required lipids (Oh *et al.*, 1997; Tehlivets *et al.*, 2007). Elo1, Elo2 and Elo3 facilitate sphingolipid biogenesis, in conjunction with accessory proteins beta-keto reductase Ybr159w and 3-hydroxyacyl Co-A dehydrase, as part of the FA elongation cycle (Browne *et al.*, 2013). Whereas Elo1 elongates C_{14}-C_{16} to C_{16}-C_{18} medium length FAs, its paralogues Elo2 and Elo3, derived from the whole-genome duplication of *S. cerevisiae*, elongate FAs shorter than C_{22} up to C_{24}, and elongate C_{24} FAs to C_{26} respectively (Oh *et al.*, 1997). As such, Elo2 and Elo3 are necessary for very long chain fatty acid (VLCFA) synthesis and their mutants show marked differences in sphingolipid composition in affected cells, thereby showing membrane generation defects. Released VLCFA is used as the substrate in AGPAT synthesis to facilitate position-2 acylation of lyso-PA (Benghezal *et al.*, 2007; Klug and Daum, 2014).

Because an excess of free cytoplasmic or ER-localised FAs from any of the three FA biosynthesis pathways (such as through inoculation in oleic-acid containing media) can disrupt cellular machinery and cause lipotoxicity, they are rapidly either: used in the synthesis of complex lipids; stored for later use as SE or TAGs in the lipid droplet; or translocated into peroxisomes for catabolic β-oxidation by the ABC transporter heterodimers Pxa1-Pxa2 (esterified long chain FAs such as oleic acid C18:1) or Ant1-Pex11 (non-activated medium chain FAs) before activation by the aforementioned acyl-CoA synthetase Faa2 (Baker *et al.*, 2015; Klug and Daum, 2014; Palmieri *et al.*, 2001).

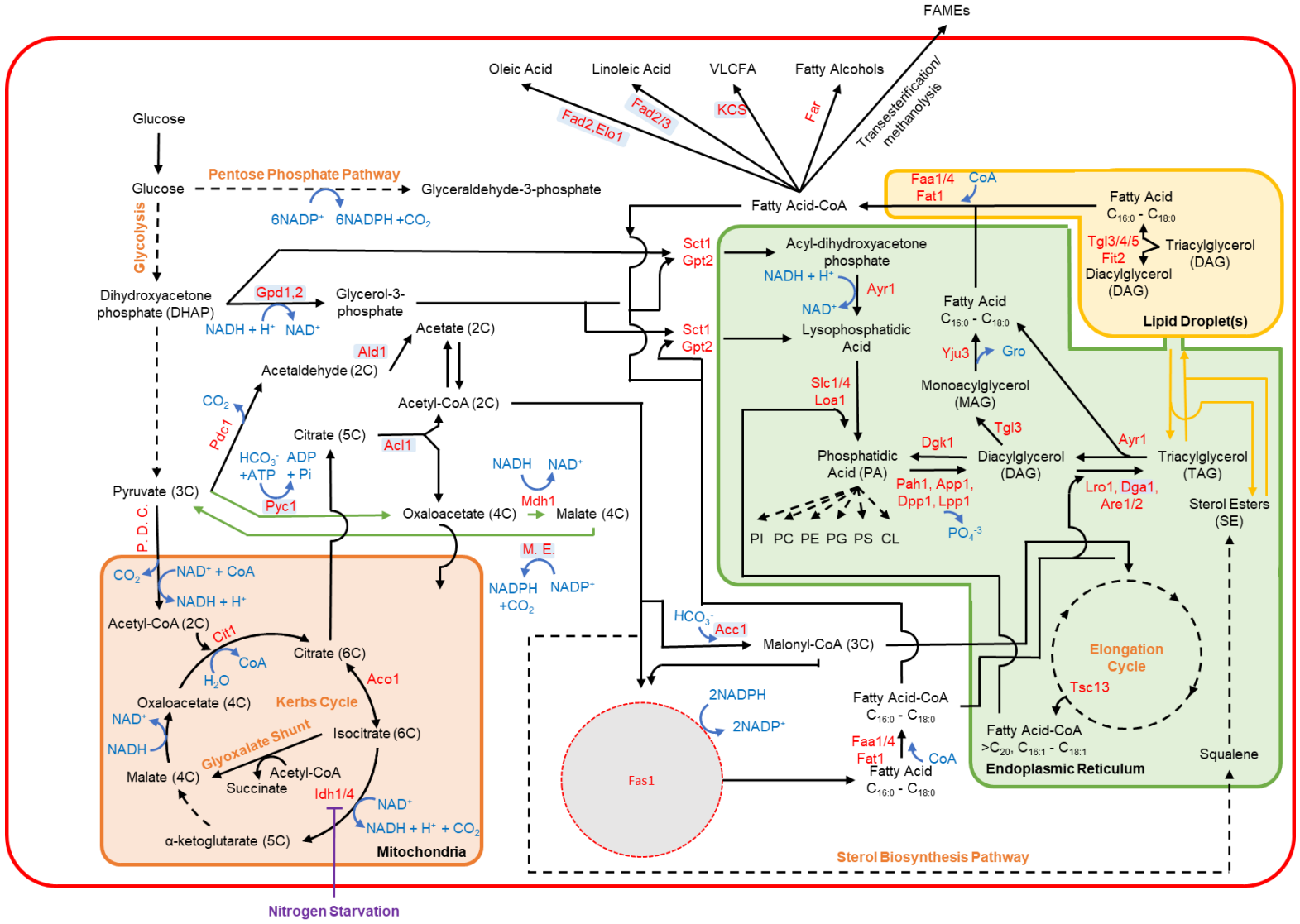
FAMEs
Oleic Acid
Linoleic Acid
VLCFA
Fatty Alcohols
Fad2,Elo1
Fad2/3
KCS
Far
Transesterification/ methanolysis
Glucose
Glucose
Pentose Phosphate Pathway
Glyceraldehyde-3-phosphate
6NADP+ 6NADPH +CO2
Glycolysis
Fatty Acid-CoA
Faa1/4 Fat1
CoA
Fatty Acid C16:0 - C18:0
Tgl3/4/5 Fit2
Triacylglycerol (DAG)
Diacylglycerol (DAG)
Lipid Droplet(s)
Dihydroxyacetone phosphate (DHAP)
Gpd1,2
Glycerol-3-phosphate
NADH + H+ NAD+
Sct1 Gpt2
Acyl-dihydroxyacetone phosphate
NADH + H+
Ayr1
NAD+
Lysophosphatidic Acid
Fatty Acid C16:0 - C18:0
Yju3
Gro
Monoacylglycerol (MAG)
Slc1/4 Loa1
Tgl3
Ayr1
Dgk1
Phosphatidic Acid (PA)
Diacylglycerol (DAG)
Triacylglycerol (TAG)
Pah1, App1, Dpp1, Lpp1
PO4-3
PI PC PE PG PS CL
Lro1, Dga1, Are1/2
Sterol Esters (SE)
Acetate (2C)
Ald1
Acetaldehyde (2C)
Acetyl-CoA (2C)
CO2
Pdc1
Citrate (5C)
Acl1
HCO3- ADP +ATP + Pi
Pyc1
NADH NAD+
Mdh1
Pyruvate (3C)
Oxaloacetate (4C)
Malate (4C)
P. D. C.
M. E.
NADPH NADP+ +CO2
CO2 NAD+ + CoA
NADH + H+
Acetyl-CoA (2C)
Cit1
Citrate (6C)
CoA
H2O
Aco1
Oxaloacetate (4C)
Kerbs Cycle
NAD+
NADH
Glyoxalate Shunt
Isocitrate (6C)
Malate (4C)
Acetyl-CoA
Succinate
Idh1/4
NAD+
NADH + H+ + CO2
α-ketoglutarate (5C)
Mitochondria
Nitrogen Starvation
HCO3-
Acc1
Malonyl-CoA (3C)
Elongation Cycle
Tsc13
2NADPH
2NADP+
Fas1
Fatty Acid-CoA C16:0 - C18:0
Faa1/4 Fat1
CoA
Fatty Acid C16:0 - C18:0
Fatty Acid-CoA >C20, C16:1 - C18:1
Endoplasmic Reticulum
Squalene
Sterol Biosynthesis Pathway

Figure 2| Overview of the main lipid biosynthesis pathways in *R. toruloides*. A summary of the biosynthetic pathways in yeast, adapted from a combination of figure 2 and figure 3 in Klug and Daum, 2014 and figure 3 in Ratledge, 2014. Nitrogen starvation response is highlighted in purple; abbreviated pathways are shown by dotted arrows and named in orange; POM cycle is indicated by green arrows; enzymes are shown in red and their gene names and functions in *S. cerevisiae* are highlighted in table 1; genes that have been experimentally overexpressed, introduced from foreign organisms or deleted in *R. toruloides* are in a light blue box; co-factors and by-products are labelled in orange text (Gro, glycerol; CoA, coenzyme A); lipid-biosynthesis products and intermediates are shown in black text. Where an enzyme shows activity in more than one organelle then the site where biosynthesis activity is highest is shown. The yellow-bordered area represents lipid droplets; the orange-bordered area represents the mitochondria; the green-bordered area represents the endoplasmic reticulum and the red-bordered white area represents the cell membrane and cytoplasm respectively.

Table 1| Key genes identified in oleaginous eukaryotic lipid biosynthesis.

Enzyme	Gene name
Acc1	Acetyl-CoA Carboxylase
Acl1	ATP citrate lyase
Aco1	Aconitase
Ald1	Cytosolic aldehyde dehydrogenase
App1	Phosphatidate phosphatase
Are1/2	Acyl-CoA:sterol acyltransferase
Ayr1	1-Acyldihydroxyacetone phosphate reductase
Cit1	Citrate synthase
Dga1	Diacylglycerol acyltransferase
Dgk1	Diacylglycerol kinase
Dpp1	Diacylglycerol pyrophosphate phosphatase
Elo1	Elongase I
Faa1	Long chain fatty acyl-CoA synthetase
Faa4	Long chain fatty acyl-CoA synthetase
Fad2	Δ12-fatty acid desaturase
Fad3	ω3 desaturase
Far	Fatty acid reductase
Fat1	Very long chain fatty acyl-CoA synthetase and fatty acid transporter
Fit2	Facilitator of Iron Transport
Gpt1	Glycerol-3-phosphate dehydrogenase
Gpt2	Glycerol-3-phosphate acyl transferase
Idh1/4	Isocitrate dehydrogenase
KCS	3-ketoacyl-CoA synthases
Loa1	Lysophosphatidic acid acyltransferase
Lpp1	Lipid phosphate phosphatase
Lro1	Lecithin cholesterol acyl transferase Related Open reading frame
M. E.	Malic Enzyme
Mdh1	Malate dehydrogenase
P. D. C.	Pyruvate dehydrogenase complex
Pah1	Mg2+-dependent phosphatidate phosphatase
Pdc1	Pyruvate decarboxylase isozyme
Pyc1/2	Pyruvate decarboxylase
Sct1	Suppressor of Choline Transport mutants
Slc1/4	1-acyl-sn-glycerol-3-phosphate acyltransferase
Tgl3	TriacylGlycerol Lipase
Tgl4	TriacylGlycerol Lipase
Tgl5	TriacylGlycerol Lipase
Tsc13	Enoyl reductase
Yju3	Monoglyceride lipase (MGL)

1.1.2. Lipid droplets

Lipid droplets (LDs) are intracellular organelles found ubiquitously in all eukaryotic, most bacterial, and some archaeal cells although their constituent lipid molecule makeup and indeed the names of these organelles are not well conserved; oil bodies, oleosomes, granules, adiposomes, lipid droplets and lipid bodies are all terms used for different taxa. Most bacteria and all archaea synthesise polyhydroxyalkanoates and their derivatives as their main lipid droplet constituents, in contrast eukaryotes (and TAG-biosynthesis capable prokaryotes) synthesise lipid droplets which contain predominantly neutral-lipid TAGs and SEs (Brandl *et al.*, 2005; Murphy, 2012).

First described in the late 19th century, LDs were considered relatively static carbon-storage organelles with a low rate-of-turnover, for much of the 20th century before a rapid acceleration in their study commenced in the 1990s, spurred by their apparent role in mammalian pathologies including atherosclerosis, obesity, dyslipidaemia and cancers (Xu, S. *et al.*, 2018). Now known to be multifaceted dynamic organelles, LDs are implicated not only in lipid storage but also in cell signalling, protein maturation, protein storage, resistance to ER and oxidative stresses by environmental insults, membrane formation, and the storage of vitamins precursors. Lipid droplet dynamics and investigations into these organelles and their intracellular interactions are now a component in most avenues of eukaryotic cellular investigations. However, it is lipid droplet biosynthesis, maintenance, and degradation processes and regulation that are most crucial in the context of *R. toruloides* as a putative oleaginous yeast for biofuel production.

As outlined in section 1.1.1, the terminal location of lipid synthesis is the ER where diacylglycerol phosphate acyl transferases (DGATs) Lro1 and Dga1 are embedded and enriched within the inner and outer leaflets respectively, forming punctate regions of TAGs within a lens. It is then thought that the barrel-shaped seipin homo-oligopeptide scans the ER bi-layer membrane until a protrusion is encountered where neutral lipids have spontaneously accumulated because of the lower free energy cost between TAGs than between TAGs and PL (Liu, X. N. *et al.*, 2016; Sui *et al.*, 2018; Thiam and Forêt, 2016). Through unknown means, this punctate region then anchors and recruits transmembrane lipid phosphatase Fit2 in the ER membrane, which specifically binds to TAGs, and GPATs, which

catalyse the rate limiting step in TAG biosynthesis as shown in Figure 3. It is thought that these proteins both structurally support the inner leaflet of the nascent LD (<200 nm diameter), thereby preventing invaginations of the LD into the ER lumen rather than the cytosol, and also constricting to provide a neck to the LD for regulation and maintenance of the ER/LD interface. In *Drosophila melanogaster* S2 cells, seipin deletion mutants are unable to develop morphologically-normal pre-LDs (300–500 nm diameter) and, instead, remain as relatively mobile puncta in the ER (Liu, X. N. *et al.*, 2016). Additionally, enrichment of negative molecular-curvature glycerolipids is found at the ER/LD interface site and mutations of *FIT2* and deactivation of *PAH1* by deletions of *PAH1* phosphatases *NEM1* and *SPO7*, which dephosphorylate phosphatidic acid to the negative-curvature diacylglycerol lipid, prevent LD emergence; this finding is consistent with computational models of ER/LD tubule development where increased convex lipids lead to spontaneous LD emergence (Choudhary *et al.*, 2018; Garay *et al.*, 2014; Miranda *et al.*, 2014).

As summarised by Schuldiner and Bohnert, (2017a), the mature LD, having a hydrophobic neutral core encapsulated by a PL monolayer, is prevented from 'normal' intracellular shuttling between aqueously-luminal organelles as found in fusion and fission of bilayer organelles. In contrast to mammalian cells, where LDs are able to either entirely disassociate from the ER or maintain contact through ER/LD bridges, mediated through a Rab18-NAG-RINT1-ZW10 (NRZ)-SNARE complex, yeast species maintain contact between the ER and LD at all times (Schuldiner and Bohnert, 2017; Wilfling *et al.*, 2013; Xu, D. *et al.*, 2018). These LD/ER contact sites help prevent ER stress and sequester cytotoxic lipid and proteins in both yeast and mammals that develop during metabolic and environmental stresses. As outlined in section 1.1.1, lipotoxic FAs are sequestered and detoxified to neutral TAGs by DGAT1 in the ER; in cells where LD biogenesis is inhibited an increased sensitivity to toxic lipids can be observed (Klecker *et al.*, 2017; Listenberger *et al.*, 2003; Nguyen *et al.*, 2017). In mammals, LDs have also been implicated in both clearance of non-functional proteins where ubiquitinated apolipoprotein B accumulates and aggregates before degradation by autophagy (Ohsaki, 2006), and in human pathologies where α-synuclein aggregates with LDs in Parkinson's disease (Colebc *et al.*, 2002). Proteotoxic-temperature derived misfolded proteins, similarly, aggregate in yeast, termed

‘inclusion bodies’ (IB). In *S. cerevisiae* these IB were found by Moldavski *et al.*, (2015) to contain 13 resident proteins, of which six are crucial for IB clearance after stress. Having found IB and LD to co-localise during stress (Szymanski *et al.*, 2007), Moldavski *et al.*, (2015) further demonstrated an interaction between the two organelles, facilitated by the IB protein ‘increased minichromosome loss’ (Iml1). Iml1 demonstrates a binding interaction with LD proteins Pet10 (Plin1) and Pdr16, with a preferential binding at 37 °C. The group then suggested a pathway by which the IB was cleared that involved LDs. *Δdga1 Δlro1* double mutants, where LDs are unable to synthesise TAGs, were able to clear the IB but *Δ*are1 *Δ*are2 double mutants, where LDs cannot synthesise sterol esters, cannot. LD-constituent neutral-lipid sterol derivatives may therefore act as a ‘chemical chaperone’ and solubilise hydrophobic interactions between integrated aggregates of IB proteins to facilitate refolding and disaggregation of the aberrant proteins.

Peripilin class proteins, which are able to sterically prevent spontaneous TAG lipolysis by preventing access by cytoplasmic lipases and fusion of established LDs, also associate to the LD outer leaflet from the cytoplasm; in yeast, the *S. cerevisiae* protein peripilin Plin1 quickly co-accumulates nascent-LDs. In common with other peripilin homologues in mammals and plants, the peripilin is thought to help anchor the PL-monolayer to the neutral-lipid core (Gao *et al.*, 2017). Peripilins may also help facilitate vectorial ER-membrane deformation towards the cytoplasm (Henne *et al.*, 2018a) because of the capacity of Plin1 mammalian-homologue Plin3 to spontaneously reorganise liposome membranes, similar to apolipoproteins (Bulankina *et al.*, 2009).

As carbon source concentrations reduce in the yeast medium, *S. cerevisiae* LDs associate with the nucleus, where Pah1 proteins also begin to accumulate. As such, during a diauxic shift, the TAG precursor diacylglycerol is increasingly synthesised, coinciding with the yeast starvation response of increased lipid droplet size (Schuldiner and Bohnert, 2017). However, as the yeast moves towards its starvation response, LDs disassociate from the nucleus and localise to sterol-rich lipid rafts on the vacuole; if starvation continues the LDs become engulfed by the vacuole and macrolipophagy occurs as TAGs are catabolised to FFAs (van Zutphen *et al.*, 2014). Additionally, FFAs can be liberated from TAG storage molecules through the activities of TAG lipases Tpl3, Tpl4, and Tpl5;

which are localised to LD outer membranes (Athenstaedt and Daum, 2003). Curiously, Tpl3 function is confounded by both a lipase and lysophosphatidic acid acylation function, though this is likely to assist with membrane stability (Rajakumari and Daum, 2010).

In *S. cerevisiae*, Atg8 protein can also be recruited to degrade lipid for FFA recycling. This occurs through microautophagy, although the direct mechanism for this process is yet to be elucidated. Briefly, Atg8 recruits additional Atg proteins to form a *de novo* preautophagosomal structure (PAS) which associates with peripilin-family proteins, the PLINs. This structure then appears to sequester and engulf small LD volumes in a piecemeal fashion (Schulze *et al.*, 2017; van Zutphen *et al.*, 2014).

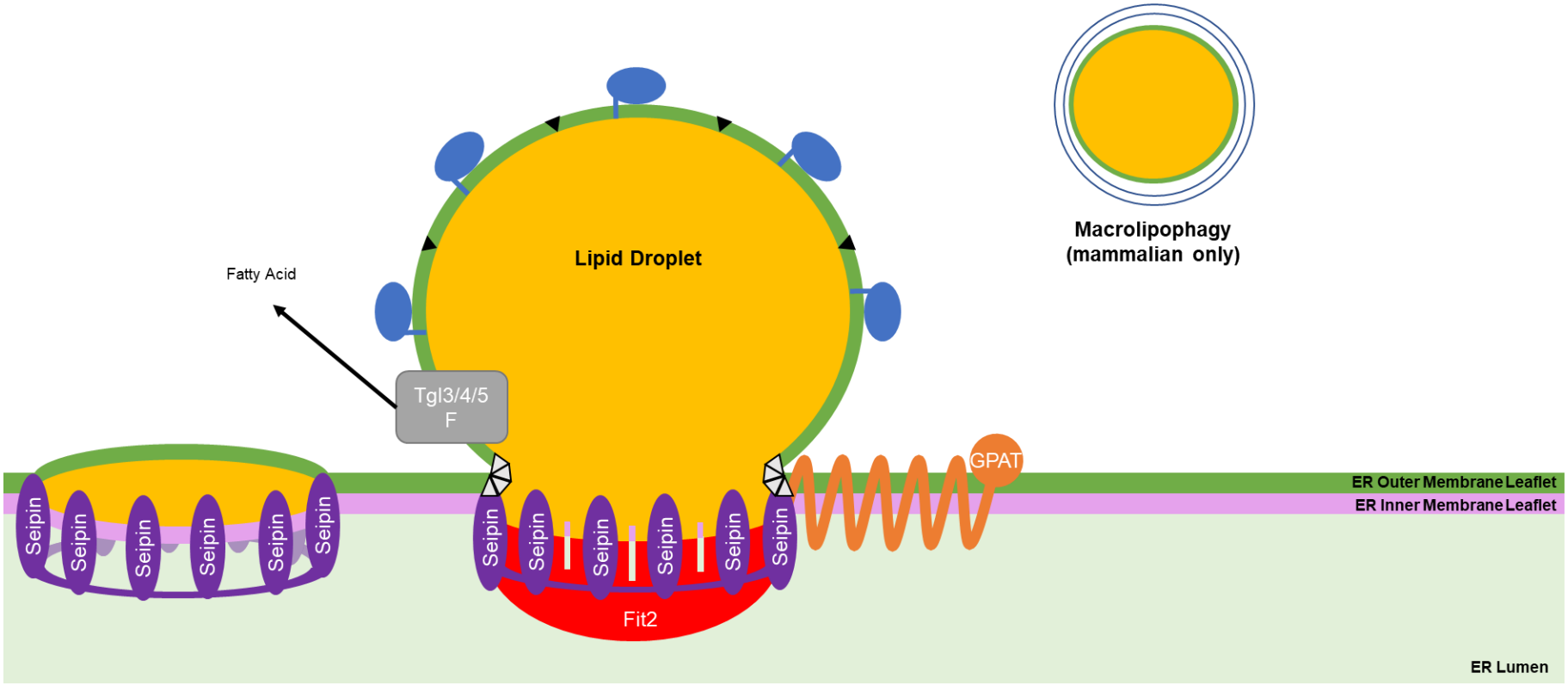

Figure 3| Model of yeast lipid droplet formation and maintenance. Initially, seipin oligopeptides scan the ER leaflets for a membrane disruption and deformation as neutral lipid accumulations form an intra-membrane lens. This then stabilises and anchors the LD in place, and recruits proteins associated with TAG and negative-curvature phospholipid-membrane biosynthesis, as indicated by grey triangles; positive-curvature phospholipids are represented in black triangles. Additionally, lipid droplets are protected from spontaneous lipolysis by sterically inhibiting peripilins, represented by blue circle with membrane-embedded tails. Mammalian macrolipophagy, whereby Atg8/LC3 protein in mammals nucleates and develops a double-membrane autophagosome, envelopes whole LDs and targets them for lipophagy-lipid recycling as lysosomes fuse to the nascent autophagolysosome. Figure is a compilation of many figures including (Gao *et al.*, 2017; Liu, X. N. *et al.*, 2016; Sui *et al.*, 2018; Sztalryd and Brasaemle, 2017; Szymanski *et al.*, 2007).

1.2. Heat shock promoters

A significant amount of work has recently been undertaken to improve and increase the genetic tools available for *R. toruloides* strains.

To date, the unreproducible method of stably introducing desired DNA constructs into the yeast through polyethylene glycol-facilitated protoplast transformation (Tully and Gilbert, 1985) has been superseded by *Agrobacterium tumefaciens*-mediated transformation (ATMT) (Johns *et al.*, 2016; Lin *et al.*, 2014; Liu, Y. *et al.*, 2013). Recent studies have also reported the successful use of electroporation and lithium acetate-mediated transformation (it may be noted, however, that I have been unable to replicate the findings of Lui *et al*., 2017, data not shown) (Liu, H. *et al.*, 2017; Otoupal *et al.*, 2019; Takahashi *et al.*, 2014; Tsai *et al.*, 2017). Endogenous gene knockouts have also recently been reported in *R. toruloides* strains: Koh *et al.*, (2014) achieved disruption of the *CAR2* gene in a *Δku70 R. toruloides* ATCC 10657 strain through the use of homologous gene flanking sequences and ATMT; *R. toruloides* DMKU3-TK16 *URA3* was successfully disrupted using an optimised lithium acetate-mediated transformation by Tsai *et al.*, (2017); and single and multiplex disruption of both *URA3* and *CAR2* genes were achieved in *R. toruloides* IFO 0880 (ATCC 10657) by CRISPR, with an editing efficiency of 3.4 % ±2.7 % to 46.2 % ±22.2 % for each of the genes respectively (Otoupal *et al.*, 2019).

The genetic toolkit in *R. toruloides* also consists of eight identified native constitutive promoters (Liu, Y. *et al.*, 2013, 2016; Wang, Y., Lin, *et al.*, 2016), one heterologous promoter from the basidiomycete *Ustilago maydis* (Liu, Y. *et al.*, 2018), with a further seven native inducible promoters, inducible or repressible under nutrient-limited conditions, having been characterised (Johns *et al.*, 2016; Liu, Y. *et al.*, 2015). However, these inducible promoters are limited in their applications in a commercial setting for synthesis of specialty chemicals where either the feed is not fully controllable (as in production of lipid and lipid-derived compounds from low-cost substrates as summarised by Xu and Liu, 2017) or where limiting the growth medium to induce promoter-driven requisite genes may cause disadvantageous metabolic remodelling (Broach, 2012; Cai *et al.*, 2011; Dechant and Peter, 2008; Klosinska *et al.*, 2011). Consequently, there is a need

for identification and development of strong, tightly controlled inducible promoters not dependent on media chemical-makeup to fulfil this biotechnological role.

One such candidate for gene induction is the environmental stress response (ESR) in yeast, where the yeast genome expression profile is dramatically altered to resist and accommodate potentially damaging physiological conditions by modulating metabolic and biosynthetic pathways. Gasch *et al.* (2000) found approximately 900 genes whose transcription levels were rapidly and significantly decreased (repressed) or increased (induced) in response to a variety of ESRs; a flurry of microarray studies in the early 2000s of global expression profiles under various environmental stresses included: temperature shocks (Causton *et al.*, 2001; Gasch, A. P. *et al.*, 2000); oxidative stresses (Gasch, A. P. *et al.*, 2000); ethanol shocks (Alexandre *et al.*, 2001); starvation of amino acids, nitrogen, in stationary phase (Gasch, A. P. *et al.*, 2000); and diauxic shifts (Gasch, A. P. *et al.*, 2000), amongst others. While some genes were almost universally either up- or down-regulated after environmental stress, it was apparent that an environmental assault does not alter all genes' transcription equally or consistently after differing assaults.

The ESR is orchestrated through a plethora of specific and general transcription factors which can antagonistically or concomitantly affect global mRNA transcription levels of *cis*-regulated proteins. The mechanisms of these transcription factors are highly conserved throughout the eukaryotes, and indeed the DNA-binding domain of key eukaryotic heat-shock factor Hsf1 with bacterial heat-shock sigma factor σ^{32} which facilitates RNA polymerase binding and transcription in bacteria (Trott and Morano, 2007). After an environmental assault, transient genetic remodelling occurs with an average relative-mRNA level shift reaching 100 % after 2-5 minutes, and reaching peak expression after 15 minutes (Causton *et al.*, 2001). In the 900 genes in *S. cerevisiae* affected by the ESR, the physiological changes can be attributed primarily to an alteration in gene expression of proteins controlling carbohydrate metabolism, oxidative stresses, protein folding and targeted degradation, autophagy, cytoskeletal rearrangement and intracellular signalling to mitigate the cytotoxic effects of the environment the cell suddenly encounters.

After an assault by many different conditions, the carbohydrate composition of yeast cells is rapidly altered. Originally thought to exist primarily in spores, trehalose, the disaccharide (α-D-glucopyranosyl-1,1-α-D-glucopyranoside), changes composition from 6.53 to 13.66 mg g^{-1} dry weight, and there is an alteration of 40.0 to 52.0 mg g^{-1} in total fatty acid, after a heat shock from 21 °C to 37 °C for 60 minutes in *S. cerevisiae* 3001 (Ballio *et al.*, 1964; Odumeru *et al.*, 1993; Shi, L. *et al.*, 2010). This trehalose carbohydrate has been implicated in cellular protection in many ways. Principally, trehalose has been shown to quench oxygen radicals which become overrepresented in heat-shocked cells (Benaroudj *et al.*, 2001; Weng and Elliott, 2015), a function critical to cell viability as an overabundance of reactive oxygen species (ROS) leads to protein crosslinking and fragmentation as protein backbones are oxidised (Berlett and Stadtman, 1997), phospholipid membrane and lipid-signalling damage through peroxidation (Ayala *et al.*, 2014), and macromolecular sugars alteration (including DNA-backbone damage) (Rowe *et al.*, 2008). Mutants of the trehalose-subunit synthase genes *TPS1* and *TPS2* lose their thermotolerance (De Virgilio *et al.*, 1994), a phenotype which can be rescued by supplemental extracellular trehalose introduction. In addition to these antioxidant properties, trehalose also prevents cytotoxic protein accumulation from heat shock-induced peptide misfolding and maintains protein activity when cells where trehalose is depleted are non-functioning, although the mechanism of this thermo-stabilisation appears to be multifaceted and is not yet fully elucidated (Benaroudj *et al.*, 2001; De Virgilio *et al.*, 1994; Singer and Lindquist, 1998; Sola-Penna *et al.*, 1997). Curiously, trehalose synthase genes *TPS1* and *TPS2*, and the neutral trehalose degradation gene *NTH1*, are all co-induced by the ESR. However, during heat shock at 40 °C, *S. cerevisiae* S288c trehalase is phosphorylated and deactivated whereas the trehalose synthases become three times more active at this temperature compared to 25 °C, implying that protein kinetics also affects the physiological ESR (Neves and François, 1992). In *R. toruloides* strain CBS 14, Evans and Ratledge (1984b) found 6.2-6.5 % of dry biomass is trehalose when cultured in nitrogen-limited medium containing 30 g L^{-1} glucose.

In the same way that an increase in temperature can cause an increase in trehalose synthase activity, a heat shock assault will alter the protein kinetics and conformational and interactive properties of all unprotected proteins and

enzymes within a cell. Non-functional protein conformers can be produced where environmental stress causes intermediate misfolded-peptides which are unable to escape their free-energy minima (Jahn and Radford, 2005). In such conformations toxic misfolded proteins often expose hydrophobic surfaces normally hidden in a protein hydrophobic core and co-aggregate (Vabulas *et al.*, 2010), before either refolded or becoming ubquinated and terminally-aggregated; aberrant proteins are then actively sequestered in inclusion bodies and targeted for degradation (Ohsaki, 2006; Tyedmers *et al.*, 2010). Lipid droplets are also implicated in detoxifying inclusion bodies through a sterol derivative, as outlined in section 1.1.2.

In addition to the carbohydrate remodelling touched on above, where trehalose is capable of detoxifying or sequestering some of the increased ROS from intra- and extracellular sources found in an environmental assault, genes encoding proteins specifically for this role are upregulated in *S. cerevisiae*. With this purpose the protein-coding genes of thioredoxin (*TRX2*), glutaredoxin (*TTR1*) and glutathionine (*ECM38*) isozymes (oxidoreductases maintain the internal oxidative and reductive-molecule homeostasis in yeast through reduction of NADPH) (Grant, 2001), antioxidants (*PRX1*), and cytosolic superoxide dismutase (*SOD1*) are upregulated (Ayer *et al.*, 2014; Causton *et al.*, 2001; Gasch, A. P. *et al.*, 2000; Gasch, Audrey P., 2007); these help prevent unmanageable oxidation of yeast macromolecules and subsequent cell death. Furthermore, lipid droplets have been associated with protection against cytotoxic ROS by sequestering the lipophilic radicals (Herms *et al.*, 2013). *In vivo*, *Drosophila melanogaster* glial cells induce LD accumulation during ROS insult, and correspondingly reduce LD accumulation during low ROS, possibly implying an inducible protective effect of LD against ROS (Liu, L. *et al.*, 2015).

These ESRs to heat shock are modulated by the conserved Msn2/4 general stress response and in invertebrate animals and yeast the transcriptional activator Hsf1; in mammals there are four HSF family members (Åkerfelt *et al.*, 2010). Ascomycete *S. cerevisiae* Msn2 and Msn4 transcription factors contain a zinc-finger domain which bind to the highly conserved stress response element (STRE) CCCCCT (Schmitt and McEntee, 1996; Underhill, 2012) which, upon an environmental assault, rapidly translocates from the cytoplasm to the nucleus (Görner *et al.*, 1998). Msn2 protein relocations to the nucleus are mediated by

hyperphosphorylation of a 250-residue sequence and subsequent disassociation from the 14-3-3 family cytosolic adapter protein Bmh2 (Beck and Hall, 1999; Boy-Marcotte *et al.*, 2006) where several hundred are down-regulated and 100-200 genes are up-regulated respectively through the binding of the cis-acting STRE sequence (Causton *et al.*, 2001; Gasch, A. P. *et al.*, 2000). Msn2 and Msn4 activity is then attenuated by either nuclear proteasomal degradation or returning to the cytoplasm, primarily through the Msn5 nuclear exportin (Bose *et al.*, 2005; Chi *et al.*, 2001; Durchschlag *et al.*, 2004).

Yeast heat shock factor 1 (Hsf1) differs from the metazoan homologue in that it constitutively remains as a DNA-bound trimer (metazoans undergo a monomer-to-trimer transition when activated), having bound to stress response elements (STE) prior to an environmental assault (Gross *et al.*, 1990). Upon heat shock, however, this basally constitutive trimer transcriptional activity increases ~20 fold as adjacent HSF trimers appear to complex together to “unmask” activator domains and complex together as they are post-translationally phosphorylated (Lee *et al.*, 2000). Additionally, an accumulation of denatured proteins, derived from heat shock assault as described above, can indirectly activate yeast Hsf1 (Moraitis and Curran, 2004; Parsell and Lindquist, 2003; Trotter *et al.*, 2002). There appears to be an intrinsic interplay between both the general stress response and the heat-specific stress responses, where many HSP gene promoters contain both STREs and STEs (Amorós and Estruch, 2001).

1.3. Project aims

R. toruloides is an oleaginous yeast with potential use as a biotechnological chassis for production of biofuel and lipid droplet-derived products such as bio-lubricants, bio-plastics and pharmaceutically relevant lipids as outlined in sections 1.1 and 1.2. However, before the yeast can be used to synthesise these desired products, further genetic tools and a greater understanding of the underlying mechanisms of lipid accumulation must be realised. To this end, this project aims to develop and begin characterisation of genetic tools for controlled induction in undefined media, through heat-shock inducible promoters, and develop tools to facilitate further investigations into lipid droplet assembly and accumulation through live-cell imaging of relevant organelles.

2. Materials and Methods

2.1. Strains and growth conditions

2.1.1. Rhodotorula toruloides

Wild-type haploid *R. toruloides* CBS 14 (MAT-A1; ATCC 10788; ATCC 15385; CCRC 20306; DBVPG 6740; IAM 13469; IFO 0559 ;IGC 4416; JCM 3792; MUCL 30249; NCYC 921; NRRL Y-1091; VKM Y-334; PYCC 4416) (BANNO, 2008; Rennerfelt, 1937) was acquired from the Westerdijk Fungal Biodiversity Institute (formerly the Centraalbureau vor Schimmelcultures).

R. toruloides was grown: initially at 25 °C in 6.9 g L^{-1} Yeast Nitrogen Base without Amino Acids (YNB) (Formedium, Hunstanton) with 790 mg L^{-1} Complete Supplement Mix (CSM) (Formedium, Hunstanton) and 20 g L^{-1} glucose before temporary heat shock at 37 °C; constitutively in YNB and CSM with a glucose concentration of 0 g L^{-1} to 20 g L^{-1} during glucose starvation studies; or as described in Zhu *et al.*, (2012) on Minimal Media with Nitrogen (MM+N) (25 g L^{-1} glucose, 0.5 g L^{-1} $MgSO_4 \cdot 7H_2O$, 3 g L^{-1} KH_2PO_4 and 5 g L^{-1} $(NH_4)_2SO_4$ pH 5.6) or Minimal Media without Nitrogen (MM-N) (25 g L^{-1} glucose, 0.5 g L^{-1} $MgSO_4 \cdot 7H_2O$, 3 g L^{-1} KH_2PO_4, 6.3 g L^{-1} K_2SO_4 and 0.2 g L^{-1} $(NH_4)_2SO_4$ pH 5.6).

2.1.2. Bacteria

Escherichia coli DH5α was used for plasmid amplification and grown in Lysogeny Broth (LB) ('LB (Luria-Bertani) liquid medium', 2006) where transformants were selected for on LB supplemented with kanamycin (50 µg mL^{-1}) at 37 °C.

Agrobacterium tumefaciens strain GV3101 (Van Larebeke *et al.*, 1974) was constitutively grown at 28 °C in LB with 100 µg mL^{-1} rifampicin and 50 µg mL^{-1} gentamycin with transformants selected for and maintained with an additional 50 µg mL^{-1} kanamycin .

2.1.3. Saccharomyces cerevisiae

S. cerevisiae BY4742 (Y10000; S288C isogenic yeast strain MATα his3Δ1 leu2Δ0 lys2Δ0 ura3Δ0) (Brachmann *et al.*, 1998; Winston *et al.*, 1995) was used to perform in yeast plasmid assembly. It was ordinarily grown in YPD at 30 °C; transformants were autotrophically selected for on 6.9 g L^{-1} YNB supplemented with 770 mg L^{-1} CSM without uracil (Formedium, Hunstanton).

2.2. Bioinformatics

2.2.1. *R. toruloides* homologous gene identification

R. toruloides homologues of desired *S. cerevisiae* S288C genes identified in the '*Saccharomyces* Genome Database' (Cherry *et al.*, 2012; Mortimer and Johnston, 1986) were identified using BLASTN searches against the annotated *R. toruloides* NP11 genome (assembly accession GCA_000320785.2) in Ensembl Fungi (Zerbino *et al.*, 2018; Zhu *et al.*, 2012).1200 bp upstream of the identified *R. toruloides* homologues were then used as the respective gene promoters.

2.2.2. Codon Optimisation

Codon optimisation was performed using Codon Optimization OnLine (COOL) (Chin *et al.*, 2014) where codon-usage from genome-wide usage patterns was derived from *R. toruloides* strain IFO 0559 (accession GCA_000988805.1). Putative 5′ splice sites (A Johns pers. comm.) located within designed constructs were manually removed and alternative codons utilised.

2.3. Plasmid construction

2.3.1. *R. toruloides* genomic DNA extraction

DNA was extracted from *R. toruloides* using an adapted phenol: chloroform method from Sambrook and Russell (2001) for yeast colonies on plates, adapted where MP Biomedicals Matrix A lysing beads (Santa Ana, CA) were used in a MP Biomedicals FastPrep-24 (Santa Ana, CA) instead of vortexing. DNA was recovered by ethanol precipitation and resuspended in TE (pH 7.6) as described by Sambrook and Russell (2001).

2.3.2. Amplification of DNA

Fragments of DNA used for cloning were amplified through PCR using Q5 DNA polymerase (NEB, Ipswich MA) and purified using a Thermo Fisher Scientific GeneJet PCR Purification Kit (Waltham, MA); during colony PCRs to verify presence of DNA within assembled plasmids PCR was achieved using *Taq* Polymerase in Standard Buffer (NEB, Ipswich MA); in both cases oligonucleotides were synthesised by Eurofins (Ebersberg).

2.3.3. Restriction digestion

Restriction digests were performed using restriction endonucleases purchased from either NEB (NEB, Ipswich) or Thermo Fisher Scientific (Waltham, MA) as

denoted in Table 2. Cloning fragments were then purified using a Thermo Fisher Scientific GeneJet PCR Purification Kit (Waltham, MA).

Table 2| Restriction endonucleases used

Enzyme	Manufacturer
***Bam*HI Fast Digest**	Thermo Fisher Scientific
***Pml*I-HF**	New England Biolabs
***Spe*I-HF**	New England Biolabs
***Afl*II-HF**	New England Biolabs

2.3.4. Plasmid recovery from micro-organisms

Plasmid constructs were isolated from *E. coli* using Thermo Fisher Scientific GeneJet plasmid miniprep kit, following the manufacturer's protocol (Waltham, MA). *S. cerevisiae* plasmids were isolated and purified through Zymolase assisted alkaline lysis using Zymoprep Yeast Plasmid Miniprep II kit following the manufacturer's protocol for single-picked colony plasmid extraction (Irvine, CA).

2.3.5. DNA gel electrophoresis

All DNA fragments were visualised in 2 % agarose gels (Melford) with Invitrogen Sybr Safe DNA stain (Thermo Fisher Scientific, Waltham, MA) unless otherwise specified. DNA bands were separated using electrophoresis at 100 V for approximately 60 minutes, until desired gel bands could be resolved. Gels were visualised through UV transillumination.

2.3.6. Bacterial transformation

E. coli DH5α was transformed using a modified protocol from Glover (1985). Competent cells were prepared by pelleting OD_{600} 0.4 mid-log *E. coli* before: washing in TF-1 (7.4 g L^{-1} KCl, 2.95 g L^{-1} CH_3COOH 1.5 g L^{-1} $CaCl_2.2H_2O$, 150 g L^{-1} glycerol, 0.2 M $MnCl_2$); cooling for 15 minutes on ice; resuspension in TF-2 (0.74 g L^{-1} KCl, 11 g L^{-1} $CaCl_2.2H_2O$, 150 g L^{-1} glycerol, 0.01 M MOPS buffer pH 6.8) and snap freezing in liquid nitrogen. Competent cells were transformed with desired plasmid constructs by: thawing on ice; addition of 1-5 µg DNA; incubation on ice for 40 minutes; 2 minutes of heat shock at 42 °C; 5 minutes of incubation on ice; 60 minutes of recovery in 37 °C LB shaken at 200

RPM; plating on 1.5 % w/vol LB agar with 50 µg mL^{-1} kanamycin; and incubation overnight at 37 °C.

A. tumefaciens GV3101 was prepared and transformed as described by Holsters *et al.*, (1978).

2.3.7. *S. cerevisiae* transformation

Yeast Recombination-Based Cloning (YRBC) was performed using a modified protocol from Kilaru and Steinberg, (2015) as DNA fragments with 40 bp end-regions homology, at a 2:1 fragment to base construct molar ratio, were co-transformed. Transformants were selected for on 3 % YNB agar supplemented with CSM without uracil.

Table 3| Primers used for DNA amplification to allow organelle visualisation in *R. toruloides*

Primer	Function	Sequence
Atg8_YRBC| F	YRBC	*atcaccctcggcatggacgagctctacaag*GGCGGCGGAGGAGGGGGCATGGTCCGCTCAAAGTTCAAGGA
Atg8_YRBC| R	YRBC	*gggaactactcacacattattatggagaaaactagt*TCATGCAGCGCCGAAGG
Cal_YRBC| F	YRBC	*aactcacccgtccaactcccaccctcccacgtgcagcccacc*ATGCAGTCCAGTGCGCAATC
Cal_YRBC| R	YRBC	*ctcctcgcccttcgagaccggatccgccat*GCCCCCTCCTCCGCCGCCCGAGCTCTCCTCCTTCTGCTT
Ldp1_YRBC| F	YRBC	*aactcacccgtccaactcccaccctcccacgtgcagcccacc*ATGGCCACCGTCAACGAGAA
Ldp1_YRBC| R	YRBC	*ctcctcgcccttcgagaccggatccgccat*GCCCCCTCCTCCGCCGCCCTGCTTCTCCCCCTCGC
Atg8 DS Check | F	Junction	CTCCCTCCGACCGCGG
Atg8 US Check | R	Junction	CTGCCTCTGCCTTGCGCTTC
CMV35 DS Check| R	Junction	TGCAAGCTTTAAGAGGAGTCCACCATGG
Calnexin DS Check| F	Junction	CCTCGTTCTCCCCGCCG
Calnexin US Check| R	Junction	GCAGCAGTGCGTAGCGCAT
Ldp1 US Check| R	Junction	TCTTTGATCACGGGGTAGTCGAGCG
Ldp1 DS Check| R	Junction	GCTGCGGACCACATTCGCAAG
PGK US Check| F	Junction	CGTTGAACTTGCACTTCTCACTCGCACT
EGFP US Check | F	Junction	CCACTACCTCTCGACCCAGTCGG
EGFP DS Check | R	Junction	TGCTTCATGTGGTCCGGGTAGC

Lowercase orange italic letters signify homologous recombination regions, uppercase italic blue letters represent coding sequences for 6x glycine ‘linker’ sequences, and black uppercase lettering depicts specific bases for PCR amplification. All primers are written from 5′ to 3′.

Table 4| Primers for HSPP fragment PCR.

Primer Name	Primer sequence
01-FL| F	*atcatcgcaagaccggcaacaggattcaat*CTGCAACCTCCTCGCCTCGCTCG
01-IG| F	*atcatcgcaagaccggcaacaggattcaat*CCTGCAGTGCACTCTGTTGCTCGT
01| R	*ctcctcgcccttcgagaccggatccgccat*GGTGGGCTGCACGGGGGAGG
02-FL| F	*atcatcgcaagaccggcaacaggattcaat*GTCGGCAGTCCTGACCGCC
02-IG| F	*atcatcgcaagaccggcaacaggattcaat*GATGGCGAGTCTCGTTGAGAGA
12| R	*ctcctcgcccttcgagaccggatccgccat*GCTGTGAGATGGGCACCGC
03-IG| F	*atcatcgcaagaccggcaacaggattcaat*TTGTCCACCGCACGCTTGAG
03-NC| F	*atcatcgcaagaccggcaacaggattcaat*CGTAGCGAGTTCGGCAGTGA
03| R	*ctcctcgcccttcgagaccggatccgccat*GGCGTCCCTGGAGAGTAGCC
04-FL| F	*atcatcgcaagaccggcaacaggattcaat*TATGCACGCTGAAAACGGCTCG
04-IG| F	*atcatcgcaagaccggcaacaggattcaat*TCGCTCCCGCTGCGAGTC
04| R	*ctcctcgcccttcgagaccggatccgccat*GGTTGCTTAGGTGCGGATAGGTG
05-FL| F	*atcatcgcaagaccggcaacaggattcaat*CACACCCGTTGGCGGCCTC
05-IG| F	*atcatcgcaagaccggcaacaggattcaat*TCCGACCGACGAACAGCTCC
05| R	*ctcctcgcccttcgagaccggatccgccat*TGTTCAAGCTGGTCGAGAAAAGCG
06-FL| F	*atcatcgcaagaccggcaacaggattcaat*CTGCAGCTACGCCGTGTTCC
06-IG| F	*atcatcgcaagaccggcaacaggattcaat*GGAGGAAGATTCGCATTGTACCGC
06| R	*ctcctcgcccttcgagaccggatccgccat*GTCGAGGTGGAGCTGCTGGA
07-FL| F	*atcatcgcaagaccggcaacaggattcaat*TGGTTGGGTCGCTGAGGAACA
07-IG| F	*atcatcgcaagaccggcaacaggattcaat*ATGTAGACGCACCTCCTCCAGC
07| R	*ctcctcgcccttcgagaccggatccgccat*TGTAGCTAGTTAGTGTTAGAAGTGA
08-FL| F	*atcatcgcaagaccggcaacaggattcaat*GTCGGATGCGGAGGGGCC
08-IG| F	*atcatcgcaagaccggcaacaggattcaat*GGCGGTGAGATGCTAGCTTGC
08| R	*ctcctcgcccttcgagaccggatccgccat*GGCTGCAGCAGTCTGTGCTG
09-FL| F	*atcatcgcaagaccggcaacaggattcaat*CCCGGACAACGACGGCATC
09-IG| F	*atcatcgcaagaccggcaacaggattcaat*CTTGACGGGCATTGTACTCGCC
09| R	*ctcctcgcccttcgagaccggatccgccat*CGTGGGCAGCTGGACTTGTA
10-FL| F	*atcatcgcaagaccggcaacaggattcaat*ATCTTGCCCGCGCTTTGCG
10-IG| F	*atcatcgcaagaccggcaacaggattcaat*CGGGGCGGACAGACGCCAG
10| R	*ctcctcgcccttcgagaccggatccgccat*CCCTCCCGCACGCGCGTC
11-IG	*atcatcgcaagaccggcaacaggattcaat*GTGCCTTTCTCTGCGTCTGTCG
11-FL| F	*atcatcgcaagaccggcaacaggattcaat*TCACGGTAGTCTCGAGGCGG
11| R	*ctcctcgcccttcgagaccggatccgccat*TGTGAGTGACTGGGTGGGTAACG
12-FL| F	*atcatcgcaagaccggcaacaggattcaat*GGGTGAGGTGCTGTTAGTGA
12-IG| F	*atcatcgcaagaccggcaacaggattcaat*TTGCCCATCCTTGCAACTCACA
12| R	*ctcctcgcccttcgagaccggatccgccat*TGTGACTGATCTGGTGTTGTTCTGA
13-FL| F	*atcatcgcaagaccggcaacaggattcaat*AAAAGAAAGGCGGAGTCGAGGA
13-IG| F	*atcatcgcaagaccggcaacaggattcaat*GACAGGCGGCTGGCGCAAG
13| R	*ctcctcgcccttcgagaccggatccgccat*CTCGTACTACTGTGCTGCGGC

R. toruloides HSPP primers ('FL' is Fixed Length 1200 bp, 'IG' is Intergenic') and then directionality of the primer ('F' is 'Forwards', 'R' is 'Reverse). Primer sequences show homology regions to the base plasmid pEGFP-Rt-YR-Hyg in lowercase coloured italics and uppercase lettering depicts specific bases for PCR amplification.

2.4. Transformation of *R. toruloides*

R. toruloides transformation was informed by methods described by Johns *et al.* (2016) for transformation of *R. toruloides* and a protocol for *Zymoseptoria tritici* transformation (Nic Hemstetter pers. comm.), giving a transformation efficiency at least x200 above that described by Johns, Love and Aves (2016). *A. tumefaciens* containing the desired transformation cassette was grown to stationary phase in LB supplemented with *A. tumefaciens* virulence plasmid maintenance antibiotics rifampicin (100 μg mL^{-1}) and gentamycin (50 μg mL^{-1}) and plasmid selection antibiotic kanamycin (50 μg mL^{-1}) at 28 °C for 36 hours. This was then diluted to an OD_{600} of 0.10 in induction medium (10 mM K_2HPO_4, 10 mM KH_2PO_4, 2.5 mM NaCl, 2mM $MgSO_4$, 0.7 mM $CaCl_2$, 10 μM $FeSO_4$, 4mM $(NH_4)SO_4$, 10 mM glucose, 40 mM 2-(N-morpholino) ethanesulphonic acid, 0.5 % w/vol glycerol adjusted to pH 5.6 with NaOH or phosphoric acid), supplemented with 200 μM acetosyrongone, 50 μg mL^{-1} rifampicin, 25 μg mL^{-1} gentamycin and 25 μg mL^{-1} kanamycin and incubated for approximately 6 hours until OD_{600} = 0.2. 500 μL *A. tumefaciens* and 500 μL mid-to-late log phase *R. toruloides* were mixed and spread over 325 P Clear Cellulose Film Discs (A. A. Packaging Limited, Lancashire, UK), placed on induction medium (as described previously, with 2 % agar) and incubated at 28 °C for 36 hours, until a pink colour began to develop. These cellulose membranes are then transferred to a YPD agar, supplemented with 150 μg mL^{-1} cefotaxime and 50 μg mL^{-1} hygromycin, incubated for 36-48 hours, and single colonies were restreaked to fresh YPD containing selective antibiotics and incubated for a further 36-48 hours for colonies to form.

2.5. CARS/SRS

Simultaneous Coherent Anti-Stokes Raman Spectroscopy (CARS) and Spontaneous Raman Spectroscopy (SRS) were performed exactly as described by Wang, *et al.*, (2018), except with a tuned Raman active mode of 2845 cm^{-1}.

2.6. Confocal microscopy

R. toruloides cells were cultured in their requisite media before immobilisation by 1:9 dilution in 15 % low melting temperature agarose (Melford, Suffolk, UK). Fluorophores were excited using a 488 nm OPSL 488 laser (Coherent Inc., Santa Clara, CA) and their fluorescence emission recorded using GFP channel filter (HyD 500-535 nm); autofluorescence channel setting (HyD 650-700 nm); and a brightfield image (PMT) in

a Leica TCS SP8 confocal laser scanning microscope (Wetzlar, Germany). The Leica was equipped with an HC PL APO 100x/1.44 oil objective at a scan speed of 200 Hz.

2.7. Quantification of lipid droplets in confocal fluorescence images

Side-profile *R. toruloides* cells were manually selected and their images recorded as described in 2.6.

Volumes of cells were ascertained using a custom ImageJ macro utilising plugins available in Fiji and a custom Python script (Oliphant, 2010; Schindelin *et al.*, 2012). Briefly, as described in Figure 4, the cell edge was selected using an appropriate brightfield slice using 4-way connectedness of similar pixel values; this cellular outline was then fitted to an ellipse to find major and minor axis angles and lengths and the original cell outline rotated about the angle of the major axis. The x and y co-ordinates for this rotated cell outline were then passed to a custom Python script to find maximum and minimum values for each y value along the x axis (to remove small artefacts in the area where connectedness had introduced invaginations of the cell profile), and the distance between the two termed the 'slice height'. The volume for each x 'slice' was determined by multiplying each 'slice height' by the pixel height, pixel width and pi; the series of summed slices, projected about the x-axis, is equal to the calculated cell volume.

Volumes of lipid were calculated again using Fiji (Schindelin *et al.*, 2012). Briefly, the GFP channel was despeckled to reduce noise and Gaussian blurred. The resultant image was auto-thresholded using the Renyi entropy algorithm (Narayana *et al.*, 2012) before volumes of each fluorescent body were calculated using the plugin '3D Objected Counter' (Bolte and Cordelières, 2006).

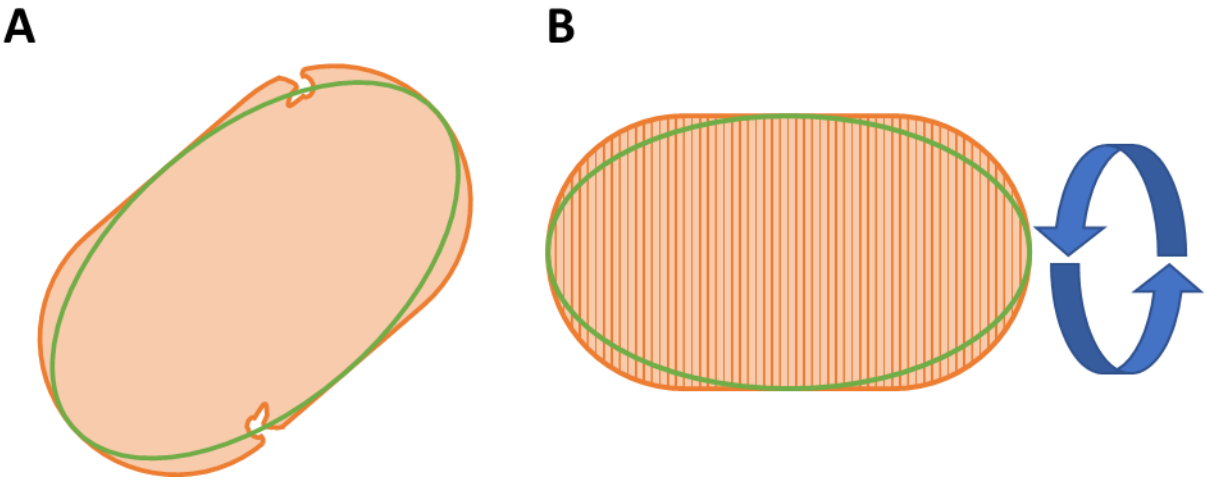

Figure 4| Ascertaining cell volume using a brightfield image. (A) A cell-outline was found from the middle slice of a side-profile cell (dark orange) and an ellipse fitted to this shape (green). The cell side-profile was then rotated to fit an x-axis aligned profile and invaginations of the cell outline (exaggerated in figure) accounted for and corrected, as in **(B)**. Each X pixel 'slice' was then projected about 360° to find volumes for each slice before each x-slice was summed.

2.8. Quantification of yeast growth rate and lipid droplet responses to different media

R. toruloides Ldp1-GFP was precultured to stationary phase in YNB + CSM with 20 g L^{-1} for 72 hours before: a single wash and dilution to OD_{600} 0.2 in Minimal Media without Nitrogen (0 g L^{-1}); and then diluted 1:99 in Minimal Media without Nitrogen supplemented with 0, 5, 10, 15, 20, or 25 g L^{-1} glucose; all incubations occurred at 30 °C.

1000 µL cultures were then loaded into a 4titude Vision 24 Plate and incubated at 500 RPM double orbital shaking, 30 °C for 72 hours in a BMG ClarioStar plate reader (Buckinghamshire, UK). Absorbance and GFP were measured every 10 minutes; for each well both values were determined using 20 orbital flashes $well^{-1}$; average well absorbance values were path-length corrected to 1 cm and GFP was measured using 428+14 nm excitation and 530+30 nm notch filters.

After 72 hours, cells were visualised in an Amnis ImageStream X Mark II Imaging Flow Cytometer (Brooks Life Science, Chelmsford, CA) through brightfield and detected fluorescence at 488 nm. Side profile cells were found by first gating a subpopulation of sharp-focused cells using brightfield intensity gradient (gradient relative mean squared 53.96 - 84.35) , then gating a brightfield Aspect Ratio: Area slice from approximately 22:0.96 - 60.3:0.67, a circularity score between 5.4 - 8.4, a gating of

brightfield Major Axis of 3-10 before finally removing cells with no GFP fluorescence detected. Values for side-profile GFP and Brightfield areas were determined using the 'Threshold' and 'Inspire' mask functions.

2.9. Measuring single-cell HSPP induction

R. toruloides transformed with EGFP controlled HSPP promoters were grown in YNB + CSM (20 g L^{-1} glucose) at 28 °C until late-log stage before dilution to OD_{600} 0.2 in pre-warmed 28 °C YNM + CSM (20 g L^{-1} glucose) and shaken for 60 minutes at 28 °C. This was followed by either heat shock to 37 °C or remaining at 28 °C for 60 minutes before further incubation at 28 °C for 5 hours. All incubation steps were at 200 RPM.

Samples were then pelleted and resuspended in F1 (4 g L^{-1} paraformaldehyde, 3.4 g sucrose) and incubated at 21 °C for 15 minutes. These were then washed in F2 (1.2 M sorbitol, 0.1 M potassium phosphate pH 7.5) before resuspension in F2. Fluorescence of each cell was then quantified using an Amnis ImageStream X Mark II Imaging Flow Cytometer (Brooks Life Science, Chelmsford, CA) using settings for side-profile cell determination described in section 2.8; the fluorescence value determined is the median pixel within the 'Inspire' mask.

2.10. Measuring HSPP induction kinetics

R. toruloides transformed with EGFP controlled HSPP promoters were grown in YNM + CSM (20 g L^{-1} glucose) at 25 °C until late-log stage before dilution to OD_{600} 0.2 in pre-warmed 25 °C YNM + CSM (20 g L^{-1} glucose), loaded into 4titiude 28-well plate and shaken for 60 min at 28 °C. This was followed by either heat shock to 37 °C or remaining at 28 °C for 120 min before further incubation at 28 °C for 4 hours. All incubation steps were at 200 RPM.

3. Results & Discussion: Organelle visualisation in *R. toruloides*

As outlined in section 1.1, *R. toruloides* is an oleaginous yeast with potential commercial uses as a more environmentally responsible method for producing carotenoids, biofuels, and other lipid-derived compounds. Work has been done to improve lipid production above the levels in wild-type yeast, which are capable of accumulation of lipid droplets to over 76 % dry biomass (Li, Q. *et al.*, 2008; LI *et al.*, 2006), through overexpression of native acetyl-CoA carboxylase and diacylglycerol acetyltransferase (Zhang, Skerker, *et al.*, 2016). However, *R. toruloides* is underdeveloped as a biotechnological chassis and requires further investigation to improve efficiency and rate of lipid production, control of gene expression, as well as improving ease of lipid/biofuel release for downstream processing. This chapter describes studies to enable the visualisation of aspects of lipid droplet dynamics and interactions in *R. toruloides*. In the next chapter, tools will be sought for the improved control of gene expression for biotechnological exploitation of this yeast.

3.1. Construction of GFP-tagged protein expression plasmids

To develop a toolkit to enable live-cell visualisation and monitoring of the lipid droplet, ER, and autophagy complex, it was necessary to fluorophore epitope-tag proteins known to localise to these organelles: Ldp1 (Zhu *et al.*, 2015), calnexin (Brandizzi *et al.*, 2004; Runions *et al.*, 2006), and Atg8 (Li, D. *et al.*, 2015) respectively. Ldp1 is a protein which localises to the boundary of lipid droplets, and its tagging with a fluorophore enables this organelle to be directly visualised in living yeast/fungal cells (Zhu *et al.*, 2015). Calnexin localises to the ER, the site of site of biogenesis of the lipid droplet and the principal site of TAG synthesis for lipid droplet formation. Tagging calnexin can enable the dynamics of lipid droplet formation to be monitored (Müller-Taubenberger *et al.*, 2001). Atg8 protein is recruited to degrade lipid droplet lipids for FFA recycling through microautophagy (Hashemi and Goodman, 2015; Wang, C. W., 2016). Tagging of these three proteins should therefore enable the dynamics of *R. toruloides* lipid droplets to be monitored via live-cell visualisation at all stages of their “life cycle”.

Successful studies on the Ldp1, calnexin and Atg8 proteins in other organisms have shown specificity for either -C or -N terminus tagging (Klionsky, 2011; Müller-Taubenberger *et al.*, 2001; Zhu *et al.*, 2015) for localised organelle-targeted fluorescence, and this information was used when designing tag constructs. A codon-

optimised eGFP tag was used which has been previously demonstrated to function efficiently in *R. toruloides* (Johns *et al.*, 2016). For transformation of *R. toruloides*, the base plasmid pEGFP-Rt-YR-Hyg was used (Figure 5), which contains a codon-optimised eGFP gene under control of the native *R. toruloides PGK1* promoter, plus elements for maintenance and selection in *S. cerevisiae*, *E. coli*, and *Agrobacterium tumefaciens* to enable transformation of *R. toruloides* by *A. tumefaciens*-mediated transformation (ATMT) (Johns *et al.*, 2016; Zhang, Skerker, *et al.*, 2016).

The strategy for constructing each of the GFP-tagged protein expression plasmids is given in Figure 6. This strategy utilised Yeast Recombination-Based Cloning (YRBC), an *in vivo* gene assembly method which utilises the highly efficient and accurate homologous recombination mechanism within the budding yeast *S. cerevisiae*; multiple linear DNA fragments with short (40 bp) overlapping sequences are transformed into *S. cerevisiae*, accurately joined to form a plasmid *in vivo*, and recovered via DNA preparation and transformation of *E. coli*. YRBC is particularly suitable for assembly of large and complex plasmids such as those required for *Agrobacterium tumefaciens*-mediated transformation (ATMT) of fungi (Johns *et al.*, 2016; Kilaru and Steinberg, 2015).

Native *R. toruloides* CBS 14 strain sequences encoding the calnexin and Atg8 proteins were identified using reciprocal BLAST searches as specified in section 2.2.1. The *R. toruloides* Ldp1, calnexin and Atg8 genes were amplified with gene sequence-specific primers containing an additional 5′ 40 bp homology region to either: *PGK1* promoter or 5′ *EGFP* with an additional codon-optimised 6x glycine residue linker sequence (*LDP1* and calnexin); or a 5′ 40 bp homology region to either: *EGFP* with an additional codon-optimised 6x glycine residue linker sequence or 5′ 40 bp homology sequence to CMV35S terminator as detailed in Table 3, Section 2. To ensure only the desired amplicon was produced in the PCR reaction, PCR products were size-fractionated by agarose gel electrophoresis to verify the fragment size: 1327 bp (*LDP1*), 2428 bp (calnexin), and 876 bp (*ATG8*) as shown in Figure 7A.

The base plasmid pEGFP-Rt-YR-Hyg (Figure 5) was cleaved with either *Afl*II (*LDP1* and calnexin) or *Pml*I (*ATG8*), and the *R. toruloides* protein coding DNA amplicons were integrated adjacent to GFP using *Saccharomyces* YRBC, as shown in Figure 6.

This led to the construction of the *R. toruloides* tagging plasmids pLDP1-EGFP-Rt-YR-Hyg, pCalnexin-EGFP-Rt-YR-Hyg, and pEGFP-Atg8-Rt-YR-Hyg respectively.

After growth of putatively transformed *S. cerevisiae* BY4742 on selective media, yeast colony PCR was performed on resultant colonies to screen for desired plasmid constructs using the ‘check’ primers, flanking each YRBC junction as demonstrated in Figure 6 with a 5′ ‘upstream’ junction and 3′ ‘downstream’ junction. Expected upstream amplicon sizes of 275 bp, 236 bp, and 343 bp and downstream amplicon sizes of 567 bp, 498 bp and 452 bp for the constructs containing *LDP1,* calnexin, and *ATG8* were found and are shown in Figure 7B. Plasmids from colonies with the correct junctions were then isolated, and these were then transformed into *E. coli* DH5α. Subsequent amplified constructed plasmid was then miniprepped from *E. coli* and verified by restriction-digestion with *Bam*HI; major expected bands of the constructs containing all contained common elements 14071 bp, 250 bp, and 21 bp with additional identifying bands of *LDP1* (1658 bp, 946 bp), calnexin (2759 bp, 946 bp), and *ATG8* (1753 bp, 403 bp) were all observed, as demonstrated om Figure 7C.

.

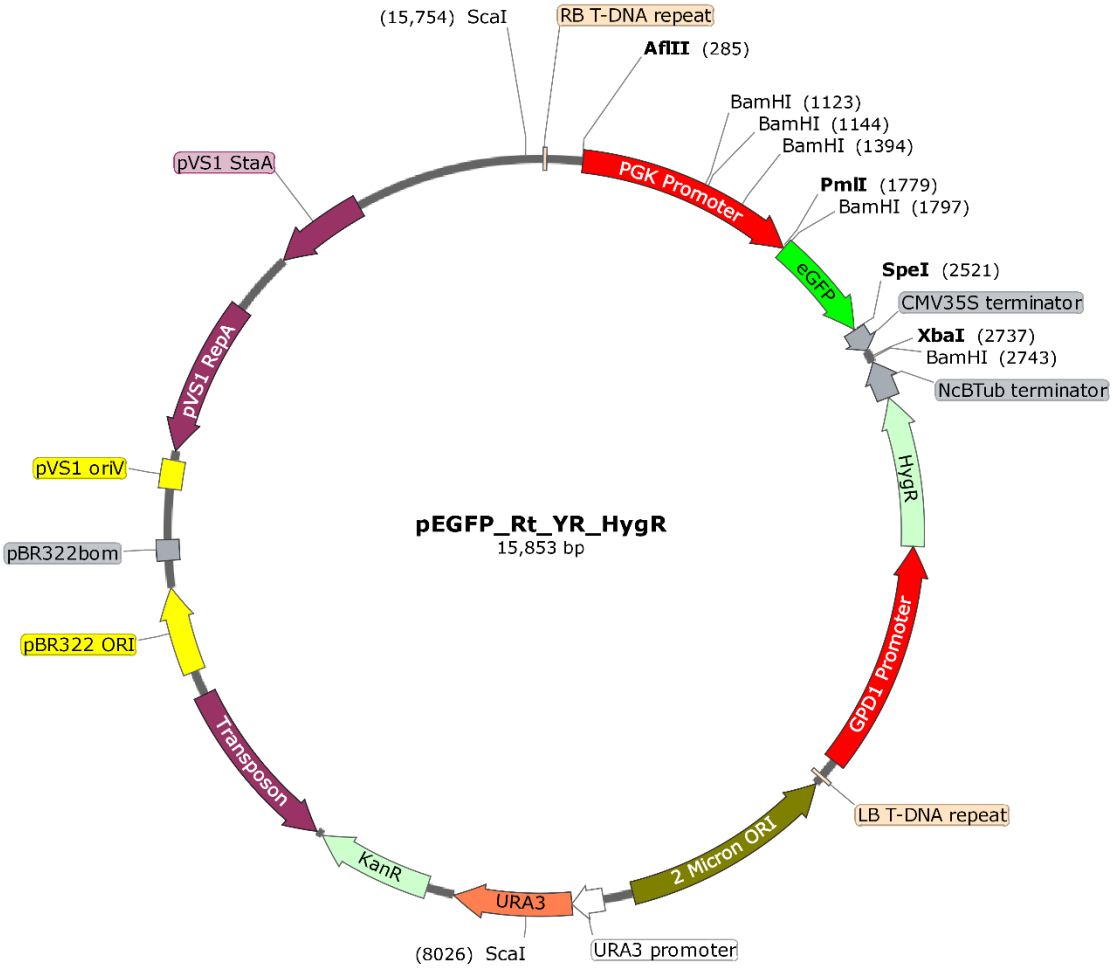

Figure 5| Map of base vector pEGFP-Rt-YR-Hyg for transformation of *R. toruloides*. This base plasmid as described by Johns et al. (2016) contains a T-DNA region between the left border (LB T-DNA) and right border (RB T-DNA) which becomes integrated into the *R. toruloides* genome, as well as sequences for propagation in *S. cerevisiae* (2µ ORI and *URA3*), and sequences for propagation in *E. coli* and *A. tumefaciens* (remainder of vector). The T-DNA region contains a codon-optimised eGFP gene regulated by the constitutive *R. toruloides PGK1* promoter and the CMV35S terminator, and a codon-optimised hygromycin resistance marker, for selection in *R. toruloides*, regulated by the *GPD1* promoter and *Neurospora crassa* β-tubulin (NcB Tub) terminator.

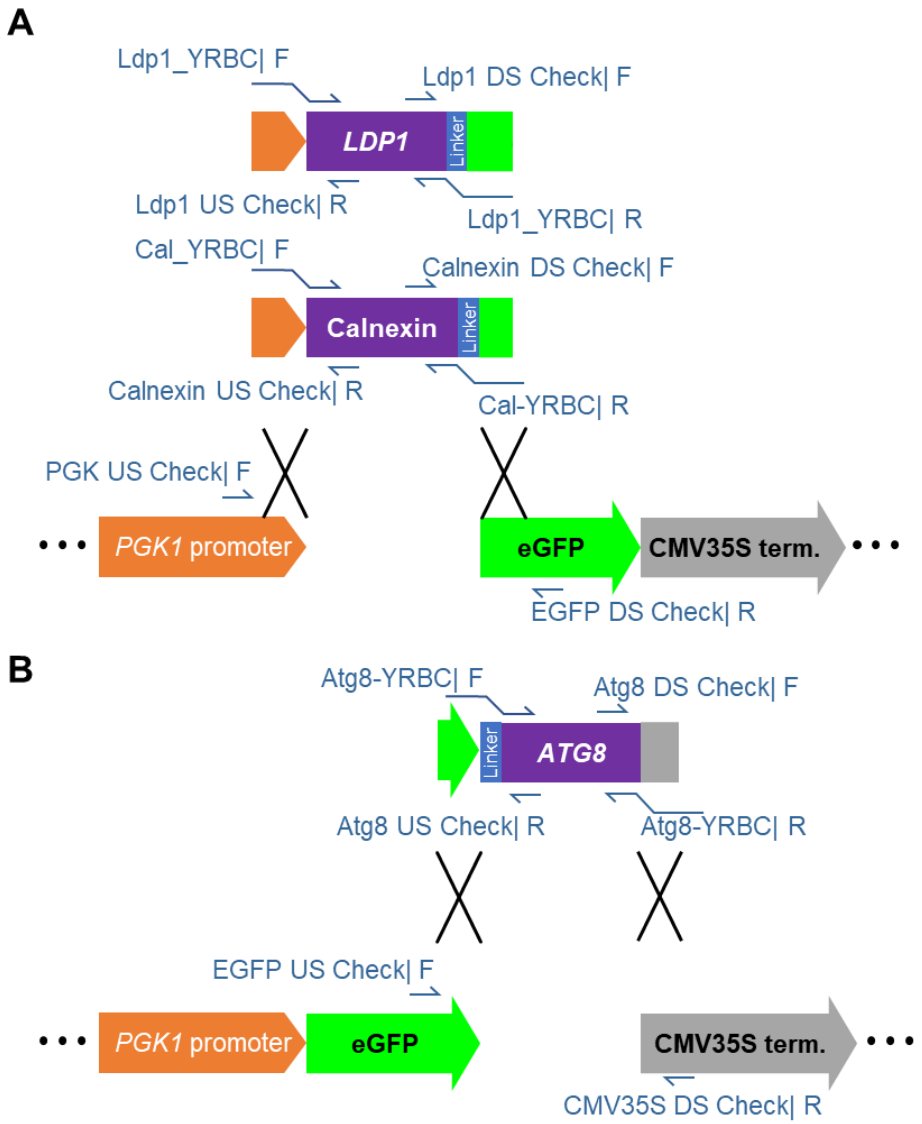

Figure 6| Yeast Recombination-Based Cloning (YRBC) strategy for construction and verification of plasmids for organelle visualisation in *R. toruloides*. Amplicons were generated by PCR containing an *R. toruloides* gene and flanking homology regions. GFP fusion constructs were then generated by homologous recombination with cleaved *R. toruloides* vector pEGFP-Rt-YR-Hyg (Figure 5), in *S. cerevisiae*. **A.** C-terminus GFP-tagged *LDP1* and calnexin amplicons generated through PCR of the respective *R. toruloides* genes using specific forward (F) primers, with an additional 5′ 40 bp homology region to the *PGK1* promoter, and reverse (R) primers, with a 5′ 40 bp homology region to eGFP, and a 'linker' sequence encoding 6x glycine residues. Amplicons were recombined via YRBC with cleaved pEGFP-Rt-YR-Hyg as illustrated. **B.** An N-terminus GFP-tagged *ATG8* amplicon was generated using the same strategy as described in A, but with the forward primer including a 5′ 40 bp eGFP homology sequence before a linker sequence, and the reverse primer containing a 5′ 40 bp CMV35S Terminator homology sequence. The amplicon is recombined via YRBC as illustrated. Relevant junction-flanking primers are also annotated (US 'Upstream'/DS 'Downstream' Check) to show their approximate locations for later verification of YRBC constructs. Primer sequences are given in Table 1 (section 2.2). Diagrams are not to scale.

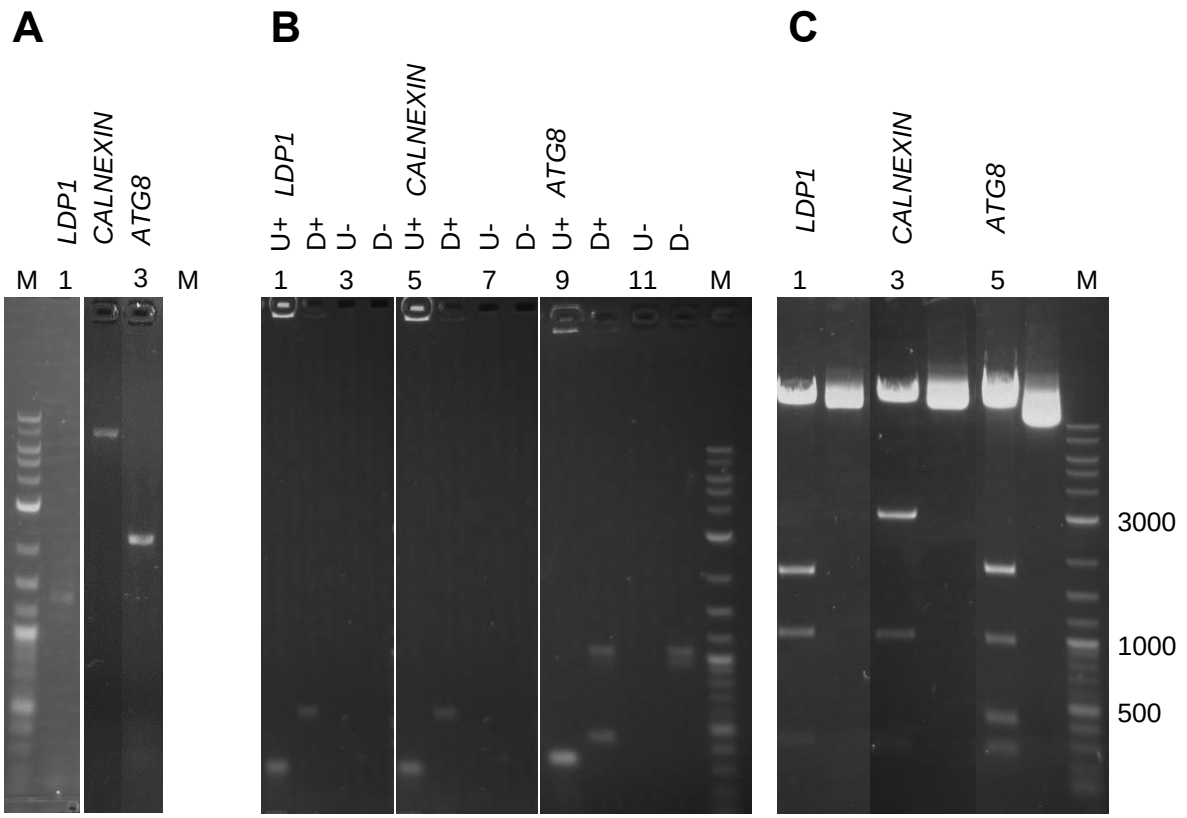

Figure 7| Construction by YRBC of *R. toruloides* GFP-tagged protein expression plasmids for organelle visualisation. Marker lanes are labelled 'M' and are loaded with NEB Log2 Ladder. **A.** Separate gels containing genes amplified through PCR from extracted *R. toruloides* CBS14 genomic DNA using primers as described in Table 4 (Section 2) to include an additional 80 bp of YRBC-required homology region above genomic CDS length. *LDP1* was loaded into lane 1 of a 1 % gel with an expected band size of 1327 bp. Calnexin and *ATG8* were loaded into lanes 2-3 of 2 % gels with an expected band size of 2428 bp and 867 bp respectively. Track M contains NEB Log2 ladder. **B.** Yeast colony PCR of junctions between pEGFP-Rt-YR-Hyg and either the Ldp1 (left), calnexin (middle) or Atg8 (right) gene, using the strategies outlined in Figure 6. In all cases, the first odd numbered tracks of each gel contained PCR products using upstream junction primers and even numbered tracks contained the applicable downstream junction primers; lanes 3-4, 7-8, and 11-12 are negative PCR controls. *LDP1*, calnexin, and *ATG8* junctions had an expected band size of 275 bp, 236 bp, and 343 bp for their upstream junctions and 567 bp, 498 bp, and 452 bp for their downstream junctions respectively. Track M contains NEB Log2 ladder. **C.** Diagnostic *Bam*HI digests of YRBC-formed plasmids for pLdp1-EGFP-Rt-YR-Hyg (lanes 1-2, expected dominant bands of 14017 bp, 1658 bp, 946 bp and 250 bp), pCalnexin-EGFP-Rt-YR-Hyg (lanes 3-4, expected dominant bands of 14017 bp, 2759 bp, 946 bp and 250 bp), and pEGFP-Atg8-Rt-YR-Hyg (lanes 5-6, expected dominant bands of 14017 bp, 1753 bp, 403 bp, 250 bp) with undigested negative controls in the even numbered tracks.

3.2. Visualisation of lipid droplets in *R. toruloides*

Ldp1 (lipid droplet protein 1) is a structural protein identified in the lipid droplet proteome of *R. toruloides* (Zhu *et al.*, 2015). An Ldp1-GFP construct expressed heterologously in *S. cerevisiae*, albeit with a different linker sequence, led to supersize lipid droplet formation (Zhu *et al.*, 2015). The most abundant lipid droplet-associated protein identified in the proteome analysis of the *R. toruloides* is Ldp1 (Zhu *et al.*, 2015). Sequence analysis of Ldp1 shows similarity to the perilipin family of proteins; the primary function of perilipins is the inhibition of lipase activity against lipid droplets by coating the organelle and physically restricting access (Sztalryd and Brasaemle, 2017; Zhu *et al.*, 2012).Recent evidence has emerged to support additional functions of the perilipins: they both promote assembly of lipid droplets in the ER membrane and stabilise the phospholipid (PL) monolayer of nascent (<200 nm diameter) and pre-lipid droplets, preventing fusion with otherwise 'unprotected' lipid droplets as can be observed in *pet10Δ S. cerevisiae* perilipin mutants (Gao *et al.*, 2017; Hashemi and Goodman, 2015).

Lipid droplet visualisation in live-cell images will be crucial for understanding lipid droplet biogenesis, lipid turnover, and lipid metabolic responses in oleaginous yeasts to external stresses and media, as well as the interactions of lipid droplets with other organelles. While conventional lipid stains, such as Nile Red, have been used to stain *R. toruloides* lipid droplets previously (Alexander Johns, pers. comm.), this stain is limited in its use for live-cell imaging of this yeast. This is primarily due to the extensive overlapping excitation and emission spectra of the stain and carotenoids of the yeast which preclude studies in stationary-phase cells, in addition to having to introduce the stain itself, which may induce artefacts into the sample or alter the lipid droplet structure. Due to the ability of *R. toruloides* Ldp1 to localise exclusively to lipid droplets in *S. cerevisiae*, this protein was chosen for a GFP fusion to attempt to visualise the lipid droplet in *R. toruloides* using the native *LDP1*-encoded perilipin.

R. toruloides was transformed through ATMT with the pLdp1-EGFP-Rt-YR-Hyg construct, using a modified protocol described in section 2.4 which generated a 200-fold greater number of transformants per plate than that reported by Johns *et al.*, 2016. To demonstrate that Ldp1-GFP specifically targets the lipid droplet, confocal microscopy was used to excite and record GFP fluorescence (Figure 8). In this figure brightfield image signal is thresholded to highlight only peaks in

signal. The spherical GFP-coated structures found closely resemble the lipid droplet shape that we would expect to observe were lipid droplet to be enveloped in the fluorophore. However, to be able to conclusively determine lipid droplet/Ldp1-GFP targeting, verification is required with colocalisation of GFP signal to a known lipid droplet marker.

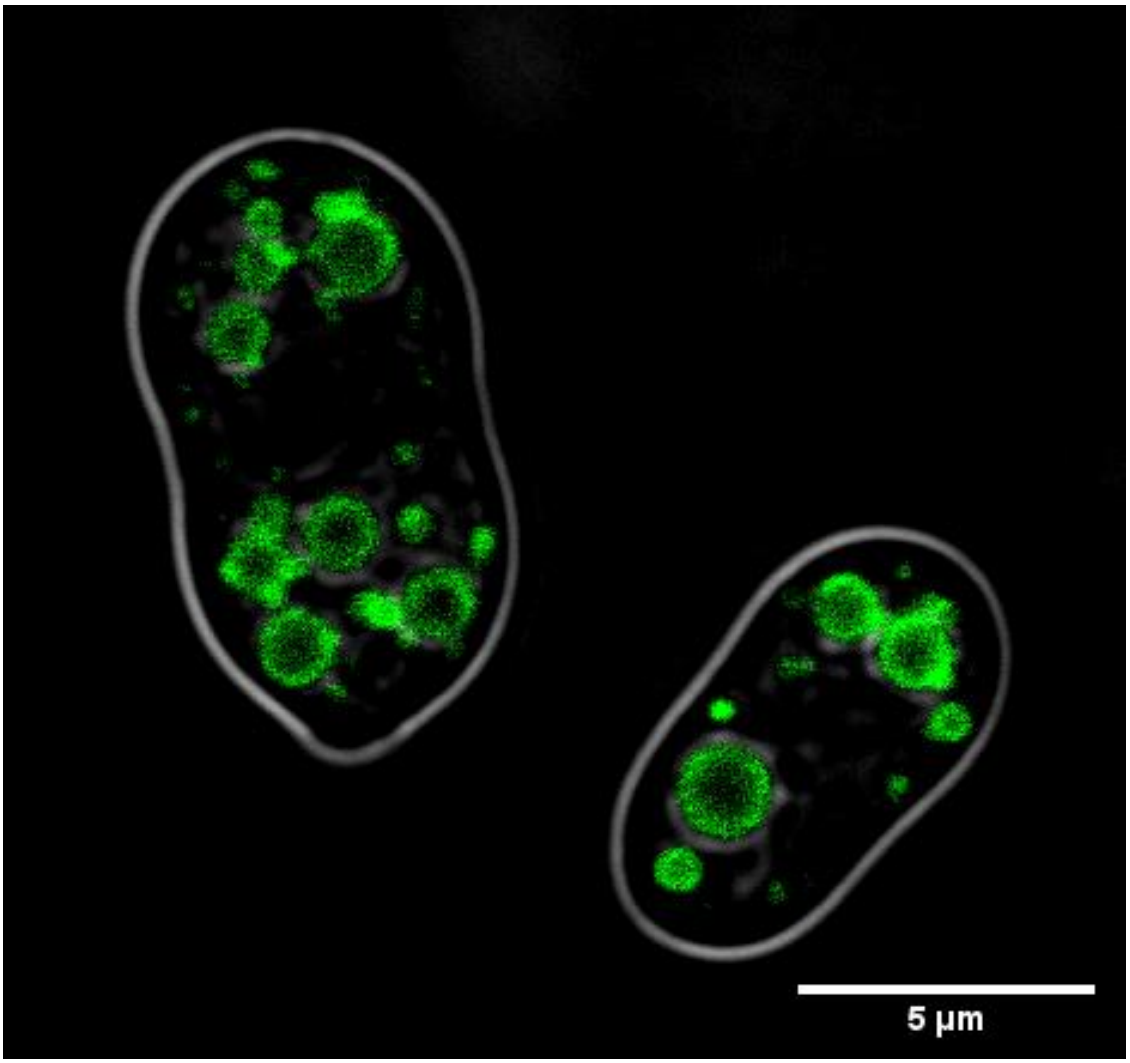

Figure 8| Single slice confocal image of *R. toruloides* cells transformed with Ldp1-GFP. *R. toruloides* CBS14 transformed with pLdp1-GFP-Rt-YR-Hyg plasmid after growth in MM+N for 48 hours was visualised with GFP excited at 488 nm and Stokes shift fluorescence detected at 500-535 nm; signal shown here in green. The brightfield image was thresholded to show signal peaks associated with 'halo' artefacts in density-change.

To show colocalisation of Ldp1-GFP to lipid droplets, it was initially planned to use simultaneous Two-Photon-EpiFluorescence (TPEF), to excite the GFP fluorophore, and a coherent pump and Stokes laser to vibrationally excite the unlabelled CH_2 bond of acyl-fatty acids for spatial mapping of the compound using Stimulated Raman Loss (SRL). As $\omega_s - \omega_p = \Omega$, and the Raman active mode (Ω) of CH_2 is 2845 cm^{-1} (3514 nm), neither the tuneable pump beam (798 nm), fixed frequency-doubled 1032 nm Stokes beam, nor outputted antistokes beam of 650 nm are able to excite the 488 nm peak GFP fluorophore. However, although more convoluted, it is possible to use CARS/SRS to show colocalisation of Ldp1-GFP and lipid droplet. Using a standard SP8 confocal microscope, GFP excitation is shown to colocalise with brighter regions in a brightfield channel as light passes through a different-phase area as shown in Figure 8 (with GFP localised to the periphery of the circular sub-cellular structures). Correspondingly, in Figure 9, brightfield-channel highlighted regions in B are spatially co-localised with peak intensity regions in CARS/fluorescence channel in A and SRS channel in C, with a 'Pearson Co-localisation Coefficient' of 0.54 between brightfield and background-subtracted CARS. As such, this microscopy data suggests that Ldp1-GFP is able to precisely localise to the periphery of organelles containing the FA palmitic acid, found within the lipid droplet of *R. toruloides*.

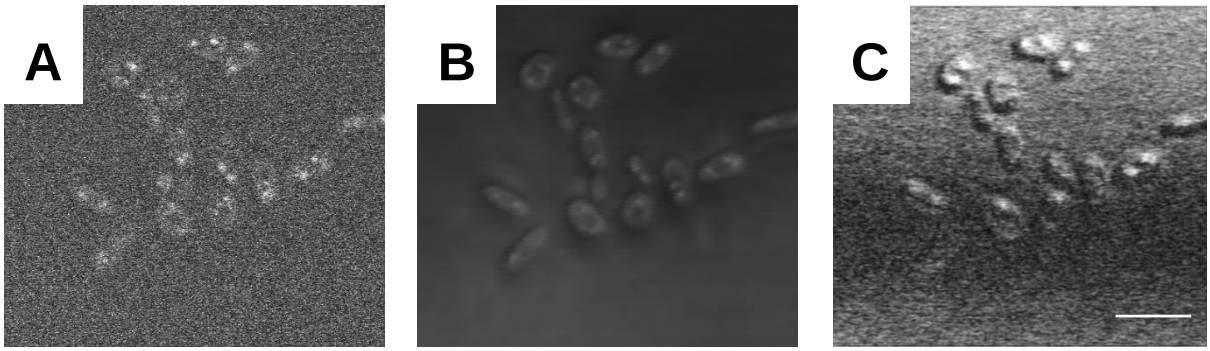

Figure 9| Composite images of CARS/SRS and Ldp1-GFP tagged *R. toruloides.* *R. toruloides* CBS14 was transformed with an Ldp1-GFP containing transformation cassette via ATMT. The transformants were cultured in Minimal Medium without Nitrogen for 48 h before visualisation on a CARS/SRS-capable microscope. **A.** Channel showing excitation with a CARS and fluorescence signal. **B.** Brightfield image of the yeast. **C.** SRS channel fluorescence. Scale bar = 15 µm

3.3. Development of a precise and a rapid method for quantification of lipid biogenesis

Having established that Ldp1-GFP localises to the periphery of lipid droplets, as suggested by Zhu *et al.*, 2015, we then wanted to establish whether it would be possible to use this as a proof-of-principle method to calculate volumes of lipid droplet within each cell and, therefore, quantify rate of and efficiency of lipogenesis in different media. Both cell and lipid droplet volumes were determined, as described in section 2.7, where confocal stacks were taken of side-profile Ldp1-GFP transformed *R. toruloides* yeast before analysis in ImageJ. The relationship between fluorescence-microscopy images (left) and lipid droplets identified by the ImageJ macro (right), where individual lipid droplets are assumed to be separated if there is no GFP-signal connectedness between their surfaces, can be shown qualitatively in Figure 10A where a representative image is shown. The yeast cell wall was identified in the brightfield channel and is outlined in orange; the cell volume for this yeast was calculated by projecting this orange-outlined profile 360° around the major axis. Figure 10B shows the relationship between cell volumes and lipid volumes determined through this method when grown in either lipid accumulating MM-N (minimal media without nitrogen; red) or MM+N (minimal media with nitrogen; green). As nitrogen starvation inhibits both amino acid and nucleic acid synthesis, in common with other yeasts, it is assumed that this will halt the cell cycle during G1 with a consequence of similarly sized cells with an increased TAG content (and lipid droplet volume) in nitrogen-limited medium. However, no statistical difference could be identified for neither cell volumes nor lipid volumes between the two growth conditions using a Student's t test. When cultured in MM-N, cell volume was an average of 78 μm^3 ±51 μm^3 and lipid droplet volumes of 18 μm^3 ±12 μm^3 (n=16); when cultured in MM+N cell volume was an average of 122 μm^3 ±78 μm^3 and lipid droplet volumes of 27 μm^3 ±20 μm^3 (n=7). Only a small number of samples were able to be analysed on the confocal microscope due to limited microscope time being available.

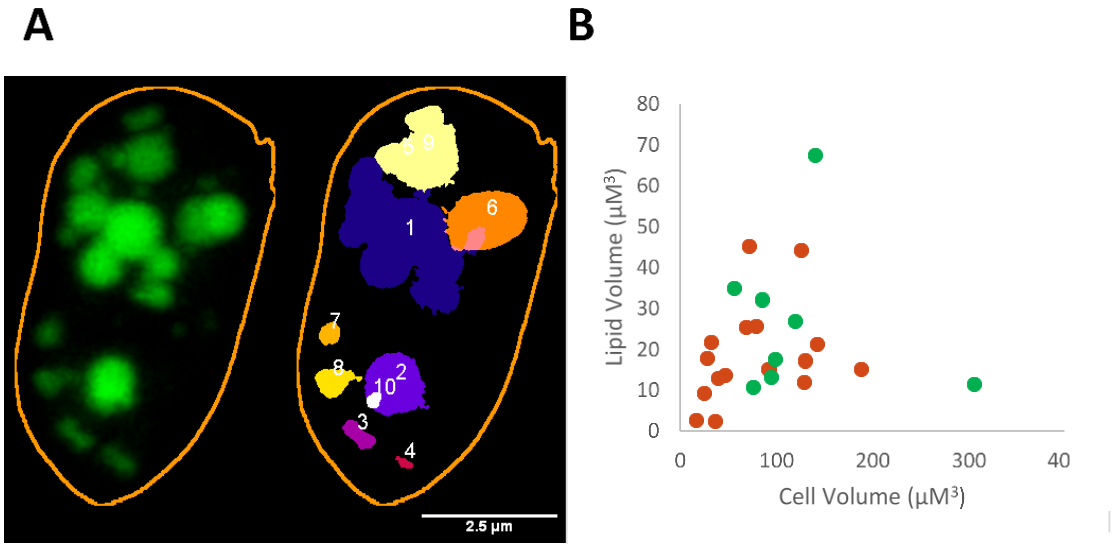

Figure 10| Comparison between raw confocal measurements of GFP-labelled Ldp1 organelles and the corresponding quantification of fluorescent intercellular compartments. A. Representative image of Maximum Projection areas identified and the volumes calculated in ImageJ. Green areas represent areas where voxels were included in the totalling of the lipid sum and white numbers labelling each lipid droplet and showing the centres of mass from of each individual vesicle within the image as calculated in section 2.7. Volumes of both whole cells and Ldp1-GFP-tagged subcellular structures were quantified as described in the 2.7. **B.** Quantitative calculated cell and lipid volumes using GFP-Ldp1, as described above, where 16 cells grown in MM-N for 48 hours (red markers) and 7 cells cultured in MM+N for 48 hours (green markers) are recorded.

3.4. Quantification of lipid biogenesis under glucose starvation conditions

To investigate whether available glucose concentration in the medium affects the rate of lipid droplet biosynthesis in *R. toruloides*, stationary phase GFP-Ldp1-transformed *R. toruloides* in MM+N was diluted into MM-N OD_{600} of 0.02, with differing concentrations of glucose from 0 g L^{-1} to 25 g L^{-1}, and the OD_{600} recorded every 15 minutes for the next 72 hours. As shown in Figure 11 it is unsurprising that yeast cell density, determined by recording light scattering, began to rise earliest in the culture with the greatest concentration of reducible carbon, approximately 14 hours earlier than yeast cultured in the absence of glucose. As shown in Figure 11, the maximum rate of cell proliferation exhibited in MM-N is $1.2x10^7$, $1.0x10^7$, $1.1x10^7$, $1.0x10^7$, $7.9x10^6$ and $5.8x10^6$ cells mL^{-1} h^{-1} for 0, 5, 10, 15, 20, and 25 g L^{-1} glucose respectively, where an OD_{600} of 1 is approximately $5x10^8$ cells mL^{-1}.

In contrast to the method for determining absolute cell-by-cell lipid droplet content using confocal microscopy above, where low sample numbers are likely to have prevented identifying statistical differences in lipid content biogenesis, we were curious to find whether it would be possible to determine any glucose-dependent differences in relative lipid droplet size with a cheaper high-throughput method. To achieve this, *R. toruloides* was inoculated as described in the glucose-dependent cell density experiment above (and section 2.8) before analysing >44 000 side-profile cells for each sample type through a flow cytometer; cell area was determined by using a root mean squared (RMS) gradient to identify cell edges, and lipid area was determined by summing known-dimension pixels fluorescing under 488 nm excitation. Figure 12 shows the plot of cell area and against lipid area from this flow cell analysis; although less useful than plotting lipid volumes for each culturing condition the resolving power of the Amnis flow cytometer was unable to distinguish each intracellular lipid droplet from one-another. Morphologically, a clustering of lipid areas and cell areas can be observed with 5-15 g L^{-1} initial glucose feeds, although as the glucose concentrations increase the lipid and cell areas appear to both decrease. While it may now be tempting to infer a relationship between the media and the cell lipid assimilation profile, this does not take into account the different growth stages of each of the yeast cultures at the point of data recording. While the 'cluster' of 5-15 g L^{-1} glucose are all still at logarithmic growth (or just entering diauxic shift), cells in 20 g L^{-1} glucose achieved stationary phase four hours before recording and cells in 25 g L^{-1} glucose had reached quiescence more than 20 hours previously. As yeasts begin to degrade lipid droplets in response to glucose limitation, to liberate and metabolise FFA, it is not surprising that cells which have apparently depleted a nutrient in their environment (and therefore reduced/stopped cell proliferation) have smaller lipid droplets.

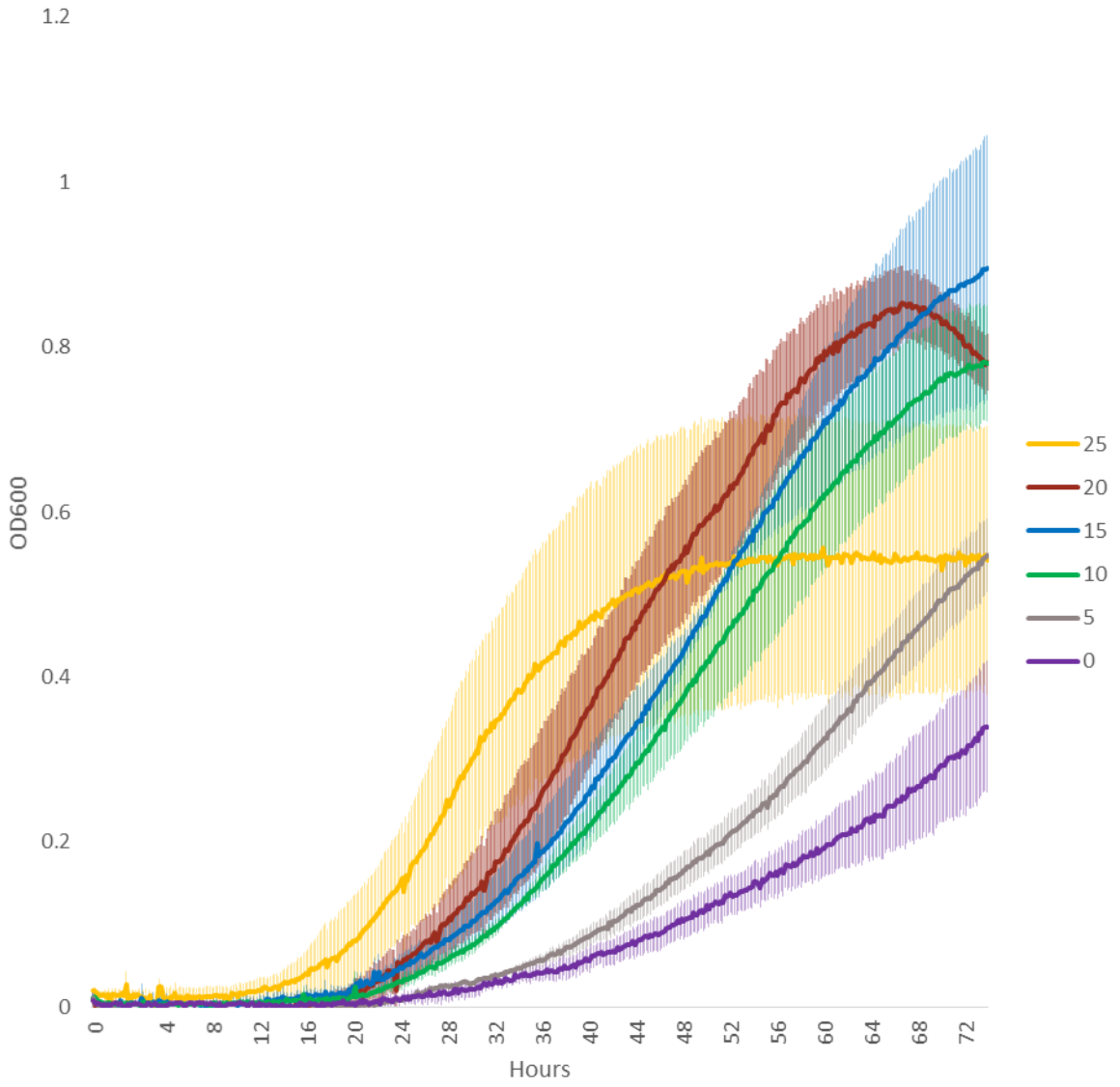

Figure 11| Rates of growth of GFP-Ldp1-transformed *R. toruloides* CBS14 with different glucose concentrations. Culture densities of *R. toruloides*, measured using OD_{600}, with different MM-N culture media with 0-25 g L^{-1} glucose supplement, as indicated (right-hand side).

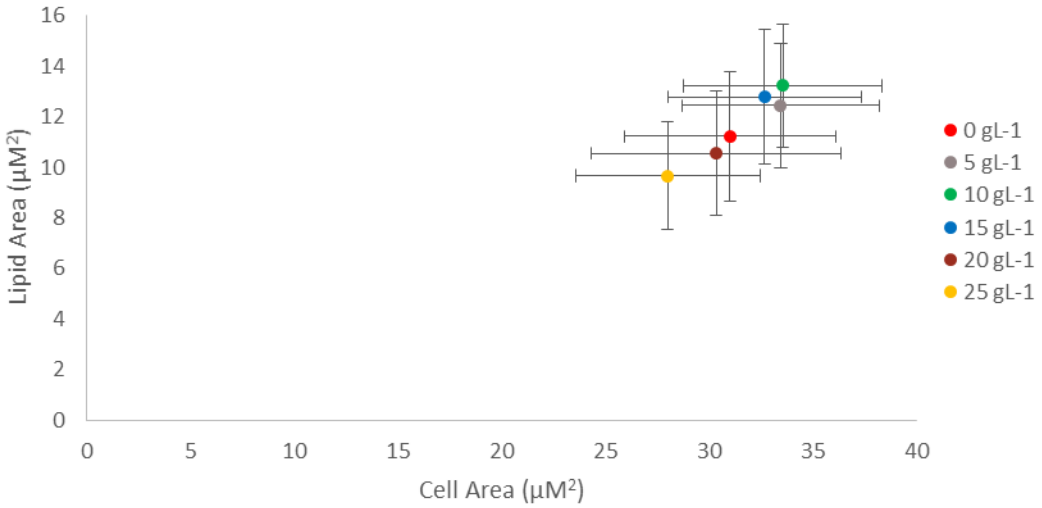

Figure 12| Median area of fluorescent regions within Ldp1-GFP-transformed *R. toruloides*. Yeast were cultured in YNB+CSM for 36 hours before paraformaldehyde fixation and sample loading into an Amnis ImageStream Mark II X. >44 000 side-profile cells were measured and their areas were determined after excitation with a 488 nm laser. Median areas are plotted; error bars represent Median Absolute Deviations.

3.5. Endoplasmic reticulum visualisation in *R. toruloides*

As described in section 1.1, the endoplasmic reticulum and lipid droplet organelles are intrinsically associated; the ER being the terminal site of the neutral lipid biogenesis pathway, the site of maintenance of the lipid droplet, the organelle which buffers against ER stresses, and the origin of many lipid droplet trafficked proteins. Throughout the lifecycle of the ER the ER and lipid droplet remain almost constantly in contact potentially through a 'lipid bridge' (Schuldiner and Bohnert, 2017). Markers for the transition zone cannot be resolved from one another through microscopy (Soni *et al.*, 2009). As such, it is crucial to developing our understanding of the oleaginous yeast, as well as organelle dynamics and interactions, that we are able to live-cell visualise the ER organelle. To achieve this, the ER calcium storage protein/chaperone 'calnexin' was fused to GFP with a 6x codon-optimised glycine residue linker through genetic engineering and the construct was transformed into *R. toruloides* as described in sections 2.3 and 3.1.

Without a counterstain which also targets the ER, it is unfortunately not possible to confirm calnexin localisation to the ER. However, as shown in Figure 13, GFP-fluorescent 'tubules' appear to have developed along the midline of the cell, with a secondary colocalisation to the two different-density organelles identified by their 'halos' in the brightfield channel – presumably the nucleus or lipid droplets. These findings support the notion that GFP-calnexin has localised to the ER, as this is where we would expect to find them, but further investigation is needed to verify this.

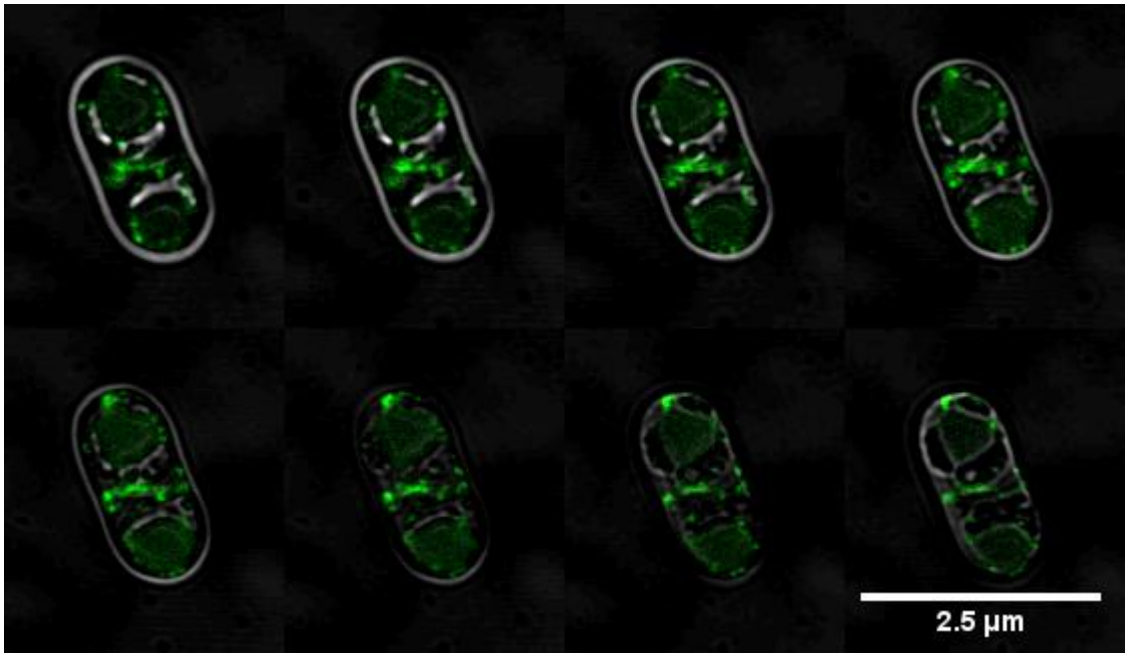

Figure 13| Z-stack montage showing localisation of calnexin-GFP in an example *R. toruloides* cell. Confocal slices showing areas of excitation at 488 nm (green) with an autofluorescence channel (650-700 nm) subtracted against a brightfield image of the yeast (grey) which was edited to highlight the refractive 'halo' artefact at the cell boundary. Cells were cultured in Minimal Medium without Nitrogen for 48 h before visualisation.

3.6. Autophagy visualisation and induction in *R. toruloides*

Autophagy ("self-eating") is a eukaryotic cellular process required in the turnover and recycling of organelles and cytoplasm implicated in the (un)selective targeted degradation of many organelles. Whereas in yeast, lipolysis occurs either through

embedded lipid droplet lipases and sterol ester hydrolases, or translocation of the entire lipid droplet to vacuoles, mammalian cells are able to undergo macroautophagy, where the entire lipid droplet organelle is enveloped by an LC-3 (Atg8 homologue)-recruited double membrane. Development of this heterologous mammalian-like macroautophagy may be of marked interest in *R. toruloides*. Targeted autophagy research is still in its infancy, but lysosomal-associated membrane protein 2 (LAMP2) has been demonstrated to translocate to lysosomal fractions, concurrent with an increase in LC3 fraction-associated increase (Cahová, 2012). Targeting of a double-membrane organelle to the lipid droplet, where lipid reservoirs account for over 70% w/w, may be useful for inducible secretion of the mature LD-containing organelle; as the only organelle capable of *de novo* double-membrane engulfment, this autophagy complex may facilitate an energetically cheap method for releasing accumulated lipid into the surrounding medium. As outlined in section 1, in a pilot study over half of the cost of the biodiesel product was derived from energy costs in isolating the lipid. Targeted release may make this second-generation biofuel commercially competitive with fossil fuels, and therefore reduce GHG emissions.

As described in 4.2, an Atg8-GFP construct was made and transformed into *R. toruloides*. Having cultured the yeast in MM-N for 48 hours, a sample of cells from each of the biological replicates were visualised through confocal microscopy; a representative image of this microscopy is shown in Figure 14. While, excitingly, Figure 14 does appear to show puncta with an association to the region of budding and a second region of higher GFP co-localisation to the artefact on brightfield imaging, this could be due to chance or accumulation of the fluorescent protein as it precipitates from solution, or accumulates in inclusion bodies. As such, from our data, we cannot yet confirm that Atg8-GFP is associated with the autophagy complex, a necessity for visualising the targeted secretion of lipid droplet mentioned above. Further studies are required to verify the colocalisation of Atg8-GFP to the autophagy complex, either through a counterstaining experiment such as immunofluorescence staining against major autophagy proteins or identification of more fluorescent puncta as the yeast are exposed to autophagy-inducing conditions such as glucose starvation.

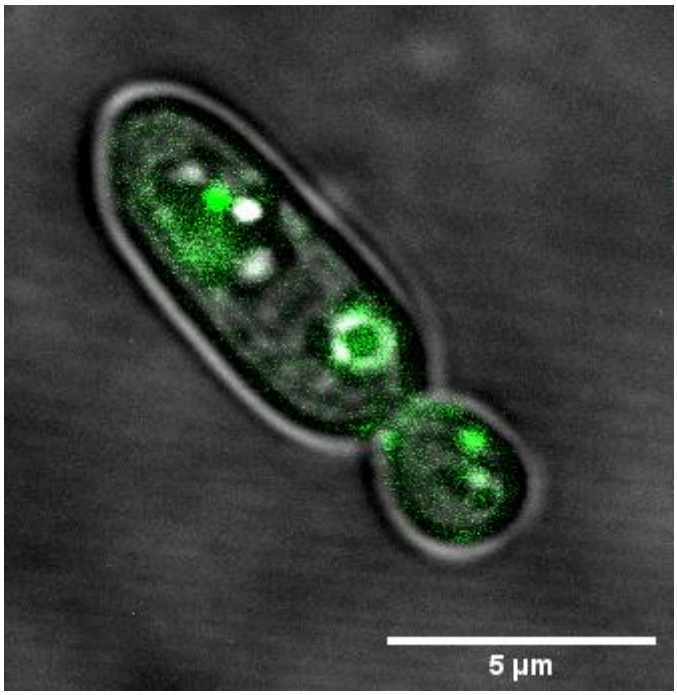

Figure 14| Example image showing localisation of GFP-Atg8 in *R. toruloides.* A single confocal slice is showing areas of excitation at 488 nm (green) with an autofluorescence channel (650-700 nm) subtracted against a brightfield image of the yeast (grey) which was edited to highlight the refractive 'halo' artefact at the cell boundary. Cells were cultured in Minimal Medium without Nitrogen for 48 h before visualisation.

4. Results & Discussion: Heat Shock Protein Promoter Induction

As outlined in section 1.2, while there has been a rapid development of genetic tools in *R. toruloides,* all of the current eight inducible promoters (*NAR1, ICL1, MET16, CTR3, DAO1, THI4, THI5 and CTR31)* in the yeast rely on nutrient-limited media (Park *et al.*, 2018). This restricts their use in a commercial setting where feed is not tightly controllable or, if feed is tightly controllable, then metabolic remodelling to accommodate the limited nutrients may have unintended physiological effects on the yeast and reduce yield of the desired specialist products. As such, a short-term environmental assault, which would induce the Environmental Stress Response (ESR) through upregulation of specific genes' transcription in the yeast, was decided as a candidate for inducible promoter investigation. Of the many assaults where global transcription has been monitored as part of an ESR (Causton *et al.*, 2001; Gasch, A. P. *et al.*, 2000), only ionising radiation or temperature shock do not involve any depletion, or changes, of composition of the media. It was therefore decided to use heat shock as the inducible ESR of choice as ionising radiation, where genes related to DNA repair are upregulated, may lead to unintended mutant variants being generated.

4.1. Promoter design and synthesis

S. cerevisiae genes were identified which were either up-regulated primarily in response to a heat-shock, as determined through microarray analysis, or which responded to a general ESR where the gene transcripts were up-regulated in response to many different types of environmental responses (Causton *et al.*, 2001; Gasch, A. P. *et al.*, 2000). Homologues of these selected 'heat shock proteins' (HSP) genes were then identified in *R. toruloides* (Table 5) and their promoters (heat shock protein promoters; HSPPs) chosen as candidates for inducible ESR-driven GFP-reporter synthesis. Forward-genetic studies by Liu, Y. *et al.*, 2018, where carotenoid biosynthesis was disrupted by random integrational mutagenesis through ATMT, showed this technique predominantly resulted in random single-copy chromosomal-integration of transfer-DNA. Previous TAIL-PCR experiments by Stephen Aves and Alexander Johns (pers. comm.) had not found any statistical differences in levels of gene expression dependent upon the site of DNA integration and were, therefore, not determined in this study.

It was also decided to investigate whether sequences of the immediately-upstream protein-coding gene contributed to HSPP induction, perhaps through transcription-factor binding in *R. toruloides* outside the intergenic region of the HSPP; the genetic schematics of the four inducible promoters previously characterised by Johns *et al.*, 2016 are shown in Figure 15. In the case of these promoters, *MET16*, *CTR3*, and *NAR1* all contained their crucial promoter regulatory elements within their intergenic regions. However, two distinct regulatory regions were identified in *ICL1* from -100 to -200, and from -200 to -400 bp. As *ICL1* intergenic region is only 218 bp, it is possible that a regulatory element is therefore found within the upstream gene; it was therefore decided to investigate whether there is any induction difference between 'fixed-length' (FL) 1200 bp or variable-length 'intergenic' (IG) promoters. This would contribute to our ability to more rapidly characterise *R. toruloides* promoters in the future as, if expression of the promoters is consistently the same between FL and IG promoters, then the number of future nested deletions of promoters (to find minimally-sized active promoters) can be reduced beyond an arbitrary 'upstream' length to just within the intergenic region. To test this, a yeast recombination-based cloning strategy was employed as described in Figure 16A. Briefly, promoter sequences of either fixed-length (FL) 1200 bp or a variable length (until the immediately upstream gene's protein coding region; intergenic (IG) length) were identified from the annotated *R. toruloides* genome (Zhu *et al.*, 2012) and primers designed with sequence specificity to either: the FL sequence, with an additional 40 bp 5′ homology sequence to the base plasmid pEGFP-Rt-YR-Hyg immediately upstream of the PGK promoter, or with sequence specificity to the reverse strand 3′ end of the HSPP gene of interest with an additional 5′ 40 bp homology to EGFP. These promoters were amplified by PCR from *R. toruloides* genomic DNA and size-verified, as shown in Figure 17.

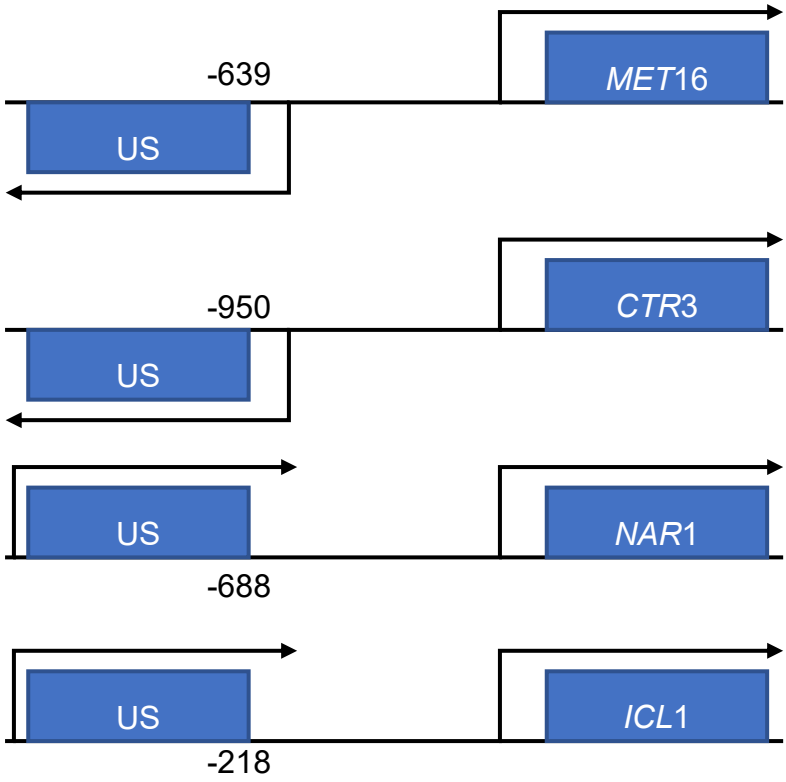

Figure 15| Schematic of inducible promoters previously characterised in *R. toruloides* CBS14. A schematic diagram (not to scale) showing directionality and distance of upstream (US) protein-coding regions in relation to previously characterised methionine-inducible *MET16*, copper-inducible *CTR3*, nitrogen-inducible *NAR1*, and acetate-inducible *ICL1* genes in *R. toruloides* CBS14; distances to the start or stop codons are shown in base-pairs.

Table 5| *R. toruloides* heat shock protein promoters

	Gene Name	*S. cerevisiae* Standard Name	*S. cerevisiae* Systemic Name	Function	Full Name	*R. toruloides* Locus & Direction	Promoter transcriptional interference	Promoter Intergenic region lengths (bp)
01	RHTO_00033	*PGK1*	YCR012W	Glycolysis	Phosphoglycerate kinase	Scaffold1: 74,979 - 76,478 : 1	T	373
02	RHTO_00323	*ENO2*	YHR174W	Glycolysis	Enolase II	Scaffold1: 783,641 - 786,135 : -1	D	873
03	RHTO_00384	*KAR2*	YJL034W	Chaperone	Hsp70 family ATPase	Scaffold1: 935,362 - 936,861 : -1	D	907
04	RHTO_01329	*TPI1*	YDR050C	Glycolysis	Triosephosphate isomerase	Scaffold13: 29,368 - 30,881 : -1	D	1488
05	RHTO_01538	*SSE1*	YPL106C	Chaperone	Adenyl-nucleotide exchange factor SSE1	Scaffold14: 28,485 - 29,984 : -1	T	506
06	RHTO_01660	*ERG20*	YJL167W	Sterol Metabolism	Farnesyl-pyrophosphate synthetase	Scaffold14: 346,860 - 348,381 : -1	T	297
07	RHTO_03043	*FBA1*	YKL060C	Glycolysis	Fructose-bisphosphate aldolase, Class II	Scaffold2: 906,477 - 908,296 : 1	T	373
08	RHTO_03322	*LHS1*	YKL073W	Chaperone	Hsp70 family chaperone LHS1	Scaffold20: 56,750-58,249 :-1	D	340
09	RHTO_03429	*LHS1*	YKL073W	Chaperone	Hsp70 family chaperone LHS1	Scaffold20: 325,239-326,738 :1	T	339
10	RHTO_03430	*NAF1*	YNL124W	Pre-rRNA Processing	RNA-binding snornp assembly protein	Scaffold20:329137:330636:1	T	598
11	RHTO_03560	*ACT1*	YFL039C	Cytoskeletal	Actin	Scaffold21:244966:246465:-1	D	782
12	RHTO_03746	*TDH3*	YGR192C	Glycolysis	Glyceraldehyde 3-phosphate dehydrogenase	Scaffold22: 315,363-317,069:-1	T	1085
13	RHTO_03759	*LHS1*	YKL073W	Chaperone	Hsp70 Family Chaperone LHS1	Scaffold22:346190:347689:1	T	~1967

Abbreviations given in column one for each *R. toruloides* gene name as derived from *R. toruloides* NP11, accession GCA_000320785.2 (Zhu *et al.*, 2012). *S. cerevisiae* S288c protein homologues in *R. toruloides NP11* were identified using tBLASTn (Madden *et al.*, 1996) and gene functions identified from UniProt (Bateman, 2019). Potential promoter transcriptional interference was determined by comparison between the *R. toruloides* gene of interest and the directionality of its immediate upstream gene (T, tandem; D, divergence).

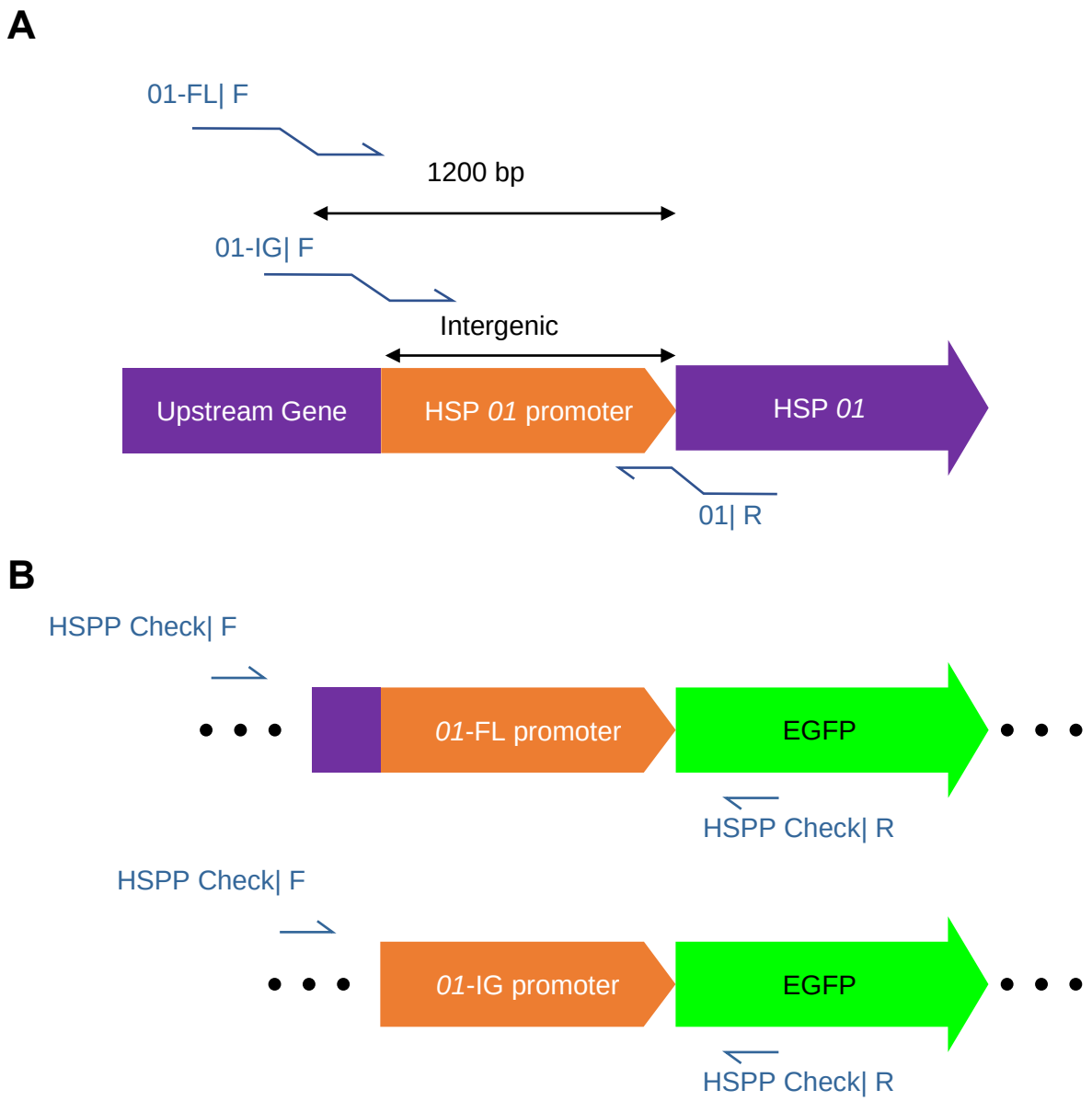

Figure 16| Strategy for generation of heat shock protein promoter (HSPP) fragment-containing reporter plasmid. A. Representative schematic diagram of HSPP primer locations relative to HSP in *R. toruloides* genome. Amplicons are produced using either a Forward (F) primer sequence specific to 1200 bp upstream of the HSP ORF ('Fixed Length' FL) or until the ORF of the immediately upstream gene ('Intergenic' IG). Both FL and IG primers are flanked with a 5′ 40 bp homology sequence to pEGFP-Rt-YR-Hyg base plasmid filler sequence, and a Reverse (R) primer containing a 5′ 40 bp homology sequence to eGFP. **B. Representative schematic diagram of HSPP primer locations relative to HSP in base plasmid construct.** Correct construction of plasmids p(01-FL)EGFP-Rt-YR-Hyg (top) or p(01-IG)EGFP-Rt-YR-Hyg (abbreviated to 01-FL and 01-IG respectively) was verified using specific flanking primers HSPP Check| F and HSPP Check| R.

4.2. Construction of HSPP reporter plasmids

Having generated insert amplicons containing HSPPs and homology regions to the base plasmid as described in section 4.1, pEGFP-Rt-YR-Hyg PGK promoter was excised through digestion with *Afl*II and *Pml*I before yeast-based recombination in *S. cerevisiae* was performed using the method described in section 2.3.7 to make HSPP-driven EGFP reporter plasmids p(HSPP)EGFP-Rt-YR-Hyg.

Yeast colony PCR was employed to screen putative *S. cerevisiae* transformants using HSPP Check Primers as shown in Figure 16B. Where correctly-sized PCR products were amplified from colonies (both FL, containing an upstream gene, and IG containing just an intergenic region), plasmids were isolated and transformed into *E. coli* DH5α. Plasmids were isolated from *E. coli* transformants and the plasmids verified through restriction digest with *Xba*I and *Sca*I. Resultant linear fragments were size-fractionated in an agarose gel, as shown in representative example Figure 19. Verified plasmids were transformed into *Agrobacterium tumefaciens* as detailed in section 2.3.6 before transformation of *R. toruloides* with the plasmid t-DNA cassette through *A. tumefaciens*-mediated transformation, as detailed in section 2.4.

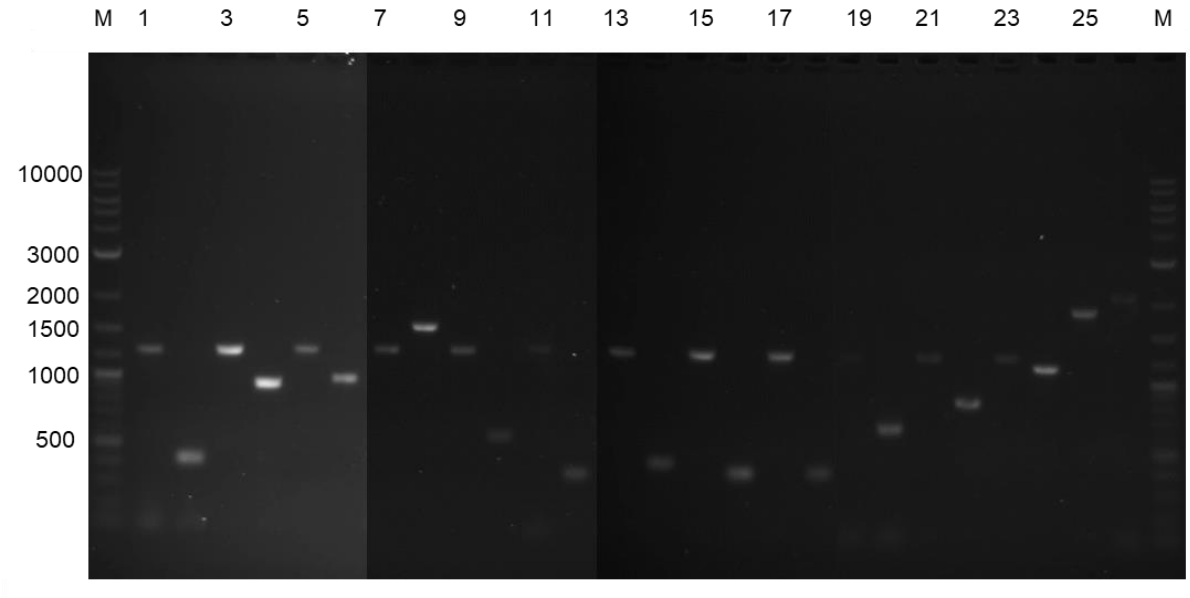

Figure 17| PCR amplicons of heat shock protein promoters. Promoter fragments were amplified from extracted genomic DNA from *R. toruloides* CBS14 using primers as described in Table 4. **(A)** NEB Log2 Ladder was loaded into lanes labelled marker (M) with full-length amplicons loaded in odd-numbered lanes and intergenic-length amplicons loaded in even-numbered lanes: lanes 1-2 HSPP01; lanes 3-4 HSPP02; lanes 5-6 HSPP03; lanes 7-8 HSPP04; lanes 9-10 HSPP05; lanes 11-12 HSPP06; lanes 13-14 HSPP07; lanes 15-16 HSPP08; lanes 17-18 HSPP09; lanes 19-20 HSPP10; lanes 21-22 HSPP11; lanes 23-24 HSPP12; lanes 25-26 HSPP13.

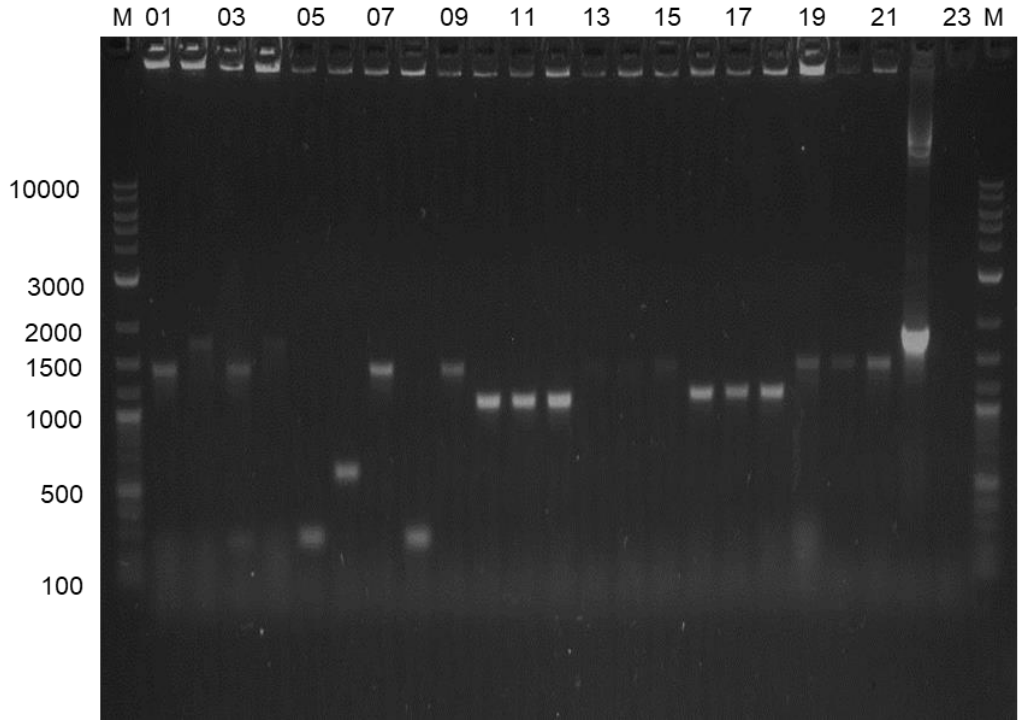

Figure 18| Example gel diagram of Yeast Colony-PCR verification of HSPPs. Three *S. cerevisiae* biological replicate colonies for each HSPP acted as template DNA for yeast colony-PCR, using flanking primers as described in Table 2, to verify desired HSPP-induced GFP plasmids for transformation into *R. toruloides* were constructed. Tracks 01 and 25 are loaded with MEB Log2 Ladder, with tracks 02-22 loaded with colonies theoretically containing 01-FL, 01-IG, 02-FL, 02-IG, 03-IG, 03-NC, 04-FL, where consecutive tracks contain one of each biological replicate respectively. Track 23 contains base plasmid as described in Figure 5 as a positive control, with track 24 as a negative control.

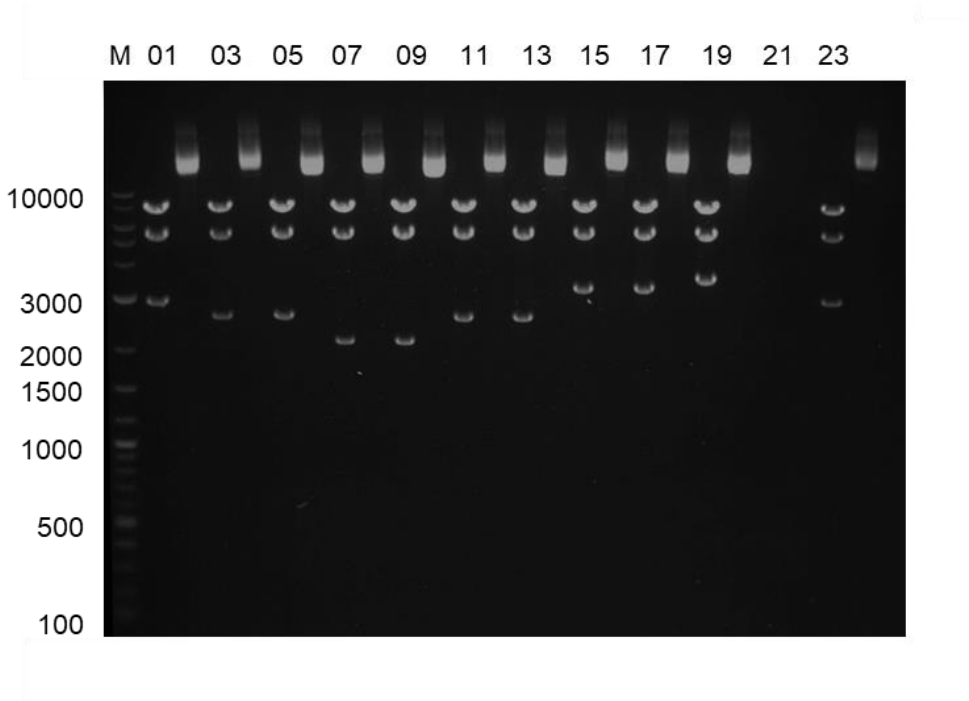

Figure 19| Representative gel of diagnostic plasmid digests of HSPP19-26. Plasmids extracted from *E. coli* containing putative HSPP-inducing GFP plasmids for transformation into *R. toruloides* containing *E. coli* before double digestion with both ThermoFisher FastDigest restriction endonucleases *Xba*I and *Sca*I. NEB Log2 ladder was loaded into column M. Representative columns were loaded as follows: 9-FL (01-02), 11-FL (03-06), 11-IG (07-10), 12-FL (11-14), 13-FL (15-18), 13-IG (19-20), *PGK1*-1500 (23-24), with even numbered columns digested and odd numbered columns undigested plasmid negative controls. Anticipated lower band sizes of 1106, 2529, 2529, 2111, 2111, 2529, 2529, 2836, 2836 and >1967 (incomplete available sequence data) were expected for digested columns respectively; 9-FL band size is unexpected and a second transformation independent colony was then verified and used (data not shown).

4.3. Heat shock promoter induction in *R. toruloides*

To determine the potential use of *S. cerevisiae* HSPP homologues in *R. toruloides* as biotechnologically useful promoters (namely strongly inducible, and tightly regulated promoter activity), three biological *R. toruloides* replicates from each *A. tumefaciens* mediated HSPP-containing transformation were inoculated into synthetic medium (to limit the level of autofluorescence observed that would otherwise be present in other media such as YPD) and heat-shocked as described in section 2.9. Briefly, late logarithmic-phase yeast cultures were diluted to an OD_{600} 0.2, given an hour to recover at 25 °C followed by either a heat shock to 37 °C or remaining at the control temperature of 25 °C, before returning to the initial temperature for five hours' growth, and the fluorescence of the yeast samples measured through flow cell cytometry.

Induction results are shown in Figure 20, where fluorescence of >16 000 cells in each group is shown for both control (blue) and heat shocked (red) conditions. Of the HSPP-driven GFP-containing yeasts, an apparent difference from wildtype (WT) is found in HSPP 1-FL (*PGK1*), 2-FL (*ENO2*), 4-IG (*TPI1*), 5-FL (*SSE1*), 6-FL (*ERG20* – heat shocked only), 11-FL (*ACT1*), and 12-FL (*TDH3*). From these transformants no statistical difference between heat shock and control conditions were identified, but 2-FL appears to show a possible difference between control and heat shock conditions which may not have been identified statistically due to the large variance in fluorescence and deserves further analysis. This suggests the identification of a further six promoters which appear constitutively expressed in *R. toruloides* and require further characterisation. It is curious that HSPP1, which is also *PGK1* promoter albeit at a cut-down of 1200 bp, had an apparent difference in fluorescence against the *PGK1*-1500 Johns *et al*., (2016) promoter and suggests further analysis is needed here.

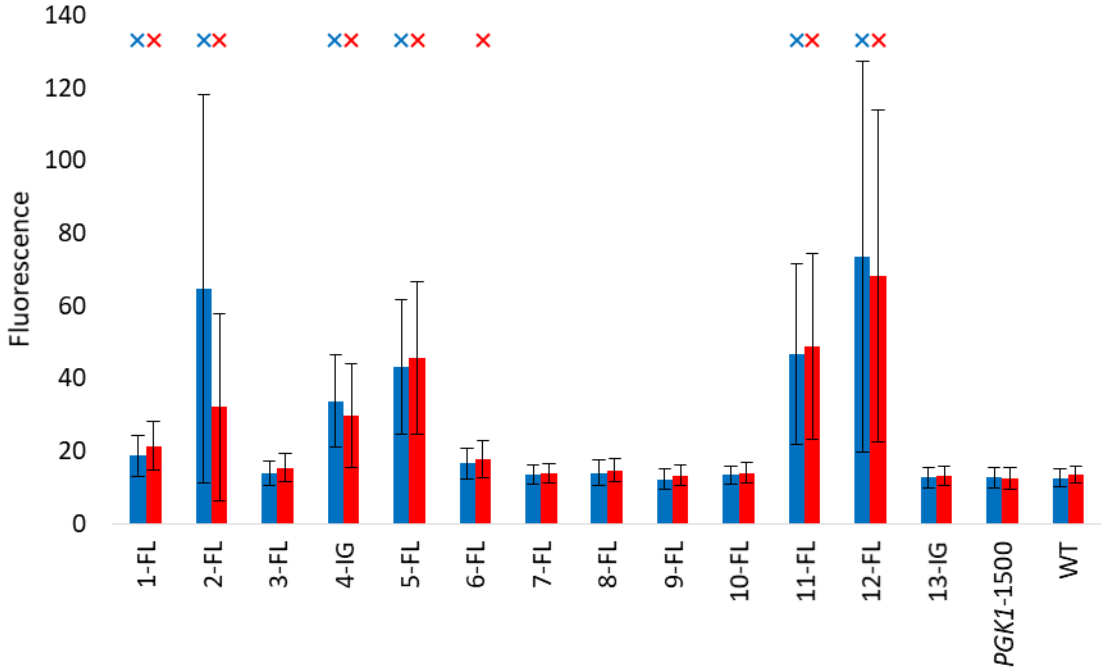

Figure 20| Induction of heat shock protein promoters controlled cell eGFP fluorescence. Median pixel intensities of logarithmic-stage *R. toruloides* cultures after dilution to an OD_{600} of 0.2 before either shock-treatment to 37 °C or remaining at 25 °C for an hour followed by a five-hour recovery period at 25 °C before: paraformaldehyde-fixation; excitation at 488 nm; and photography with an Amnis ImageStream X Mark II Imaging Flow Cytometer**.** X-axis numbers represent the HSPPs denoted in Table 5, where >16 000 images from three biological replicates of each HSPP-EGFP of each were treated; error bars represent Median Absolute Deviation. Blue and red crosses denote an identified statistical difference between HSPP and WT fluorescence medians respectively using a Student's *t*-test p=0.05. No statistical differences were identified between HSPPs under heat-shock conditions.

4.4. Heat Shock promoter kinetics in *R. toruloides*

Having initially measured the final HSPP-driven fluorescence at six hours, it was decided to measure promoter kinetics from the initial heat-shock in case an induction peak was being temporally missed. In *S. cerevisiae*, RNA transcription is upregulated for all of the selected HSPs within 5 minutes, with the majority of HSPs' RNA transcripts reaching maximal expression between 15-20 minutes. As detailed in section 2.10, logarithmic-stage *R. toruloides* was normalised to an OD_{600} of 0.2 in a 24-well plate; both OD and fluorescence were then measured at regular intervals during a two hour heat shock to 37 °C, and the following four hour recovery time at 25 °C (Causton *et al.*, 2001; Gasch, A. P. *et al.*, 2000). Although unlikely, GFP stability in *R. toruloides* has not yet been determined experimentally and it is probable that the five promoters identified in section 4.3 are constitutively expressing GFP, thereby replenishing degraded fluorescent protein, whereas in a briefly-expressed RNA transcript, such as that only produced while Msn2/4 is nucleus-localised while hyperphosphorylated, the unstable fluorophore would not be detectable after degradation and non-replenishment.

Kinetic assays of the promoters HSPP 1-FL (*PGK1*), 2-FL (*ENO2*), 2-IG (*ENO2*), and 12-FL (*TDH3*) are shown in Figure 21. Statistical differences were determined by Student's *t*-test, and differences between WT and HSPP-induced GFP under heat-shock are identified by red crosses; differences between WT and HSPP-induced GFP when remaining at 25 °C for the duration of the experiment are identified in blue crosses; and differences in fluorescence between HSPP-GFP at heat shock and control 25 °C are represented by black crosses. Curiously, 02-FL showed a rapid accumulation of fluorescence during recovery, reaching maximum fluorescence after 50 minutes. This is statistically different to HSPP-driven GFP under control conditions, suggesting the presence of an inducible heat-shock response. However, the HSPP appears to "leak", as a weaker control fluorescence constantly increased, becoming not statistically distinguishable from the fluorescence level of the heat-shocked transformants after 4.5 hours. Interestingly, heat-shocked WT also shows a 'bounce' of fluorescence shortly after heat shock; this is potentially due to autofluorescence as part of the ESR. Even more curiously, 02-IG HSP-driven GFP also continuously increases, as for 02-FL. However, this transformant does not exhibit an inducible heat-shock fluorescence-associated response, therefore suggesting the loss of a crucial

stress-response element contained within the upstream coding DNA sequence. Interestingly, 12-FL does not show significant difference between WT and HSPP-transformants until after 5 hours; this suggests the presence of a weak constitutive promoter. This data corroborates the fluorescence characteristics determined for this promoter in Figure 20, where stronger fluorescence was observed than for WT 6 hours after heat shock.

These kinetic experiments suggest that it may be prudent for future experiments on *R. toruloides* seeking to identify inducible HSPPs to focus primarily on the first 2-4 hours after heat shock, after which any sudden inducibility may be masked. To this end, kinetic assays of fluorescence of all HSPPs (FL and IG) were undertaken, but no statistical differences were observed between the other HSPPs and WT in these cases (data not shown).

This experiment does not appear to corroborate findings by Johns *et al.*, (2016) and Wang, Y. *et al.*, (2016), with regards to the strongly constitutive promoter *PGK1*. Through this time-course experiment, no statistical difference between WT and *PGK1*-controlled GFP could be observed, despite it being a well-characterised and strong constitutive promoter. However, a trend can be observed where, although WT continues to stably not fluoresce, a continuous upward trend in fluorescence can be seen for both the heat-shocked and non-heat-shocked HSP-transformant. This may indicate that other 'HSP'-transformants may not be biologically useful heat-shock inducible protein promoters but may be constitutive promoters which have not yet been identified due to truncation of the experimental kinetic time series at 6 hours. It may, therefore, be prudent to extend this time course in the future to allow possible constitutive promoters, like *PGK1*, to be identified.

Possible reasons for the low induction in all chosen *S. cerevisiae* HSPP homologues in *R. toruloides* are numerous and, from this study, no definitive conclusions can be drawn. However, one likely cause is that the native ESR was not adequately induced in this organism during heat shock to 37 °C because CBS14 strain of the yeast may be ordinarily tolerant to short stresses found at 37 °C as reported in CBS349 by Zhu *et al.*, (2012b). To determine CBS14 strain thermotolerance in the future WT yeast cultures could be temporarily heat-shocked at increasing temperatures before plating until a maximum viable temperature is found. As outlined in section 1, the oleaginous yeast natively produces compounds which are capable of actively mitigating damage

from heat shock-derived deleterious compounds (developing 940.2 µg/g carotenoids in *R. toruloides* strain NP11 (Lin *et al.*, 2017)) and capable of sequestering reactive oxygen species generated during heat shock. Additionally, the physiological presence of a large lipid droplet in *R. toruloides*, which sequesters misfolded proteins in the ascomycete yeast *S. cerevisiae*, may have prevented the necessity for additional molecular chaperones and the associated additional transcriptional- and translational-energy burden of up-regulating these proteins under a 'milder' heat shock (Henne *et al.*, 2019).

It is possible that a stronger induction of HSPP-driven heterologous genes could be found in thermotolerant strains of the yeast. Wu *et al.*, (2018) employed an adaptive breeding strategy to selectively drive and isolate a thermotolerant *R. toruloides* TK16 strain which maintained viability when grown at 37 °C, whereas WT growth was attenuated above 36 °C. Indeed, dry biomass was comparable with higher titres of lipid produced at 37 °C between the mutant strain when compared to WT at 30 °C. If the mechanism of acquired *R. toruloides* thermotolerance mirrors that of *S. cerevisiae*, where heat shock proteins are more strongly up-regulated (Satomura *et al.*, 2013, 2016), then it is possible that a stronger and more sustained HSPP-driven response could be identified.

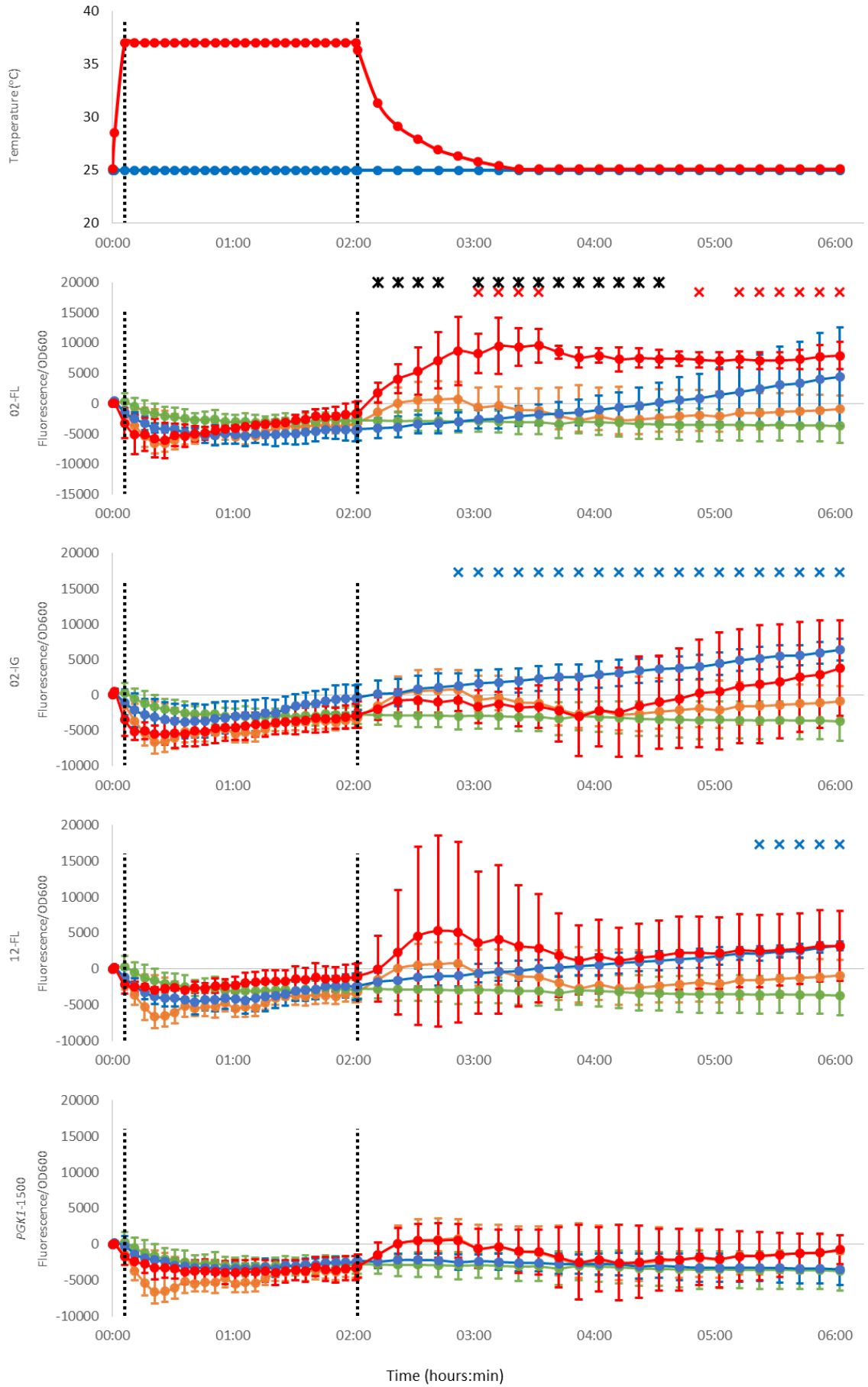
Temperature (°C)
40
35
30
25
20
00:00
01:00
02:00
03:00
04:00
05:00
06:00
02-FL
Fluorescence/OD600
20000
15000
10000
5000
0
-5000
-10000
-15000
02-IG
12-FL
PGK1-1500
Time (hours:min)

Figure 21| Graphical series of measured fluorescence of heat shock protein promoters (HSPP) controlled eGFP after heat shock. Time-dependent response of EGFP fluorescence of a representative tested HSPPs (as annotated in Table 5) after excitation at 488 nm. As shown in the top graph (red), after 5 min the temperature of the ClarioStar platereader rises to 37 °C before cooling back to 25 °C after 2 hours; the negative control (blue) remains constantly at 25 °C. The remaining 4 graphs show OD_{600} normalised fluorescence of the HSPP-GFP (red and blue) and WT *R. toruloides* yeast (orange and green) after either heat-shock or constant temperature respectively. Black crosses represent a statistical different between HSPP-EGFP containing yeast under heat-shock or negative control conditions; red crosses represent a statistical difference observed between HSPP-EGFP containing and WT yeast under heat-shock conditions; and blue crosses represent a statistical difference observed between WT and HSPP-EGFP containing yeast under negative control conditions.

5. Conclusion

As the crisis of climate change becomes more apparent, it is self-evident that a change in global methods for reducing anthropogenic carbon emissions is urgently required. While inroads in other renewable energy technologies capable of eventually fulfilling static and small-distance energy requirements through low-density batteries can be fulfilled, there is not yet a current feasible alternative to the mobile energy density fuels necessitated by longer distance transport than petrochemicals. Recent progress in developing *R. toruloides* as a biotechnological chassis for high-titre neutral lipid synthesis and accumulation from low-cost organic matter, which can undergo transesterification to drop-in FAME biodiesel, offers an alternative to continued release of sequestered carbon as greenhouse gases. Additionally, *R. toruloides* has demonstrated increased or exotic production of high-value lipids and products through expression of foreign genes, including carotenoids, used in food colourants, and essential lipids for dietary supplements or as a therapy for certain neurological and metabolic pathologies.

We have demonstrated the first use of fluorescently epitope-tagged protein probes for live-cell imaging lipid droplets in *R. toruloides*. This can now be shown to quantify lipid biogenesis in this oleaginous yeast and can be used to monitor and investigate mechanisms of lipid droplet formation and maintenance in the yeast in conjunction with the ER, which we have also putatively tagged with the GFP fluorophore. To aid characterisations between the dynamics between the two, different fluorophore tags, such as RFP or Venus yellow, will have to be synthesised. Furthermore, the autophagy complex has been targeted, but the specificity of this tag requires further verification.

Having set out to identify heat-shock inducible promoters for genetic manipulation in undefined media, we instead firmly identified five constitutive promoters. However, one of these identified promoters (RHTO_00323; *ENO2*) is also potentially heat-shock inducible. However, at their current level of characterisation, each of these promoters requires further experimentation to become a biotechnologically useful genetic tool. We have, however, indicated that the rate of heat-shock in *R. toruloides* is rapid, and further experiments to characterise and identify HSPPs should focus on the immediate two hours after heat shock to identify differences in protein expression.

6. Acknowledgements

In the first instance, I am eternally grateful to my academic supervisor Dr Stephen Aves for his long-standing support, patience, and assistance in all aspects of this project, from the initial experimental designs to troubleshooting to suggesting changes to this manuscript.

I am also grateful for the companionship, technical expertise and moral support from my colleagues in the Mezzanine Laboratory and beyond in the Biosciences department, namely Francesco Valente, Stefan Sassmann, Alex Johns, Tom Chaloner, William Kay, Corey Holt, Dominic Wiredu Boakye, Andy Foster, Anke Lange, Jamie Gilman, Skye Marshall, Nick Gaunt, Peggy Dousseaud, Richard Tennant, Paul James, Ann Power, Katy Jones, Maulood Turfah, Dominic Arnaud, Sheera Abdulla and Chloe Singleton.

Finally, I should like to thank my parents, Richard and Sue, for their continued encouragement and belief in me.

7. Bibliography

Agbogbo, F. K., and Wenger, K. S. (2007) Production of ethanol from corn stover hemicellulose hydrolyzate using *Pichia stipitis*. *Journal of Industrial Microbiology and Biotechnology* 34(11): 723–727.

Åkerfelt, M., Morimoto, R. I., and Sistonen, L. (2010) Heat shock factors: Integrators of cell stress, development and lifespan. *Nature Reviews Molecular Cell Biology* 11(8): 545–555.

Alexandre, H., Ansanay-Galeote, V., Dequin, S., and Blondin, B. (2001) Global gene expression during short-term ethanol stress in *Saccharomyces cerevisiae*. *FEBS Letters* 498(1): 98–103.

Amminger, G. P., Schäfer, M. R., Klier, C. M., Slavik, J. M., Holzer, I., Holub, M., Goldstone, S., Whitford, T. J., McGorry, P. D., and Berk, M. (2012) Decreased nervonic acid levels in erythrocyte membranes predict psychosis in help-seeking ultra-high-risk individuals. *Molecular Psychiatry* 17(12): 1150–1152.

Amorós, M., and Estruch, F. (2001) Hsf1p and Msn2/4p cooperate in the expression of *Saccharomyces cerevisiae* genes HSP26 and HSP104 in a gene- and stress type-dependent manner. *Molecular Microbiology* 39(6): 1523–1532.

Athenstaedt, K., and Daum, G. (2003) YMR313c/TGL3 encodes a novel triacylglycerol lipase located in lipid particles of *Saccharomyces cerevisiae*. *Journal of Biological Chemistry* 278(26): 23317–23323.

Ayala, A., Muñoz, M. F., and Argüelles, S. (2014) Lipid peroxidation: Production, metabolism, and signaling mechanisms of malondialdehyde and 4-hydroxy-2-nonenal. *Oxidative Medicine and Cellular Longevity* 2014: 360438.

Ayer, A., Gourlay, C. W., and Dawes, I. W. (2014) Cellular redox homeostasis, reactive oxygen species and replicative ageing in *Saccharomyces cerevisiae*. *FEMS Yeast Research* 14(1): 60–72.

Baker, A., Carrier, D. J., Schaedler, T., Waterham, H. R., van Roermund, C. W., and Theodoulou, F. L. (2015) Peroxisomal ABC transporters: functions and mechanism. *Biochemical Society Transactions* 43(5): 959–965.

Ballio, A., Di Vittorio, V., and Russi, S. (1964) The isolation of trehalose and polyols

from the conidia of *Penicillium chrysogenum* Thom. *Archives of Biochemistry and Biophysics* 107(2): 177–183.

BANNO, I. (2008) Studies on the Sexuality of *Rhodotorula*. *The Journal of General and Applied Microbiology* 13(2): 167–196.

Bateman, A. (2019) UniProt: A worldwide hub of protein knowledge. *Nucleic Acids Research* 47(D1): D506–D515.

Bathiany, S., Dakos, V., Scheffer, M., and Lenton, T. M. (2018) Climate models predict increasing temperature variability in poor countries. *Science Advances* 4(5): eaar5809.

Bebber, D. P., Ramotowski, M. A. T., and Gurr, S. J. (2013) Crop pests and pathogens move polewards in a warming world. *Nature Climate Change* 3(11): 985–988.

Beck, T., and Hall, M. N. (1999) The TOR signalling pathway controls nuclear localization of nutrient- regulated transcription factors. *Nature* 402(6762): 689–692.

Benaroudj, N., Lee, D. H., and Goldberg, A. L. (2001) Trehalose accumulation during cellular stress protects cells and cellular proteins from damage by oxygen radicals. *Journal of Biological Chemistry* 276(26): 24261–24267.

Benghezal, M., Roubaty, C., Veepuri, V., Knudsen, J., and Conzelmann, A. (2007) SLC1 and SLC4 encode partially redundant acyl-coenzyme A 1-acylglycerol-3-phosphate O-acyltransferases of budding yeast. *Journal of Biological Chemistry* 282(42): 30845–30855.

Berlett, B. S., and Stadtman, E. R. (1997) Protein oxidation in aging, disease, and oxidative stress. *Journal of Biological Chemistry* 272(33): 20313–20316.

Biodiesel Standards & Properties (n.d.). Accessed: <https://www.dieselnet.com//tech/fuel_biodiesel_std.php. >.

Black, P. N., and DiRusso, C. C. (2007) Yeast acyl-CoA synthetases at the crossroads of fatty acid metabolism and regulation. *Biochimica et Biophysica Acta - Molecular and Cell Biology of Lipids* 1771(3): 286–298.

Bolte, S., and Cordelières, F. P. (2006/December) A guided tour into subcellular colocalization analysis in light microscopy. *Journal of Microscopy*.

Bose, S., Dutko, J. A., and Zitomer, R. S. (2005) Genetic factors that regulate the

attenuation of the general stress response of yeast. *Genetics* 169(3): 1215–1226.

Boy-Marcotte, E., Garmendia, C., Garreau, H., Lallet, S., Mallet, L., and Jacquet, M. (2006) The transcriptional activation region of Msn2p, in *Saccharomyces cerevisiae*, is regulated by stress but is insensitive to the cAMP signalling pathway. *Molecular Genetics and Genomics* 275(3): 277–287.

BP (2004) Statistical Review of World Energy, BP Statistical Review.

Brachmann, C. B., Davies, A., Cost, G. J., Caputo, E., Li, J., Hieter, P., and Boeke, J. D. (1998) Designer deletion strains derived from *Saccharomyces cerevisiae* S288C: A useful set of strains and plasmids for PCR-mediated gene disruption and other applications. *Yeast* 14(2): 115–132.

Brandizzi, F., Irons, S. L., Johansen, J., Kotzer, A., and Neumann, U. (2004) GFP is the way to glow: Bioimaging of the plant endomembrane system. *Journal of Microscopy* 214(2): 138–158.

Brandl, H., Gross, R. A., Lenz, R. W., and Fuller, R. C. (2005) Plastics from bacteria and for bacteria: Poly(β-hydroxyalkanoates) as natural, biocompatible, and biodegradable polyesters. *Microbial Bioproducts* 41: 77–93.

Broach, J. R. (2012/September) Nutritional control of growth and development in yeast. *Genetics*.

Browne, C. M., Samir, P., Fites, J. S., Villarreal, S. A., and Link, A. J. (2013) The yeast eukaryotic translation initiation factor 2B translation initiation complex interacts with the fatty acid synthesis enzyme YBR159W and endoplasmic reticulum membranes. *Molecular and Cellular Biology* 33(5): 1041–1056.

Bulankina, A. V., Deggerich, A., Wenzel, D., Mutenda, K., Wittmann, J. G., Rudolph, M. G., Burger, K. N. J., and Höning, S. (2009) TIP47 functions in the biogenesis of lipid droplets. *Journal of Cell Biology* 185(4): 641–655.

Cahová, M. (2012) Autophagy-lysosomal pathway is involved in lipid degradation in rat liver. *Physiological Research* 61(3): 287–297.

Cai, L., Sutter, B. M., Li, B., and Tu, B. P. (2011) Acetyl-CoA induces cell crowth and proliferation by promoting the acetylation of histones at growth genes. *Molecular Cell* 42(4): 426–437.

Causton, H. C., Ren, B., Koh, S. S., Harbison, C. T., Kanin, E., Jennings, E. G., Lee, T. I., True, H. L., Lander, E. S., and Young, R. A. (2001) Remodeling of yeast genome expression in response to environmental changes. (Silver, P. A., Ed.)*Molecular Biology of the Cell* 12(2): 323–337.

Chae, M., Han, G. S., and Carman, G. M. (2012) The *Saccharomyces cerevisiae* actin patch protein app1p is a phosphatidate phosphatase enzyme. *Journal of Biological Chemistry* 287(48): 40186–40196.

Charles, H., Godfray, J., Beddington, J. R., Crute, I. R., Haddad, L., Lawrence, D., Muir, J. F., Pretty, J., Robinson, S., Thomas, S. M., and Toulmin, C. (2010) Food Security: The Challenge of Feeding 9 Billion People. 812.

Cherry, J. M., Hong, E. L., Amundsen, C., Balakrishnan, R., Binkley, G., Chan, E. T., et al. (2012) *Saccharomyces* Genome Database: The genomics resource of budding yeast. *Nucleic Acids Research* 40(D1): D700–D705.

Chi, Y., Huddleston, M. J., Zhang, X., Young, R. A., Annan, R. S., Carr, S. A., and Deshaies, R. J. (2001) Negative regulation of Gcn4 and Msn2 transcription factors by Srb10 cyclin-dependent kinase. *Genes and Development* 15(9): 1078–1092.

Chin, J. X., Chung, B. K. S., and Lee, D. Y. (2014) Codon Optimization OnLine (COOL): A web-based multi-objective optimization platform for synthetic gene design. *Bioinformatics* 30(15): 2210–2212.

Choudhary, V., Golani, G., Joshi, A. S., Cottier, S., Schneiter, R., Prinz, W. A., and Kozlov, M. M. (2018) Architecture of lipid droplets in endoplasmic reticulum is determined by phospholipid intrinsic curvature. *Current Biology* 28(6): 915-926.e9.

Coelho, M. A., Rosa, A., Rodrigues, N., Fonseca, Á., and Gonçalves, P. (2008) Identification of mating type genes in the bipolar basidiomycetous yeast *Rhodosporidium toruloides*: First insight into the MAT locus structure of the Sporidiobolales. *Eukaryotic Cell* 7(6): 1053–1061.

Colebc, N. B., Murphy, D. D., Grider, T., Rueter, S., Brasaemle, D., and Nussbaum, R. L. (2002) Lipid droplet binding and oligomerization properties of the Parkinson's disease protein α-synuclein. *Journal of Biological Chemistry* 277(8): 6344–6352.

De Virgilio, C., Hottiger, T., Dominguez, J., Boller, T., and Wiemken, A. (1994) The role of trehalose synthesis for the acquisition of thermotolerance in yeast: I. Genetic

evidence that trehalose is a thermoprotectant. *European Journal of Biochemistry* 219(1–2): 179–186.

Dechant, R., and Peter, M. (2008/December) Nutrient signals driving cell growth. *Current Opinion in Cell Biology*.

Delgenes, J. P., Moletta, R., and Navarro, J. M. (1996) Effects of lignocellulose degradation products on ethanol fermentations of glucose and xylose by *Saccharomyces cerevisiae*, *Zymomonas mobilis*, *Pichia stipitis*, and *Candida shehatae*. *Enzyme and Microbial Technology* 19(3): 220–225.

Durchschlag, E., Reiter, W., Ammerer, G., and Schüller, C. (2004) Nuclear localization destabilizes the stress-regulated transcription factor Msn2. *Journal of Biological Chemistry* 279(53): 55425–55432.

Evans, C. T., and Ratledge, C. (1984a) Effect of nitrogen source on lipid accumulation in oleaginous yeasts. *Microbiology* 130(7): 1693–1704.

Evans, C. T., and Ratledge, C. (1984b) Phosphofructokinase and the regulation of the flux of carbon from glucose to lipid in the oleaginous yeast *Rhodosporidium toruloides*. *Microbiology* 130(12): 3251–3264.

Fahy, E., Cotter, D., Sud, M., and Subramaniam, S. (2011) Lipid classification, structures and tools. *Biochimica et Biophysica Acta - Molecular and Cell Biology of Lipids* 1811(11): 637–647.

Fakas, S., Qiu, Y., Dixon, J. L., Han, G. S., Ruggles, K. V., Garbarino, J., Sturley, S. L., and Carman, G. M. (2011) Phosphatidate phosphatase activity plays key role in protection against fatty acid-induced toxicity in yeast. *Journal of Biological Chemistry* 286(33): 29074–29085.

Fillet, S., Ronchel, C., Callejo, C., Fajardo, M. J., Moralejo, H., and Adrio, J. L. (2017) Engineering *Rhodosporidium toruloides* for the production of very long-chain monounsaturated fatty acid-rich oils. *Applied Microbiology and Biotechnology* 101(19): 7271–7280.

Fischer, M., Rhinow, D., Zhu, Z., Mills, D. J., Zhao, Z. K., Vonck, J., and Grininger, M. (2015) Cryo-EM structure of fatty acid synthase (FAS) from *Rhodosporidium toruloides* provides insights into the evolutionary development of fungal FAS. *Protein Science* 24(6): 987–995.

Gao, Q., Binns, D. D., Kinch, L. N., Grishin, N. V., Ortiz, N., Chen, X., and Goodman, J. M. (2017) Pet10p is a yeast perilipin that stabilizes lipid droplets and promotes their assembly. *Journal of Cell Biology* 216(10): 3199–3217.

Garay, L. A., Boundy-Mills, K. L., and German, J. B. (2014) Accumulation of high-value lipids in single-cell microorganisms: a mechanistic approach and future perspectives. *Journal of agricultural and food chemistry* 62(13): 2709–27.

Gasch, A. P., Spellman, P. T., Kao, C. M., Carmel-Harel, O., Eisen, M. B., Storz, G., Botstein, D., and Brown, P. O. (2000) Genomic expression programs in the response of yeast cells to environmental changes. (Silver, P. A., Ed.)*Molecular Biology of the Cell* 11(12): 4241–4257.

Gasch, Audrey P. (2007) The environmental stress response: a common yeast response to diverse environmental stresses. In *Yeast Stress Responses*. Berlin, Heidelberg: Springer Berlin Heidelberg doi:10.1007/3-540-45611-2_2.

Glover, D. M. (1995) *DNA cloning: a practical approach, Volume 1*. *DNA Cloning: A Practical Approach* (1st ed.). IRL Press.

Görner, W., Durchschlag, E., Martinez-Pastor, M. T., Estruch, F., Ammerer, G., Hamilton, B., Ruis, H., and Schüller, C. (1998) Nuclear localization of the C_2H_2 zinc finger protein Msn2p is regulated by stress and protein kinase A activity. *Genes & development* 12(4): 586–597.

Grant, C. M. (2001) Role of the glutathione/glutaredoxin and thioredoxin systems in yeast growth and response to stress conditions. *Molecular Microbiology* 39(3): 533–541.

Gross, D. S., English, K. E., Collins, K. W., and Lee, S. (1990) Genomic footprinting of the yeast HSP82 promoter reveals marked distortion of the DNA helix and constitutive occupancy of heat shock and TATA elements. *Journal of Molecular Biology* 216(3): 611–631.

Hashemi, H. F., and Goodman, J. M. The life cycle of lipid droplets. , 33 Current Opinion in Cell Biology 119–124 (2015). Elsevier Current Trends.

Henne, W. M., Reese, M. L., and Goodman, J. M. (2019) The assembly of lipid droplets and their roles in challenged cells. *The EMBO Journal* 38(9): e101816.

Herms, A., Bosch, M., Ariotti, N., Reddy, B. J. N., Fajardo, A., Fernández-Vidal, A.,

Alvarez-Guaita, A., Fernández-Rojo, M. A., Rentero, C., Tebar, F., Enrich, C., Geli, M. I., Parton, R. G., Gross, S. P., and Pol, A. (2013) Cell-to-cell heterogeneity in lipid droplets suggests a mechanism to reduce lipotoxicity. *Current Biology* 23(15): 1489–1496.

Holsters, M., de Waele, D., Depicker, A., Messens, E., van Montagu, M., and Schell, J. (1978) Transfection and transformation of *Agrobacterium tumefaciens*. *MGG Molecular & General Genetics* 163(2): 181–187.

Hu, C., Zhao, X., Zhao, J., Wu, S., and Zhao, Z. K. (2009) Effects of biomass hydrolysis by-products on oleaginous yeast *Rhodosporidium toruloides*. *Bioresource Technology* 100(20): 4843–4847.

Jackson, R. B., Canadell, J. G., Le Quéré, C., Andrew, R. M., Korsbakken, J. I., Peters, G. P., and Nakicenovic, N. (2016) Reaching peak emissions. *Nature Climate Change* 6(1): 7–10.

Jacquier, N., and Schneiter, R. (2010) Ypk1, the yeast orthologue of the human serum- and glucocorticoid-induced kinase, is required for efficient uptake of fatty acids. *Journal of Cell Science* 123(13): 2218–2227.

Jahn, T. R., and Radford, S. E. (2005) The Yin and Yang of protein folding. *FEBS Journal* 272(23): 5962–5970.

Johns, A. M. B., Love, J., and Aves, S. J. (2016) Four inducible promoters for controlled gene expression in the oleaginous yeast *Rhodotorula toruloides*. *Frontiers in Microbiology* 7(OCT).

Kilaru, S., and Steinberg, G. (2015) Yeast recombination-based cloning as an efficient way of constructing vectors for *Zymoseptoria tritici*. *Fungal Genetics and Biology* 79: 76–83.

Kitahara, Y., Yin, T., Zhao, X., Wachi, M., Du, W., and Liu, D. (2014) Isolation of oleaginous yeast (*Rhodosporidium toruloides*) mutants tolerant of sugarcane bagasse hydrolysate. *Bioscience, Biotechnology and Biochemistry* 78(2): 336–342.

Klecker, T., Braun, R. J., and Westermann, B. (2017) Lipid droplets guard mitochondria during autophagy. *Developmental Cell* 42(1): 1–2.

Klionsky, D. J. (2011) For the last time, it is GFP-Atg8, not Atg8-GFP (and the same goes for LC3). *Autophagy* 7(10): 1093–1094.

Klosinska, M. M., Crutchfield, C. A., Bradley, P. H., Rabinowitz, J. D., and Broach, J. R. (2011) Yeast cells can access distinct quiescent states. *Genes and Development* 25(4): 336–349.

Klug, L., and Daum, G. (2014) Yeast lipid metabolism at a glance. *FEMS Yeast Research* 14(3): 369–388.

Koh, C. M. J., Liu, Y., Moehninsi, Du, M., and Ji, L. (2014) Molecular characterization of KU70 and KU80 homologues and exploitation of a KU70-deficient mutant for improving gene deletion frequency in *Rhodosporidium toruloides*. *BMC Microbiology* 14(1): 50.

Kutty, S. N., and Philip, R. (2008) Marine yeasts - A review. *Yeast* 25(7): 465–483.

LB (Luria-Bertani) liquid medium (2006) *Cold Spring Harbor Protocols* 2006(1): pdb.rec8141.

Lee, S., Carlson, T., Christian, N., Lea, K., Kedzie, J., Reilly, J. P., and Bonner, J. J. (2000) The yeast heat shock transcription factor changes conformation in response to superoxide and temperature. (Pelham, H. R. B., Ed.)*Molecular Biology of the Cell* 11(5): 1753–1764.

Leibundgut, M., Jenni, S., Frick, C., and Ban, N. (2007) Structural basis for substrate delivery by acyl carrier protein in the yeast fatty acid synthase. *Science* 316(5822): 288–290.

Li, D., Song, J. Z., Shan, M. H., Li, S. P., Liu, W., Li, H., Zhu, J., Wang, Y., Lin, J., and Xie, Z. (2015) A fluorescent tool set for yeast Atg proteins. *Autophagy* 11(6): 954–960.

Li, Q., Du, W., and Liu, D. (2008) Perspectives of microbial oils for biodiesel production. *Applied microbiology and biotechnology* 80(5): 749–56.

LI, Y. H., LIU, B., ZHAO, Z. B., and BAI, F. W. (2006) Optimization of Culture Conditions for lipid production by *Rhodosporidium toruloides*. *Chinese Journal of Biotechnology* 22(4): 650–656.

Lin, X., Gao, N., Liu, S., Zhang, S., Song, S., Ji, C., Dong, X., Su, Y., Zhao, Z. K., and Zhu, B. (2017) Characterization the carotenoid productions and profiles of three *Rhodosporidium toruloides* mutants from *Agrobacterium tumefaciens*-mediated transformation. *Yeast* 34(8): 335–342.

Lin, X., Wang, Y., Zhang, S., Zhu, Z., Zhou, Y. J., Yang, F., Sun, W., Wang, X., and Zhao, Z. K. (2014) Functional integration of multiple genes into the genome of the oleaginous yeast *Rhodosporidium toruloides*. 14(4): 547–555.

Ling, J., Nip, S., Cheok, W. L., de Toledo, R. A., and Shim, H. (2014) Lipid production by a mixed culture of oleaginous yeast and microalga from distillery and domestic mixed wastewater. *Bioresource Technology* 173: 132–139.

Listenberger, L. L., Han, X., Lewis, S. E., Cases, S., Farese, R. V., Ory, D. S., and Schaffer, J. E. (2003) Triglyceride accumulation protects against fatty acid-induced lipotoxicity. *Proceedings of the National Academy of Sciences* 100(6): 3077–3082.

Liu, H., Jiao, X., Wang, Y., Yang, X., Sun, W., Wang, J., Zhang, S., and Zhao, Z. K. (2017) Fast and efficient genetic transformation of oleaginous yeast *Rhodosporidium toruloides* by using electroporation. *FEMS Yeast Research* 17(2).

Liu, L., Zhang, K., Sandoval, H., Yamamoto, S., Jaiswal, M., Sanz, E., Li, Z., Hui, J., Graham, B. H., Quintana, A., and Bellen, H. J. (2015) Glial lipid droplets and ROS induced by mitochondrial defects promote neurodegeneration. *Cell* 160(1–2): 177–190.

Liu, X. N., Lin, Q., Walther, T. C., Upadhyayula, S., Farese, R. V, Housden, B. E., et al. (2016) Seipin is required for converting nascent to mature lipid droplets. *eLife* 5: 1–28.

Liu, Y., Koh, C. M. J., Ngoh, S. Te, and Ji, L. (2015) Engineering an efficient and tight d-amino acid-inducible gene expression system in *Rhodosporidium*/*Rhodotorula* species. *Microbial Cell Factories* 14(1): 170.

Liu, Y., Koh, C. M. J., Sun, L., Hlaing, M. M., Du, M., Peng, N., and Ji, L. (2013) Characterization of glyceraldehyde-3-phosphate dehydrogenase gene RtGPD1 and development of genetic transformation method by dominant selection in oleaginous yeast *Rhodosporidium toruloides*. *Applied microbiology and biotechnology* 97(2): 719–29.

Liu, Y., Koh, C. M. J., Yap, S. A., Du, M., Hlaing, M. M., and Ji, L. (2018) Identification of novel genes in the carotenogenic and oleaginous yeast *Rhodotorula toruloides* through genome-wide insertional mutagenesis. *BMC Microbiology* 18(1): 14–39.

Liu, Y., Yap, S. A., Koh, C. M. J., and Ji, L. (2016) Developing a set of strong intronic

promoters for robust metabolic engineering in oleaginous *Rhodotorula* (*Rhodosporidium*) yeast species. *Microbial Cell Factories* 15(1): 200.

Lui, Y., Koh, C. M., and Ji, L. (2015) Methods for efficient production of Polyunsaturated Fatty Acids (PUFA) in *Rhodosporidium* and *Rhodotorula* species. Singapore: World Intellectual Property Organization.

Macool, D. J., Zhixiong, X., and Quinn Qun, Z. (2013/March) Expression of cytosolic malic enzyme in transgenic yarrowia to increase lipid production.

Madden, T. L., Tatusov, R. L., and Zhang, J. (1996) Applications of network BLAST server. *Methods in enzymology* 266: 131–41.

Miranda, D. A., Kim, J. H., Nguyen, L. N., Cheng, W., Tan, B. C., Goh, V. J., Tan, J. S. Y., Yaligar, J., Kn, B. P., Velan, S. S., Wang, H., and Silver, D. L. (2014) Fat storage-inducing transmembrane protein 2 is required for normal fat storage in adipose tissue. *Journal of Biological Chemistry* 289(14): 9560–9572.

Mishina, M., Rogguenkamp, R., and Schweizer, E. (1980) Yeast mutants defective in Acetyl-Coenzyme A carboxylase and biotin: Apocarboxylase ligase. *European Journal of Biochemistry* 111(1): 79–87.

Moldavski, O., Amen, T., Levin-Zaidman, S., Eisenstein, M., Rogachev, I., Brandis, A., Kaganovich, D., and Schuldiner, M. (2015) Lipid droplets are essential for efficient clearance of cytosolic inclusion bodies. *Developmental Cell* 33(5): 603–610.

Moraitis, C., and Curran, B. P. G. (2004) Reactive oxygen species may influence the heat shock response and stress tolerance in the yeast *Saccharomyces cerevisiae*. *Yeast* 21(4): 313–323.

Mortimer, R. K., and Johnston, J. R. (1986) Genealogy of principal strains of the yeast genetic stock center. *Genetics* 113(1): 35–43.

Müller-Taubenberger, A., Lupas, A. N., Li, H., Ecke, M., Simmeth, E., and Gerisch, G. (2001) Calreticulin and calnexin in the endoplasmic reticulum are important for phagocytosis. *EMBO Journal* 20(23): 6772–6782.

Murphy, D. J. (2012) The dynamic roles of intracellular lipid droplets: From archaea to mammals. *Protoplasma* 249(3): 541–585.

Naik, S. N., Goud, V. V., Rout, P. K., and Dalai, A. K. (2010) Production of first and

second generation biofuels: A comprehensive review. *Renewable and Sustainable Energy Reviews*.

Narayana, C. V., Sreenivasa Reddy, E., and Seetharama Prasad, M. (2012) A new method for gray level image thresholding using spatial correlation features and ultrafuzzy measure. *Global Journal of Computer Science and Technology* 12(15): 33–42.

Neves, M. J., and François, J. (1992) On the mechanism by which a heat shock induces trehalose accumulation in *Saccharomyces cerevisiae*. *Biochemical Journal* 288(3): 859–864.

Nguyen, T. B., Louie, S. M., Daniele, J. R., Tran, Q., Dillin, A., Zoncu, R., Nomura, D. K., and Olzmann, J. A. (2017) DGAT1-dependent lipid droplet biogenesis protects mitochondrial function during starvation-induced autophagy. *Developmental Cell* 42(1): 9-21.e5.

Nilsson, A., Gorwa-Grauslund, M. F., Hahn-Hägerdal, B., and Lidén, G. (2005) Cofactor dependence in furan reduction by *Saccharomyces cerevisiae* in fermentation of acid-hydrolyzed lignocellulose. *Applied and Environmental Microbiology* 71(12): 7866–7871.

Odumeru, J. A., D'Amore, T., Russell, I., and Stewart, G. G. (1993) Alterations in fatty acid composition and trehalose concentration of *Saccharomyces* brewing strains in response to heat and ethanol shock. *Journal of Industrial Microbiology* 11(2): 113–119.

Oh, C. S., Toke, D. A., Mandala, S., and Martin, C. E. (1997) ELO2 and ELO3, homologues of the *Saccharomyces cerevisiae ELO1* gene, function in fatty acid elongation and are required for sphingolipid formation. *Journal of Biological Chemistry* 272(28): 17376–17384.

Ohsaki, Y. (2006) Cytoplasmic lipid droplets are sites of convergence of proteasomal and autophagic degradation of Apolipoprotein B. (Brodsky, J., Ed.)*Molecular Biology of the Cell* 17(6): 2674–2683.

Okunuki, K. (1931) Beiträge zur Kenntnis der rosafarbigen Sprosspilze. *Journal of Japanese Botany* 5: 285–322.

Oliphant, T. E. (2010) *Guide to NumPy*. *Methods* (Vol. 1).

Otoupal, P. B., Ito, M., Arkin, A. P., Magnuson, J. K., Gladden, J. M., and Skerker, J. M. (2019) Multiplexed CRISPR-Cas9-based genome editing of *Rhodosporidium toruloides*. *mSphere* 4(2).

Pacifici, M., Foden, W. B., Visconti, P., Watson, J. E. M., Butchart, S. H. M., Kovacs, K. M., et al. (2015) Assessing species vulnerability to climate change. *Nature Climate Change* 5(3): 215–225.

Palmieri, L., Rottensteiner, H., Girzalsky, W., Scarcia, P., Palmieri, F., and Erdmann, R. (2001) Identification and functional reconstitution of the yeast peroxisomal adenine nucleotide transporter. *EMBO Journal* 20(18): 5049–5059.

Park, Y. K., Nicaud, J. M., and Ledesma-Amaro, R. (2018/March) The engineering potential of *Rhodosporidium toruloides* as a workhorse for biotechnological Applications. *Trends in Biotechnology*.

Parsell, D. A., and Lindquist, S. (2003) The Function of Heat-Shock Proteins in Stress Tolerance: Degradation and reactivation of damaged proteins. *Annual Review of Genetics* 27(1): 437–496.

Pascual, F., and Carman, G. M. (2013) Phosphatidate phosphatase, a key regulator of lipid homeostasis. *Biochimica et Biophysica Acta - Molecular and Cell Biology of Lipids* 1831(3): 514–522.

Polburee, P., Yongmanitchai, W., Honda, K., Ohashi, T., Yoshida, T., Fujiyama, K., and Limtong, S. (2016) Lipid production from biodiesel-derived crude glycerol by Rhodosporidium fluviale DMKU-RK253 using temperature shift with high cell density. *Biochemical Engineering Journal* 112: 208–218.

Rajakumari, S., and Daum, G. (2010) Janus-faced enzymes yeast Tgl3p and Tgl5p catalyze lipase and acyltransferase reactions. (Munro, S., Ed.)*Molecular Biology of the Cell* 21(4): 501–510.

Ratledge, C. (2014/August) The role of malic enzyme as the provider of NADPH in oleaginous microorganisms: A reappraisal and unsolved problems. *Biotechnology Letters*.

Rennerfelt, E. (1937) Undersökningar över svampinfektionen i slipmassa och dess utveckling däri. *Svenska Skogsvårdsföreningens Tidskrift* 35(1): 43–159.

Robson, M. (/1981) World energy prices. *Futures*.

Rogelj, J., Meinshausen, M., and Knutti, R. (2012) Global warming under old and new scenarios using IPCC climate sensitivity range estimates. *Nature Climate Change* 2(4): 248–253.

Rowe, L. A., Degtyareva, N., and Doetsch, P. W. (2008) DNA damage-induced reactive oxygen species (ROS) stress response in *Saccharomyces cerevisiae*. *Free Radical Biology and Medicine* 45(8): 1167–1177.

Runions, J., Brach, T., Kühner, S., and Hawes, C. (2006) Photoactivation of GFP reveals protein dynamics within the endoplasmic reticulum membrane. *Journal of Experimental Botany* 57(1): 43–50.

Sambrook, J., and Russel, D. W. (2012) *Moleculare Cloning: A Laboratory Manual*. (3rd ed.). New York, NY: Cold Spring Harbor Laboratory Press.

Satomura, A., Katsuyama, Y., Miura, N., Kuroda, K., Tomio, A., Bamba, T., Fukusaki, E., and Ueda, M. (2013) Acquisition of thermotolerant yeast *Saccharomyces cerevisiae* by breeding via stepwise adaptation. *Biotechnology Progress* 29(5): 1116–1123.

Satomura, A., Miura, N., Kuroda, K., and Ueda, M. (2016) Reconstruction of thermotolerant yeast by one-point mutation identified through whole-genome analyses of adaptively-evolved strains. *Scientific Reports* 6(1): 23157.

Schindelin, J., Arganda-Carreras, I., Frise, E., Kaynig, V., Longair, M., Pietzsch, T., Preibisch, S., Rueden, C., Saalfeld, S., Schmid, B., Tinevez, J. Y., White, D. J., Hartenstein, V., Eliceiri, K., Tomancak, P., and Cardona, A. (2012) Fiji: An open-source platform for biological-image analysis. *Nature Methods* 9(7): 676–682.

Schmitt, A. P., and McEntee, K. (1996) Msn2p, a zinc finger DNA-binding protein, is the transcriptional activator of the multistress response in *Saccharomyces cerevisiae*. *Proceedings of the National Academy of Sciences* 93(12): 5777–5782.

Schuldiner, M., and Bohnert, M. (2017) A different kind of love – lipid droplet contact sites. *Biochimica et Biophysica Acta - Molecular and Cell Biology of Lipids* 1862(10): 1188–1196.

Schulze, R. J., Sathyanarayan, A., and Mashek, D. G. (2017) Breaking fat: The regulation and mechanisms of lipophagy. *Biochimica et Biophysica Acta - Molecular and Cell Biology of Lipids* 1862(10): 1178–1187.

Schweizer, E., and Hofmann, J. (2004) Microbial Type I Fatty Acid Synthases (FAS): Major Players in a Network of Cellular FAS Systems. *Microbiology and Molecular Biology Reviews* 68(3): 501–517.

Schweizer, M., Roberts, L. M., Höltke, H. J., Takabayashi, K., Höllerer, E., Hoffmann, B., Müller, G., Köttig, H., and Schweizer, E. (1986) The pentafunctional FAS1 gene of yeast: its nucleotide sequence and order of the catalytic domains. *MGG Molecular & General Genetics* 203(3): 479–486.

Shi, L., Sutter, B. M., Ye, X., and Tu, B. P. (2010) Trehalose Is a Key Determinant of the Quiescent Metabolic State That Fuels Cell Cycle Progression upon Return to Growth. (Lew, D. J., Ed.)*Molecular Biology of the Cell* 21(12): 1982–1990.

Shi, S., and Zhao, H. (2017) Metabolic engineering of oleaginous yeasts for production of fuels and chemicals. *Frontiers in Microbiology* 8(NOV): 2185.

Singer, M. A., and Lindquist, S. (1998) Multiple effects of trehalose on protein folding in vitro and in vivo. *Molecular Cell* 1(5): 639–648.

Soccol, C. R., Dalmas Neto, C. J., Soccol, V. T., Sydney, E. B., da Costa, E. S. F., Medeiros, A. B. P., and Vandenberghe, L. P. de S. (2017) Pilot scale biodiesel production from microbial oil of *Rhodosporidium toruloides* DEBB 5533 using sugarcane juice: Performance in diesel engine and preliminary economic study. *Bioresource Technology* 223: 259–268.

Sola-Penna, M., Ferreira-Pereira, A., Lemos, A. dos P., and Meyer-Fernandes, J. R. (1997) Carbohydrate protection of enzyme structure and function against guanidinium chloride treatment depends on the nature of carbohydrate and enzyme. *European Journal of Biochemistry* 248(1): 24–29.

Soni, K. G., Mardones, G. A., Sougrat, R., Smirnova, E., Jackson, C. L., and Bonifacino, J. S. (2009) Coatomer-dependent protein delivery to lipid droplets. *Journal of Cell Science* 122(11): 1834–1841.

Sui, X., Arlt, H., Brock, K. P., Lai, Z. W., DiMaio, F., Marks, D. S., Liao, M., Farese, R. V., and Walther, T. C. (2018) Cryo–electron microscopy structure of the lipid droplet–formation protein seipin. *Journal of Cell Biology* 217(12): 4080–4091.

Sztalryd, C., and Brasaemle, D. L. (2017) The perilipin family of lipid droplet proteins: Gatekeepers of intracellular lipolysis. *Biochimica et Biophysica Acta - Molecular and*

Cell Biology of Lipids 1862(10): 1221–1232.

Szymanski, K. M., Binns, D., Bartz, R., Grishin, N. V., Li, W.-P., Agarwal, A. K., Garg, A., Anderson, R. G. W., and Goodman, J. M. (2007) The lipodystrophy protein seipin is found at endoplasmic reticulum lipid droplet junctions and is important for droplet morphology. *Proceedings of the National Academy of Sciences* 104(52): 20890–20895.

Takahashi, S., Okada, H., Abe, K., and Kera, Y. (2014) Genetic transformation of the yeast Rhodotorula gracilis ATCC 26217 by electroporation. *Applied Biochemistry and Microbiology* 50(6): 624–628.

Tanaka, K., Shimizu, T., Ohtsuka, Y., Yamashiro, Y., and Oshida, K. (2007) Early dietary treatments with Lorenzo's oil and docosahexaenoic acid for neurological development in a case with Zellweger syndrome. *Brain and Development* 29(9): 586–589.

Tang, W., Zhang, S., Wang, Q., Tan, H., and Zhao, Z. K. (2009) The isocitrate dehydrogenase gene of oleaginous yeast Lipomyces starkeyi is linked to lipid accumulation . *Canadian Journal of Microbiology* 55(9): 1062–1069.

Tehlivets, O., Scheuringer, K., and Kohlwein, S. D. (2007) Fatty acid synthesis and elongation in yeast. *Biochimica et Biophysica Acta - Molecular and Cell Biology of Lipids* 1771(3): 255–270.

Thiam, A. R., and Forêt, L. (2016) The physics of lipid droplet nucleation, growth and budding. *Biochimica et Biophysica Acta - Molecular and Cell Biology of Lipids* 1861(8): 715–722.

Thliveros, P., Uçkun Kiran, E., and Webb, C. (2014) Microbial biodiesel production by direct methanolysis of oleaginous biomass. *Bioresource Technology* 157: 181–187.

Trott, A., and Morano, K. A. (2007) The yeast response to heat shock. In *Yeast Stress Responses*. Berlin, Heidelberg: Springer Berlin Heidelberg doi:10.1007/3-540-45611-2_3.

Trotter, E. W., Kao, C. M. F., Berenfeld, L., Botstein, D., Petsko, G. A., and Gray, J. V. (2002) Misfolded proteins are competent to mediate a subset of the responses to heat shock in *Saccharomyces cerevisiae*. *Journal of Biological Chemistry* 277(47): 44817–44825.

Tsai, Y. Y., Ohashi, T., Kanazawa, T., Polburee, P., Misaki, R., Limtong, S., and Fujiyama, K. (2017) Development of a sufficient and effective procedure for transformation of an oleaginous yeast, *Rhodosporidium toruloides* DMKU3-TK16. *Current Genetics* 63(2): 359–371.

Tsai, Y. Y., Ohashi, T., Wu, C. C., Bataa, D., Misaki, R., Limtong, S., and Fujiyama, K. (2019) Delta-9 fatty acid desaturase overexpression enhanced lipid production and oleic acid content in *Rhodosporidium toruloides* for preferable yeast lipid production. *Journal of Bioscience and Bioengineering* 127(4): 430–440.

Tully, M., and Gilbert, H. J. (1985) Transformation of *Rhodosporidium toruloides*. *Gene* 36(3): 235–240.

Tyedmers, J., Mogk, A., and Bukau, B. (2010) Cellular strategies for controlling protein aggregation. *Nature Reviews Molecular Cell Biology* 11(11): 777–788.

Tyner, W. E. (2010) Commentary: Comparison of the US and EU approaches to stimulating biofuels. *Biofuels* 1(1): 19–21.

Ulvestad, A. (2018) A Brief Review of Current Lithium Ion Battery Technology and Potential Solid State Battery Technologies.

UNCTAD (2016) Rewiev of Maritime Transport 2016.

Underhill, J. (2012) The *Saccharomyces cerevisiae* zinc finger proteins Msn2p and Msn4p are required for transcriptional induction through the stress response element (STRE). *The EMBO journal* 15(9): 2227–2235.

Vabulas, R. M., Raychaudhuri, S., Hayer-Hartl, M., and Hartl, F. U. (2010) Protein folding in the cytoplasm and the heat shock response. *Cold Spring Harbor perspectives in biology* 2(12): a004390–a004390.

Van Larebeke, N., Engler, G., Holsters, M., Van Den Elsacker, S., Zaenen, I., Schilperoort, R. A., and Schell, J. (1974) Large plasmid in *Agrobacterium tumefaciens* essential for crown gall-inducing ability. *Nature* 252(5479): 169–170.

van Zutphen, T., Todde, V., de Boer, R., Kreim, M., Hofbauer, H. F., Wolinski, H., Veenhuis, M., van der Klei, I. J., and Kohlwein, S. D. (2014) Lipid droplet autophagy in the yeast *Saccharomyces cerevisiae*. *Molecular Biology of the Cell* 25(2): 290–301.

Walker, T. R. (2016) Green Marine: An environmental program to establish

sustainability in marine transportation. *Marine Pollution Bulletin* 105(1): 199–207.

Walker, T. R., Adebambo, O., Del Aguila Feijoo, M. C., Elhaimer, E., Hossain, T., Edwards, S. J., Morrison, C. E., Romo, J., Sharma, N., Taylor, S., and Zomorodi, S. (2018) Environmental effects of marine transportation. In *World Seas: An Environmental Evaluation*. Elsevier doi:10.1016/b978-0-12-805052-1.00030-9.

Wang, C. C., Moorhouse, S., Stain, C., Seymour, M., Green, E., Penfield, S., and Moger, J. (2018) In situ chemically specific mapping of agrochemical seed coatings using stimulated Raman scattering microscopy. *Journal of Biophotonics* 11(11): e201800108.

Wang, C. W. (2016) Lipid droplets, lipophagy, and beyond. *Biochimica et Biophysica Acta - Molecular and Cell Biology of Lipids* 1861(8): 793–805.

Wang, H., Airola, M. V., and Reue, K. (2017) How lipid droplets "TAG" along: Glycerolipid synthetic enzymes and lipid storage. *Biochimica et Biophysica Acta - Molecular and Cell Biology of Lipids* 1862(10): 1131–1145.

Wang, Q. M., Yurkov, A. M., Göker, M., Lumbsch, H. T., Leavitt, S. D., Groenewald, M., Theelen, B., Liu, X. Z., Boekhout, T., and Bai, F. Y. (2015) Phylogenetic classification of yeasts and related taxa within Pucciniomycotina. *Studies in Mycology* 81: 149–189.

Wang, Y., Lin, X., Zhang, S., Sun, W., Ma, S., and Zhao, Z. K. (2016) Cloning and evaluation of different constitutive promoters in the oleaginous yeast *Rhodosporidium toruloides*. *Yeast* 33(3): 99–106.

Wang, Y., Zhang, S., Pötter, M., Sun, W., Li, L., Yang, X., Jiao, X., and Zhao, Z. K. (2016) Overexpression of Δ12-fatty acid desaturase in the oleaginous yeast *Rhodosporidium toruloides* for production of linoleic acid-rich lipids. *Applied Biochemistry and Biotechnology* 180(8): 1497–1507.

Weng, L., and Elliott, G. D. (2015) Distinctly different glass transition behaviors of trehalose mixed with Na_2HPO_4 or NaH_2PO_4: evidence for its molecular origin. *Pharmaceutical Research* 32(7): 2217–2228.

Wilfling, F., Wang, H., Haas, J. T., Krahmer, N., Gould, T. J., Uchida, A., Cheng, J. X., Graham, M., Christiano, R., Fröhlich, F., Liu, X., Buhman, K. K., Coleman, R. A., Bewersdorf, J., Farese, R. V., and Walther, T. C. (2013) Triacylglycerol synthesis

enzymes mediate lipid droplet growth by relocalizing from the ER to lipid droplets. *Developmental Cell* 24(4): 384–399.

Winston, F., Dollard, C., and Ricupero-Hovasse, S. L. (1995) Construction of a set of convenient *Saccharomyces cerevisiae* strains that are isogenic to S288C. *Yeast* (Vol. 11).

Wu, C. C., Tsai, Y. Y., Ohashi, T., Misaki, R., Limtong, S., and Fujiyama, K. (2018) Isolation of a thermotolerant *Rhodosporidium toruloides* DMKU3-TK16 mutant and its fatty acid profile at high temperature. *FEMS Microbiology Letters* 365(21).

Xu, D., Li, Y., Wu, L., Li, Y., Zhao, D., Yu, J., Huang, T., Ferguson, C., Parton, R. G., Yang, H., and Li, P. (2018) Rab18 promotes lipid droplet (LD) growth by tethering the ER to LDs through SNARE and NRZ interactions. *Journal of Cell Biology* 217(3): 975–995.

Xu, J., and Liu, D. (2017) Exploitation of genus Rhodosporidium for microbial lipid production. *World Journal of Microbiology and Biotechnology* 33(3): 54.

Xu, S., Zhang, X., and Liu, P. (2018) Lipid droplet proteins and metabolic diseases. *Biochimica et Biophysica Acta - Molecular Basis of Disease* 1864(5): 1968–1983.

Yang, F., Zhang, S., Zhou, Y. J., Zhu, Z., Lin, X., and Zhao, Z. K. (2012) Characterization of the mitochondrial NAD +-dependent isocitrate dehydrogenase of the oleaginous yeast *Rhodosporidium toruloides*. *Applied Microbiology and Biotechnology* 94(4): 1095–1105.

Zerbino, D. R., Achuthan, P., Akanni, W., Amode, M. R., Barrell, D., Bhai, J., et al. (2018) Ensembl 2018. *Nucleic Acids Research* 46(D1): D754–D761.

Zhang, S., Ito, M., Skerker, J. M., Arkin, A. P., and Rao, C. V. (2016) Metabolic engineering of the oleaginous yeast *Rhodosporidium toruloides* IFO0880 for lipid overproduction during high-density fermentation. *Applied Microbiology and Biotechnology* 100(21): 9393–9405.

Zhang, S., Skerker, J. M., Rutter, C. D., Maurer, M. J., Arkin, A. P., Rao, C. V., Skerker, J. M., Maurer, M. J., and Arkin, A. P. (2016) Engineering *Rhodosporidium toruloides* for increased lipid production. *Biotechnology and Bioengineering* 113(5): 1056–1066.

Zheng, Z., and Zou, J. (2001) The initial step of the glycerolipid pathway: Identification

of glycerol 3-phosphate/dihydroxyacetone phosphate dual substrate acyltransferases in *Saccharomyces cerevisiae*. *Journal of Biological Chemistry* 276(45): 41710–41716.

Zhu, Z., Ding, Y., Gong, Z., Yang, L., Zhang, S., Zhang, C., Lin, X., Shen, H., Zou, H., Xie, Z., Yang, F., Zhao, X., Liu, P., and Zhao, Z. K. (2015) Dynamics of the lipid droplet proteome of the oleaginous yeast *Rhodosporidium toruloides*. *Eukaryotic cell* 14(3): 252–64.

Zhu, Z., Zhang, S., Liu, H., Shen, H., Lin, X., Yang, F., Zhou, Y. J., Jin, G., Ye, M., Zou, H., and Zhao, Z. K. (2012) A multi-omic map of the lipid-producing yeast *Rhodosporidium toruloides*. *Nature Communications* 3: 1112.